4-30-2011

Formation of geomorphic features as a response to sea-level change at Ritidian Point, Guam, Mariana Islands

Blaz Miklavic

FORMATION OF GEOMORPHIC FEATURES AS A RESPONSE TO SEA-LEVEL CHANGE AT RITIDIAN POINT, GUAM, MARIANA ISLANDS

By

Blaž Miklavič

A Thesis
Submitted to the Faculty of
Mississippi State University
in Partial Fulfillment of the Requirements
for the Degree of Master's of Science
in Geosciences
in the Department of Geosciences

Mississippi State, Mississippi

April 2011

FORMATION OF GEOMORPHIC FEATURES AS A RESPONSE TO SEA-LEVEL CHANGE AT RITIDIAN POINT, GUAM, MARIANA ISLANDS

By

Blaž Miklavič

Approved:

John E. Mylroie Professor of Geology Director of Thesis	Chris P. Dewey Associate professor of Geology Graduate Coordinator
Craig B. Grimes Assistant Professor of Geology Committee Member	Brenda Kirkland Associate Professor of Geology Committee Member
Gary L. Myers College of Arts and Sciences Dean	

Name: Blaž Miklavič

Date of Degree: April 30, 2011

Institution: Mississippi State University

Major Field: Geosciences

Major Professor: John E. Mylroie

Title of Study: FORMATION OF GEOMORPHIC FEATURES AS A RESPONSE TO SEA-LEVEL CHANGE AT RITIDIAN POINT, GUAM, MARIANA ISLANDS

Pages in Study: 195

Candidate for Degree of Master's of Science

Geomorphic features have been one of the major tools for sea-level change studies. The present work shows an example of sea-level change study on karst terrain in the tropics. Sea-level notches as well as flank margin caves were identified in the research area and their elevation measured. The time of formation of the sea-level indicators was constrained by lithology study and dating methods such as facies comparison and U-Th dating. Denudation and uplift were also studied for the same purpose.

From this study it can be concluded that sea-level stands within the glacial cycle can cause the formation of flank margin caves and that the position of these sea-level stands can be determined. The research area was estimated to have cumulatively uplifted ~22 m in the past 125 ka years (~0.18 mm/yr) while the surface has been denuded some 8 m in the same span of time (~0.064 mm/yr).

Keywords: karst, karst hydrology, flank margin caves, sea-level change, denudation rate, uplift rate, sea-level notches, bioerosional notches, last interglacial, MIS 5e, mid-Holocene sea-level highstand, reef limestone, Guam

ACKNOWLEDGEMENTS

In first place I would like to thank my advisors, John Mylroie and John Jenson, for making this masters research possible and for all the valuable help in the field, with the manuscripts and endless paperwork that was encountered during the research. For my extended stay on Guam I also owe thanks to the Water and Environmental Research Institute of the Western Pacific (WERI) Director, Gary Denton, and Mark Lander.

The study and research would not be possible without the combined funding of the Guam Hydrologic Survey, USGS-NIWR (National Institutes for Water Resources), NOAA, WERI, Mississippi State University, and Slovene Human Resources Development and Scholarship Fund.

Special thanks go to volunteers Tomoko Bell, Peter Sakisat, Akashi Rouse, Kennedy Tolenoa, Judson Partin, Von Apuya, Liang Guo, Chris Halligan, Michael Hazel, Nathan Habana and Bryan Duell for invaluable help in digging out the buried entrances of some of the caves and for other field assistance. I am truly indebted and thankful to Richard Randall for providing critical assistance and guidance in the field.

Thanks go also to Shahram Khosrowpanah for training in surveying and providing the survey equipment, Maria Kottermair for dealing with ArcMap, Jennifer Cruz, Chrispina Tagudin and Carmen Kautz for the assistance in the laboratory, Jennifer Kenne Kivett for the quick course of Photoshop and Yuming Wen for GIS and surveying tips.

I'm obliged for all the administrative help to Gwen Mangloña, Norma Blas, Eden Suarez-Galvez, Miyuki Reklai and Remy Babauta Cristobal at the University of Guam, Patricia Willson, Kim Chewe, Mary Dean, Tina Davis and Stephen Cottrell at the Mississippi State University. Thanks also to the librarians Paul Drake, Suzanne Bell and Moses Francisco for all the help in finding unfindable literature. The research would not be possible without the collaboration of the Jackson School of Geosciences of the University of Texas at Austin where U-Th dating was done; special thanks go to Jay Banner, Judson Partin, Lawrence Mack and Eric James.

I would also like to thank the Guam National Wildlife Refuge, for permission to work in the restricted areas and its friendly personal, Jospeh Scwagerl, Cary and Chris Eggleston, Gabriel Cruz, Paul Castro and Emily Sablan-Torres. Thanks go also to the Anderson Air Force Base Environmental Office for permission and providing escorts to support work on the Ritidian cliff top and Tarague embayment. Thanks go also to Guam Homeland Security Office of Civil Defense, Department of Land Management Land Survey Division, Office of the Governor of Guam, Bureau of Statistics and Plans, and UOG Residence Halls. Thanks also to WERI and Danko Taboroši for providing the necessary funds for participating at two conferences where the results of this research were presented.

I owe sincere and earnest thankfulness to Joan Mylroie and the rest of the Mylroie family (Leif, Lars, Erik and Bika) for all the given help while in Starkville. Thanks go also to Cheri Jenson for the various help in settling on Guam.

I would like to show my gratitude also to my roommates Dušan Kunec, Florian Yatilman, Liang Guo, Benjamin Ratilmay, Lorelei Ford and Claudia Hohn for various kind of assistance and support. Thanks go also to the graduate student gang at Mississippi

State University, Maggie Corley, Andrew Birmingham, John Eric Ezel, Charlotte Buehler and Keith Puckett.

Last but not least I thank my parents for all the support in all the years of my education as well as for the moral support while on Guam. Precious and of special importance were the culinary treats sent from Slovenia..>

TABLE OF CONTENTS

LIST OF TABLES

LIST OF FIGURES

CHAPTER I

INTRODUCTION

Sea-level change research has drawn high attention at least since the 19th century, when the first tide-gauges were placed, mainly due to its importance because of high population density along the coasts and high economic importance of the ports. No matter the relative long history of the study, the dynamics of sea-level change and its relation to climate change are not yet fully understood and further research is needed to better understand changes in sea level as a response to changes in climate. While a lot of research has been done in the temperate zones, less attention has been paid to the more remote environments such as the tropics where Guam is located.

The objective of this study is to help to determine the long term relative sea-level change on Guam using geomorphic features. This study also meets the increasing demand of coastal management, hydrogeologists, archeologists, and the tourist industry on Guam. The research area is on carbonate terrain, which is prone to karstification and the various geomorphic phenomena connected to that process.

To understand the geomorphic features and their relation to relative sea-level change, one has to carefully study a variety of different geological clues. In tectonically active areas special attention has to be paid to the regional tectonic setting and known uplift trends. Besides the dynamics, driving forces and known fluctuations of the sea level, the sea-level indicators have to be well understood--how they form, how can be recognized, what they represent, their strengths and limitations, and how can they be

dated. For proper comprehension of the genesis of geomorphic features on limestone terrains a thorough knowledge of karst processes is a prerequisite.

The chosen research area was thus thoroughly examined and the key geomorphic features identified and thoroughly described. Besides the geomorphology, attention was also paid to the lithology and local geologic structure. In contrast to other similar research, greater attention was paid to the surface lowering and related problems and pitfalls. In addition to the selected research area, the adjacent areas were also briefly examined for comparison, especially the area(s) that were thoroughly examined before by earlier researchers. The findings are therefore described separately for each examined area.

CHAPTER II

LITERATURE REVIEW

Geography

Guam is the largest of the Mariana Islands, located at 13°28' N and 144°45' E (Tracey et al., 1964), approximately half way between Japan and Australia. It is situated in the western Pacific between the Pacific Ocean to the east and the Philippine Sea to the west (Figure 1). It covers an area of 550 km^2 and is 48 km long and 6-19 km wide.

The island can be divided in two distinct provinces: northern and southern. The northern part of the island is a limestone plateau (Figure 1) with a mean elevation about 100 m with only very minor and restricted surface drainage. The plateau reaches its highest limestone elevation at the very north being Mt. Machanao near Ritidian Point at 183.5 m above sea level. The plateau is gently inclined towards the south with an average slope of about 5 m per 1 km (Tracey et al., 1964). There are two small volcanic outcrops forming smaller topographic highs above the plateau, the higher of the two, Mt Santa Rosa, being 253 m high. The terrain of the south, on the other hand, is predominantly composed of volcanic rocks and has a well expressed topography of mountains and stream valleys, but isolated interior limestone outcrops and a strip of coastal limestone (Figure 1) create sections of karst. A cuesta of low mountains stands above the western coast of the southern part of the island. The peaks are from about 300 to 400 m high. The highest is Mt. Lamlam, 407 m high, and capped with limestone. Fringing reefs surround

most of the island ranging from narrow cut benches around headlands to broad reef flats more than 900 m wide.

The average tidal range between the mean lower low water and mean Higher High Water is ~0.7 m, while the water-level range between the minimum and maximum observed water level is more than 2 m. The Mean Higher High Water is 0.68 m above the Mean Lower Low Water Level and 0.26 m above Mean Sea Level (Table 1) (NOAA, 2011).

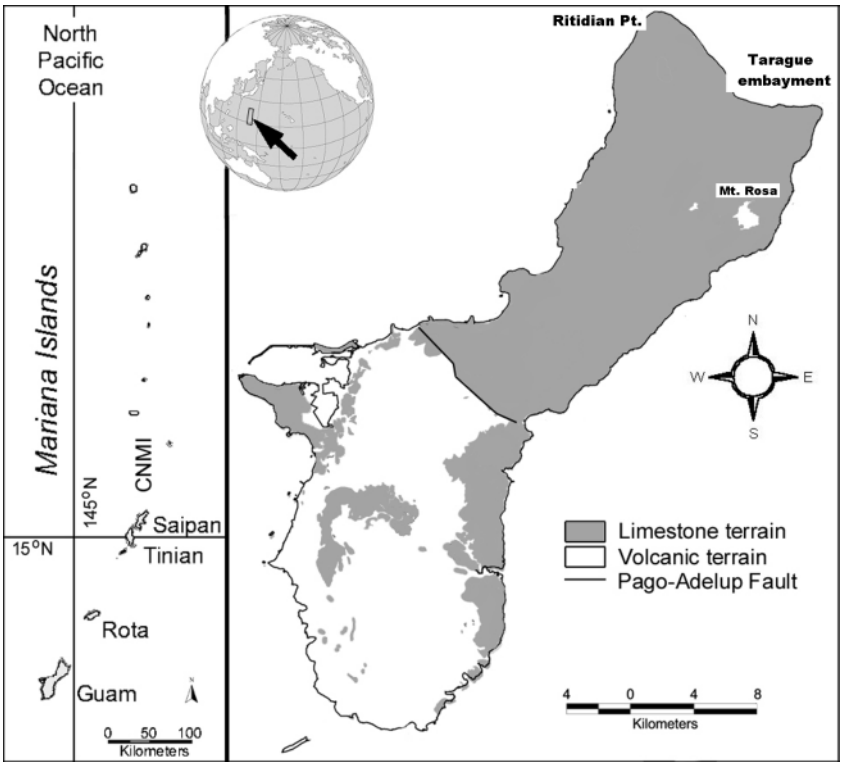

Figure 1 Geographic position of Guam (upper left corner and left side) and limestone terrain on Guam. (From Taboroši et al., 2005, with permission.)

Table 1 Elevations of tidal datums referred to the Mean Lower Low Water in meters. The averages are based on records between January 1983 and December 2001. (NOAA, 2011.)

Highest observed water level (08/12/1992)	1.302 m
Mean Higher High Water	0.715 m
Mean High Water	0.678 m
Mean Tide Level	0.432 m
Mean Sea Level	0.412 m
Mean Low Water	0.185 m
Mean Lower Low Water	0.000 m
Lowest observed water level (10/24/1972)	- 0.712 m

Climate and hydrology

Guam's climate is tropical marine with a well-expressed dry and wet season. The mean annual temperature is 27°C with little seasonal variation (Tracey et al., 1964; Mink and Vacher, 1997). The mean daily low temperature is 24°C and the mean high 30°C. The dry season is characterized by westward-moving trade winds that last from January until May. July through November is the wet season, when the trades are frequently interrupted by tropical storms with heavy rainfall. June and December are transitional months. Mean annual rainfall on Guam is about 2400 mm (Jocson et al., 2002); on the northern plateau between 2200 and 2500 mm (Mink and Vacher, 1997, Lander and Guard, 2003) and between 2300 and 2400 mm in the Ritidian Point area (Figure 2) (Lander and Guard, 2003). About 70% of mean annual rainfall arrives in the wet season. Somewhat more than 60% of the annual rainfall is estimated to contribute to the

groundwater recharge (Jocson et al., 2002). The average water budget for northern Guam could therefore be estimated to be ~1400 mm. During the wet season, tropical storms and typhoons can cross the island, releasing large amounts of water in a short time. The chances that a typhoon will pass within 220 km of Guam in any given year are 2 in 3 (Tracy et al., 1964). During El Niño events, however, severe droughts may occur.

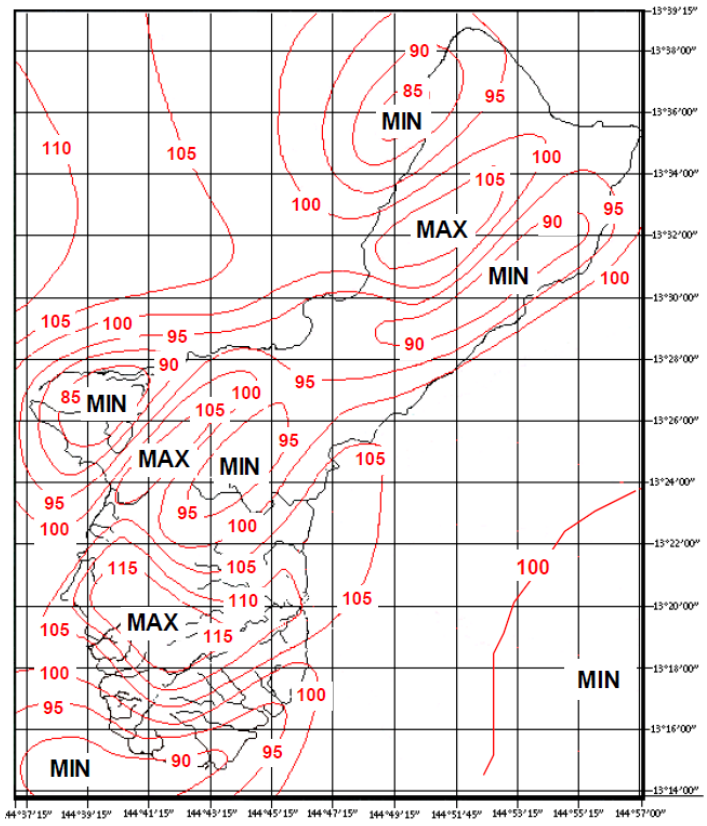

Figure 2 Mean annual rainfall distribution for Guam based on 1950-1999 rainfall database. Isohyets are in inches, 1 in = 25.4 mm, 90 in = 2286 mm. (From Lander and Guard, 2003, with permission.)

Tectonic setting and movements on Guam

Regional tectonic setting

The Mariana island arc is part of the Izu-Bonin-Mariana arc system that extends 2800 km from near Tokyo, Japan to near Guam and is an example of intra-oceanic convergent margin (Stern et al., 2003) where, in this case, the Pacific Plate subducts under the Philippine Sea Plate. The system is interpreted to have formed when an oceanic transform fault was converted into a subduction zone due to the change in motion of the Pacific Plate from northerly to more westerly motion about 43 Ma ago (Stern and Bloomer, 1992; Stern et al., 2003). Since then, the arc split twice to form the present Mariana system, which includes a trench (Mariana Trench), frontal arc (Mariana Ridge), inter-arc or back-arc basin (Mariana Trough), and third arc (West Mariana Ridge) (e.g. Karig, 1971; Stern et al., 2003). The forearc of the Mariana ridge is composed of uplifted Eocene igneous basement partly surmounted by reefal limestone and produces the chain of islands from Guam in the south to Ferdinand de Medinilla in the northern Mariana Islands. The active arc is located just west from the forearc forming a chain of predominantly submerged volcanoes that stretch from near Guam to Oshu. The West Mariana ridge and further east-lying Palau-Kyushu ridge are remnant arcs that were rifted away during opening of the Parece-Vela remnant back-arc basin and Mariana Trough back-arc basin, respectively. The Mariana Trough is characterized by active back-arc spreading with spreading rates from 15 mm/yr near Arighan to 45 mm/yr near Guam, implying arc movement to the east relative to the Philippine Sea plate (Kato et al., 2003). Martinez and Fryer (2000) estimate a 65 mm/yr spreading rate near Guam based on magnetic inversions on the seafloor. Subduction rates of the Pacific Plate beneath the Mariana forearc range from 35-45 mm/yr near Arighan and 60-70 mm near Guam (Kato

et al., 2003). Because of the curved shape and different velocities, the arc is being stretched and fragmented with radiating normal faults (Martinez and Fryer, 2000; Kato et al., 2003). Vertical movements are also associated with the arc system. Uplift is generally associated with compression, while subsidence is associated with extension (Kobayashi, 1995). The solid support of the arc is being pushed by the subsiding plate. When spreading occurs, the remnant arc, as well as the spreading basin, looses the support of the underlying subsiding plate so they tend to subside in order to achieve isostatic equilibrium (Kobayashi, 1995).

Uplift estimates for Guam based on geologic evidence

On several places on Guam a set of well-defined terraces is present. On the assumption of a constant uplift, Bureau and Hengsh (1994) tried to correlate each of these terraces to the sea-level curve, each of the terraces representing a sea-level high stand, with the lowest terrace representing the youngest high stand. The resulting estimates were between 0.56 and 0.64 mm/yr of uplift for southern and central Guam (Figure 3). For northern Guam, however, the estimates were considerably higher. The estimated uplift at Pagat Point was 1.06 mm/yr while Ritidian Point would have an uplift rate of 0.92 mm/yr or 1.55 mm/yr, depending on the interpretation of the terraces' correlation to the sea-level curve. Based on either of these assumptions, the level of the MIS 5e sea-level highstand (~125 ka) would be at or near the top of the Ritidian cliff.

Randall and Siegrist (1996), on the other hand, estimated the uplift of northern Guam by considering the elevation of the highest Mariana Limestone outcrop (180 m) and its age of deposition (1.8 to 2 million yrs) resulting in an estimate of about 0.1 mm/yr of average uplift. However, they did not consider the erosion of the limestone in such a

time span, possible subsidence episodes, or the actual sea-level position during each phase of the deposition of the Mariana Limestone.

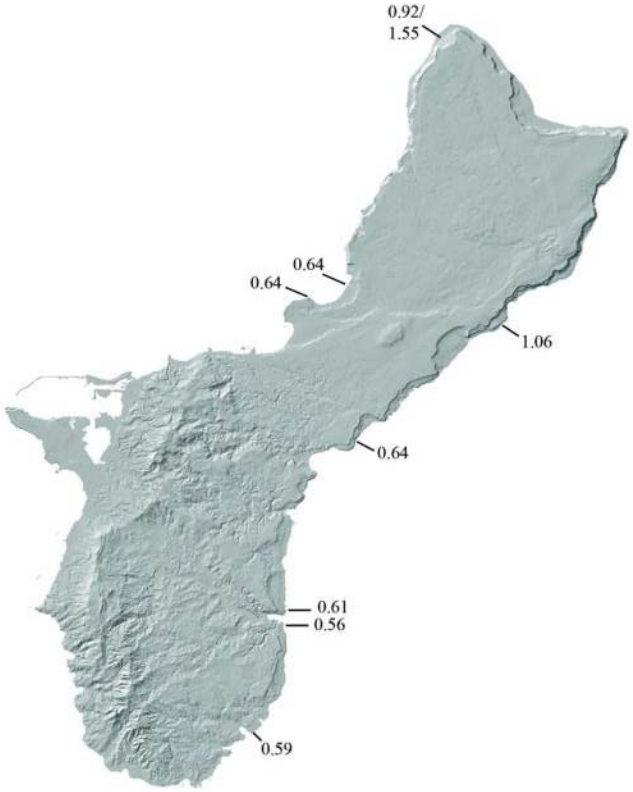

Figure 3 Locations of marine terraces with calculated uplift rates based on terraces elevations. Note the higher trend of uplift values in northern Guam. All the values are in millimeters per year. (Constructed with the data from Bureau and Hengsh, 1994, map from Taboroši et al., 2005, with permission.)

Recent uplift and subsidence on Guam

Geodetic survey was performed in The Commonwealth of the Northern Mariana Islands in years 1968 and 1969, and in Guam in 1963 (Carlson et al., 2009). The mean sea level was used as datum for Guam and was based on the average of 13 years and 10 months of tide gauge records spanning January 1949 to October 1962. For the new vertical control network established in 2004, mean sea level relative to the 1983-2001 National Tidal Datum Epoch was used as a datum. The benchmarks established in 1963

that were considered the most stable and undisturbed were re-measured in the 2004 survey and the results compared (Table 2). On average, the elevations of the benchmarks were 4.1 cm lower than in 1963. The differences in elevations, however, ranged from +16.2 to −24.3 cm. Even by removing four points exhibiting changes larger than 10 cm (i.e., considering them as anomalous outliers) the residual average change would still be about −3 cm. The change of local mean sea level computed for the time span between 1948 to 1999, however, indicates a 0.4 cm rise in sea level. Thus, assuming the surveys are accurate, the sea level rise between 1948 and 1999 does not significantly account for the measured subsidence between the 1963 and 2004 and thus tectonic activity is believed to be the cause (Carlson et al., 2009).

Table 2 Difference in benchmark elevations between the 2004 and 1963 measurements ion Guam. (Modified after Carlson, 2009.)

Benchmark	2004 measurement (m)	1963 measurement (m)	H Difference (m)
163 0000 TIDAL 6	1.537	1.531	0.006
163 0000 TIDAL 7	2.264	2.263	0.001
ASALONSA	73.973	74.063	-0.090
AAFB 1	160.784	160.805	-0.021
AAFB 21	160.322	160.354	-0.032
AAFB 27	161.011	161.049	-0.038
BEACH	1.858	1.897	-0.039
BIXBY	3.539	3.608	-0.069
CASTRO	184.693	184.710	-0.017
CRUSHER	87.451	87.493	-0.042
GAYINERO	166.784	166.816	-0.032
H 2	3.072	3.089	-0.017
HAWAIIAN	112.012	112.064	-0.052
MANALISAY	0.898	0.966	-0.068
NCS	133.167	133.172	-0.005
NSD 5	9.211	9.221	-0.010
SABANON	167.476	167.520	-0.044

Table 2 (Continued)

SALISBURY	187.872	187.710	0.162
SASA	3.298	3.442	-0.144
SOLEDAD	44.194	44.437	-0.243
SPLIT	139.69	139.731	-0.041
SPUR	122.851	122.895	-0.044
SYLAR	177.853	177.878	-0.025
TAMUNING	33.812	33.833	-0.021
TART	7.993	8.065	-0.072
UMATAC	5.585	5.575	0.010
USO	3.480	3.621	-0.141
V 1	3.747	3.794	-0.047
WETTENGEL	90.176	90.195	-0.019
		Average	-0.041
		Std. Dev.	0.066

In 1993 a magnitude 8.1 (momentum magnitude Mw7.7) earthquake occurred, with its epicenter slightly offshore southeast of Guam. Pre- and post-earthquake GPS measurements at a number of sites on Guam documented a coseismic subsidence of about 10 cm, with about 25 cm of displacement to the southeast (Beavan et al., 1994). The earthquake ruptured a shallow-dipping thrust fault that corresponds to the subduction interface under Guam (Campos et al., 1996). In contrast to other subduction zones, there

have not been earthquakes with Mw greater than 8 in the Mariana Island Arc system in recorded history (Bureau and Hengsh, 1994).

The regional recurrence time for Guam has been calculated as:

$\text{Log } N = 5.596 - 0.599M$

where N is the number of events per year of magnitude $\geq$ M (Bureau and Hengsh, 1994).

Several equations that express the relation between the magnitude (M) and coseismic displacement (D) have been reported (Wang and Law, 1994 and references therein):

$\text{Log } D = 0.55M - 3.71$ (worldwide)

$\text{Log } D = 0.96M - 6.69$ (worldwide)

$\text{Log } D = 0.57M - 3.91$ (USA)

$\text{Log } D = 0.6M - 4.0$ (vertical displacement, continental Japan)

$\text{Log } D = 0.57M - 3.19$ (USA)

$\text{Log } D = 0.67M - 4.33$ (Japan)

None of them seem to fit the 1993 Guam earthquake, as the displacement would have to be several meters for each of these equations. Therefore, even with a known recurrence it is not possible to calculate the coseismic displacement over a given time period. Further, none of the given equations gives the direction of the displacement, and usually uplift is assumed.

Recent data from a permanent GPS station on the northern part of the island revealed an average uplift of 1.18 ±0.73 mm/yr in a 10-year time span between January 1997 and November 2006 (Bouin and Wöppelmann, 2010).

Geology of Guam

General

Guam is a part of the Mariana island arc which has split twice in the geologic history to form two remnant ridges (Palau-Kyushu Ridge and West Mariana Ridge) (Reagan and Meier, 1983). The formation of the arc began about 43 Ma ago, which is also the age of the oldest rocks found on Guam.

Geologic sequence

Geologically, Guam can be divided into two physiographic provinces: northern Guam, composed mostly of carbonate rocks, and southern Guam, mainly composed of volcanic rocks (Fig. 1; Appendix A). The two provinces are separated by the Pago-Adelup fault approximately in the middle of the island. Most of southern Guam was uplifted and subaerally exposed in the Miocene, while the northern part was still submerged and limestones were being deposited, with short intervals of emergence. During the Pleistocene, the entire island emerged (Tracey et al., 1964). Volcanic rocks form the foundations of the whole island (Tracey et al., 1964; Reagan and Meier, 1983).

The oldest rocks on the island are part of the Facpi Formation, and are Eocene in age (Regan and Meier, 1983). They consist of boninite pillow lavas and breccias deposited in a submarine environment (Appendix A). Basaltic and andesitic dikes of middle Eocene to early Oligocene age are found throughout the formation. The Facpi Formation is exposed in the southeast portion of the island.

On top of the Facpi Formation, the Oligocene Alutom Formation was also deposited in a submarine environment (Regan and Meier, 1983). The Alutom Formation is composed of volcanic breccias interbeded with tuffaceous sandstones, shales,

limestones, minor lava flows, and sills. The Alutom Formation dominates the northern part of southern Guam and crops out on Mt. Santa Rosa and Mataguac Hill in northern Guam.

The Miocene Umatac Formation overlies the Facpi and Alutom Formations (Regan and Meier, 1983). The lower part consists of the Geus River Member (Siegrist & Reagan, 2008), followed by pillow lavas of the Schroeder Member and pyroclastic rocks of the Bolanos Member which are the main components of the formation. The formation is capped with the lava flow of the Dandan Member. The Umatac Formation is dominant in the southern part of southern Guam. The Miocene Maemong Limestone Formation, which overlies the Umatac Formation (Siegrist & Reagan, 2008), is the oldest limestone on Guam to show significant karstification (Taboroši et al., 2004).

The southern part of the island has extensive remnants of Alifan Limestone with lagoonal and backreef facies. It is Miocene in age and covers the northern part of the western cuesta in southern Guam. A small outcrop of Alifan Limestone is also found on the flank of Mt. Santa Rosa in northern Guam.

The Bonya and Janum Limestones are detrital, foraminiferal, off-reef limestones of shallow and deep water environments, respectively. They are of Miocene to Pliocene age and are found in small outliers and exposures in northern and southern Guam.

The northern part of the island is mainly covered by younger limestones, from Miocene to Holocene age (Tracey et al., 1964; Siegrist and Reagan, 2008). The oldest is represented by the Miocene to Pliocene open and deep water foraminiferal Barrigada Limestone and its deep fore-reef but rather restricted equivalent, the Janum Limestone.

The Barrigada Limestone gradually grades upwards into the most widespread unit on the surface of northern Guam, the Mariana Limestone. The Pliocene to

Pleistocene Mariana Limestone was deposited in an atoll environment in different facies: reef-crest facies, fore-reef facies, detrital facies, and molluscan facies. In the central area of the island and in the south-west part is found the Marina Limestone Argillaceous Member which was deposited in the proximity of aerially-exposed volcanic rocks, and as a result contains argillaceous material.

The youngest limestones are the Late Pleistocene Tarague Limestone and the Holocene Merizo Limestone (Randall and Siegrist, 1996; Siegrist & Reagan, 2008). Prior to this research, the Tarague Limestone had been identified only in a small strip along Tarague embayment in the north-east part of the island (Randall and Siegrist, 1996). The Merizo Limestone, on the other hand, has been found in small patches along the rim of the entire island.

Net tectonic uplift is estimated to be more than 1000 m since the Eocene in the area now occupied by Guam (Tracey et al., 1964). The uplift was intermittent and was interrupted by periods of minor subsidence. Each period of uplift appears to have been accompanied by normal faulting.

Late Pleistocene and Holocene Limestones on Guam

The studied Tarague Limestone outcrop along Tarague Beach is a terrace from 3 to 8 m high (Randall and Siegrist, 1996). It is interpreted as a fossil coral reef with local detrital facies. On the backward or landward side of the terrace the limestone is sometimes veneered with reddish brown to light reddish, well-cemented paleosol with recrystallized coral clasts and land-snail shells. The outcrops are mainly barren, with a moss cover, but are covered in places with organic-rich soil. U/Th dating of two aragonitic fossil corals (Goniastrea retiformis) in the Tarague Limestone, found at

elevations of +4.8 m and +5.3 m showed ages of 126.4 and 131.9 ka, respectively (Randall and Siegrist, 1996). These dates place the time of deposition of the Tarague Limestone during the last interglacial sea-level highstand (MIS 5e) . The estimated duration of sea-level stand at the elevation of the near-present level or higher is from 128 ka to 116 ka (Muhs, 2002). This estimate takes into account coral records from locations in the Pacific (Hawaii and Western Australia). The maximum sea-level of the highstand is generally estimated to have been +6 m. Time and elevation of sea-level peaks can differ from place to place, however, as shown by observations and models of more recent sea-level changes (e.g. Fleming et al., 1998; Mitrovica and Milne, 2002; Peltier, 2002).

The Merizo Limestone is found in patches all around the rim of the island along the beach and seaward to just behind the reef margin (Tracey et al. 1964; Randall and Siegrist, 1996; Siegrist and Reagan, 2008). It is about 2 m thick and found at elevations from 2 to 4 m. Dating of corals by 14C showed mid-Holocene age (Randall and Siegrist, 1996). Analysis of Montastrea curta coral gave an age of 4,250 ±70 BP. Five Acropora sp. corals were dated from 3,380-3,310 ± 70 years BP, while rudstone infill gave a value of 2,750 ± 60 years BP. The position and age of Merizo limestone indicate it must have formed during the mid-Holocene highstand, with perhaps some tectonic overprint.

Porosity of limestones on Guam

The post-Miocene limestones of Guam have a high porosity due to their relatively young age and the lack of deep burial. The average porosity has been reported to be from 10 to 25%, with 13 % average porosity deduced from a gravity survey (Mink and Vacher, 1997). Reale et al. (2004) reported a 27.3% average porosity from more than one-hundred thin sections of Barrigada and Mariana Limestones, while Ayers and Clayshutle (1984)

reported a porosity ranging between 3 to 26% for the same limestones, based on thin sections and core samples. In primary carbonates, original porosity ranges from 40-70%, but reduces to 36-57% when primary aragonite recrystallizes to calcite (Mink and Vacher, 1997).

It may be noted, in contrast, that the Miocene Maemong and Bonya limestones found in southern Guam are diagenetically mature and compact limestones (Schlanger, 1964). They show an average porosity as low as 3 %. This has a major effect on surface dissolutional features (karren), which are distinct from those formed on diagenetically immature eogenetic limestones elsewhere on Guam (Taboroši et al., 2004).

Soils of Northern Guam

The soils of Northern Guam were classified in two major units, Guam series and Ritidian-Rock outcrop complex (Young, 1988). The Guam-series soils are very shallow, well drained, nearly level to moderately sloping soils on that occupy the top of the plateau. The Ritidian-Rock outcrop complex is partly Ritidian rock outcrop and partly Ritidian soil, which also comprises very shallow, well drained, gently sloping to extremely steep soils. It is found on plateaus, and escarpments.

The Ritidian soil is made of extremely cobbly clay loam and 35% rock outcrop. The soil occurs in small pockets that are intricately intermingled with the rock outcrop. Normally 60 to 90% of the surface is covered with gravel, cobbles, and stones. The soil is a dark reddish-brown extremely cobbly clay loam ~10 cm thick overlying porous coral limestone. The loam is composed of 7 to 27% clayey particles, 28 to 50% silt and <52% sand. The clay is gibbsitic and non-acid. Cobbly soil is defined by volume more than 60% of rounded or semi rounded rocks of 7.5 to 25 cm diameter. The depth of the soil

ranges from 5 to 25 cm, and it is mildly to moderately alkaline. Its permeability is moderately rapid, with very low water retention capacity.

Along the shoreline the Shioya loamy sand is also found. It formed in water-deposited coral sand. Typically, the surface layer is dark brown loamy sand about 25 cm thick while the underlying 150 cm and deeper is very pale brown sand.

Below are summarized some of the Ritidian soil properties (Table 3).

Table 3 The selected Ritidian soil properties. (After Young, 1988.)

Moist bulk density	0.7-0.9 g/cm^3	Salinity	<1280 ppm
Permeability	5-15 cm/h	Shrink and swell potential	Low
Available H_2O cap.	0.05-0.08 cm/cm	Org. matter	6-9 %
pH	6.6-7.8	Clay content	35-60 %

Previous geologic studies in the Ritidian Point area

Most of the known work in the Ritidian area was done by Randall and Baker (1989). Their research comprises the area from Achae Point to Pajon Point (see Figure 24). In this area no major faulting was observed (Tracey et al., 1964; Randall and Baker, 1989; Siegrist and Reagan, 2008). A minor fault (so-called Ritidian Fault) stretches N-S at the tip of the Ritidian Point, the eastern side being downthrown (Appendix A). Randall and Baker (1989) further argue that such a displacement could have only occurred between Ritidian Point and a distance of ~1.3 km SE from it.

Along the coast of this area Randall and Baker (1989) did many transects. Between Achae Point and Ritidian Point they describe the lowermost terrace as an

accumulation of unconsolidated storm deposits. Recent archaeological investigations (Carson, 2010) confirmed by 14C dating of the detritus from the tops to the bottoms of the pits indicate that these deposits are indeed late Holocene, 2,500 to 3,500 yr old. At the very bottom of the exploratory pits, reef-flat material was found, and a Heliopora coral gave a 14C age 4,100 ± 50 BP. Randall and Baker (1989) also mention a prominent notch along the cliff above the unconsolidated Holocene deposits, visible where the latter do not obscure it. At Achae Point in the West Ritidian area they also report two notches at elevations of 2.5 to 2.7 m and 3.5 to 3.7 m above mean low low water (MLLW) with the lower notch being veneered with Holocene Porites and Heliopora corals still retaining their original color. Further towards Ritidian Point they observed two Holocene bioclastic beach deposits, the highest being 2.5 m above MLLW. A Pleistocene dissolutional rampart is described to form the outer edge foundation of the active reef.

On the immediate east side of the Ritidian Point, Randall and Baker (1989) describe a 1-km-long outcrop of seaward-dipping imbricate beachrock with a maximum exposure less than a meter above MLLW. Further southeast along the coast they describe massive Holocene concave algal ridge deposits 3 to 3.5 m and 4 to 4.5 m above MLLW and with or without a backreef platform facies up to 50 m wide and veneered with storm deposits. The concave algal ridge facies indicate a high-energy environment. Notches cut into Holocene deposits as well as into older limestone just above the Holocene deposits were also observed.

According to Randall and Baker (1989) the active reef in the West Ritidian area laps on a Pleistocene terrace that has the more or less the same elevation as the modern sea level; and part of it is still visible on the seaward margin of the reef whereas on the East Ritidian side the Pleistocene terrace is 4 to 8 m below the modern sea level. Because

of the constant wave assault, the reef on the East Ritidian has developed a coral-algal ridge up to 1 m above the reef flat. Because the West Ritidian side is calmer, the algal ridge here is not as well developed.

In the Randall and Baker (1989) interpretation the sea level rise reached its maximum of 3 to 3.5 m above the present sea level (MLLW) about 5 ka BP, then regressed between 5 and 3 ka BP by 1.5 m, dropping by ~2 m (to the present sea level) between 3 to 2.8 ka BP.

On East Ritidian, midway between Pajon Point and Ritidian Point, Randall and Baker (1989) describe remarkably well preserved in situ corals. The abundance of rubble on this terrace is believed to be due to the trees that have their roots penetrating along fissures and other voids and thus breaking the rock (Randall and Baker, 1989). The effect is then strongly accelerated because of the toppling of the trees during frequent typhoons.

Sea-level change

Definitions of eustasy, relative sea-level change and water depth

Eustasy or eustatic sea level is global sea level and is a measure of the distance between the sea surface and a fixed datum, usually taken as the center of the Earth. Variations in eustasy are controlled by changes in ocean water or basin volume; thus

- *glacio-eustasy* is controlled by varying the volume of water locked up in glaciers, while
- *tectono-eustasy* is controlled by the change in the volume of the ocean basins.

Relative sea-level change on the other hand is the distance between the sea surface and the local datum, e.g. the top of the basement rocks of the basin. Relative sea-level change is therefore influenced by either eustasy or changes in elevations of the

continents or sea-floor. Thus, relative sea-level is a better term to use when considering sea-level change in a local area, as it accounts for both, local subsidence/uplift and eustatic changes in sea level (Coe et al., 2005). Local sea-level change can be used as an alternative term (Mylroie, 1990).

Sea-level depth is the distance between the sea bed, i.e. the top of the sediments or bedrock on the sea floor, and the sea surface or water level. Basin subsidence/uplift and eustatic sea level can be static while water depth can be reduced as sediments fill the basin.

Processes controlling sea-level change

Long term

There are two main types of processes that control sea-level change: those which require the *volume of seawater* to change and those which require *the volume of basins* containing seawater to change (Coe et al., 2005).

Changes in the volume of the seawater can be due to addition of water through volcanism or removal due to subduction of oceanic crust. These processes, however, cause minor fluctuations in the time scale of concern (Quaternary). The major processes controlling the change in volume of the seawater are (Coe et al., 2005):

- the formation and melting of ice-caps and glaciers (causing *glacio-eustatic* sea-level change): melting of the present-day Antarctic ice-cap and Greenland ice sheet would lead to sea level-rise of ~60-80 m,
- thermal expansion of water: an increase in the average global seawater temperature of 10°C would result in a sea-level rise of about 10 m.

Changes in the volume of basins containing seawater result from changes in basin size and shape. On short time-scale the following mechanisms may play a major role (Coe et al., 2005; Lambeck, 2004):

- Deformation of continental crust near major ice centers (so-called "*near field*") associated with the ice loading causing the crust to subside and isostatic rebound (uplift) following ice melting, together termed *glacioisostasy*.
- Subsidence of the oceanic crust due to melt water load delivered far from major ice centers (so called "*far field*"), and the subsequent rebound after the glaciers grow back again, together termed *hydroisostasy*.
- Sediment loading within a sedimentary basin: as sediment is deposited within a basin, the added weight causes the basin and its margins to subside.
- Fault movement along coastal regions may cause rapid uplift or subsidence.

Processes having a longer-time-scale influence on the volume of the ocean basins are ocean spreading and continental collision. Sediment supply from weathering continents to the oceans decreases the volume of the basins (Coe et al., 2005). Long term differences in sea level can also result from changes in density of the mantle and shifts in the heterogeneity of the Earth's crust, resulting in shifting anomalies of Earth's gravity field and departures from the gravitational norm at sea level. At hot spots, for example, the lateral gravitational field is stronger and the sea level higher (Coe et al., 2005).

Short term

Short term climate fluctuations of rapid shifts from cold to warm conditions termed Dasgaard-Oeschger cycles with a typical duration of ~1470 yr can cause a sea-level change of several tens of meters (Murray-Wallace, 2007). Other sea-level changes

that can have higher frequency are ocean and atmospheric circulation, both associated with long or short climate fluctuations (Milne and Shennan, 2007). Wind can cause the so called seiche, a sea-leve rise ("standing wave") in enclosed or partly enclosed bodies of water such as bays in the down-wind direction (Allaby and Allaby, 1999). Lunar tides are the shortest-term sea-level changes that can range up to several meters in some places.

Sea level change and Milanković cycles

According to Milanković theory the perturbations of the Earth's tilt and orbit control the amount of incoming solar radiation or insolation at different latitudes (Coe et al., 2005). The resulting temperature variations cause climate change and as a consequence formation and melting of ice caps, and the thermal expansion and contraction of the oceans. Both result in global sea-level fluctuations. The three parameters of Milanković cycles are:

- Eccentricity. It refers to the change of the shape of Earth's orbit from an ellipse to a circle (and back again). The resultant periodicities of this motion include the 95 ka, 123 ka and the 413 ka aspects at the present time.

- Obliquity. It describes the angle of tilt of the Earth's axis with respect to the plane in which it orbits the sun. The tilt angle changes from 21.8 to 24.4°. This change occurs every 41 ka at the present time.

- Wobble. It refers to the change in precession that is made of two components: that related to its axis of rotation and that relating to the elliptical orbit of the Earth. The main resultant periodicities are 19 ka and 23 ka at present time giving a mean cycle of 21 ka.

The interaction of the above cycles gives results in other cycles with different periods.

Sea-level change during the Quaternary

General

The dominant mechanism responsible for the sea-level change during the Quaternary has been the accumulation and melting of massive ice sheets in response to Milanković cycles of insolation changes (Murray-Wallace, 2007). From late Pliocene through early Pleistocene time (2.47 Ma B.P. to about 0.735 Ma B.P.) the dominant cycle controlling the climate and sea-level respectively was the 41 ka obliquity cycle. Since then until the present day the orbital eccentricity cycle has been dominating with glacial cycles occurring about every 100 ka (Ruddiman et al., 1986). Seven glacial cycles occurred since this shift in frequency. Of all the interglacial stages, only the interglacial stages MIS 5e, MIS 9 and possibly MIS 11 have been warmer with the sea level higher than the present (Murray-Wallace, 2007). Sea-level dropped as much as about 135 m below the present sea-level during glacial cycles. There have been local variations in the sea level due to glacio-hydro-isostatic feedback effects on continental shelves of contrasting widths and, in the near field of former ice sheets, progressive mantle adjustments in response to fluctuating ice volumes and differences in mantle properties (Murray-Wallace, 2007. These effects can be further complicated by the changes in volume of sea water due to its temperature changes.

The last glacial cycle in the Pacific

The last interglacial, MIS 5e

The last glacial cycle is the period since the last interglacial up to the present one. The last interglacial, also termed Marine Isotope Stage 5e (MIS 5e), peaked about 125 ka ago though evidence based on different proxies show different peak times and spans of the last interglacial. Dated reef terraces from Hawaii, Western Australia and Barbados suggest that the sea-level was above the present one for about 12,000 years between 128 to 116 yr B.P. (Muhs, 2002). Fossil corals from the Bahamas suggest 131 to 119 ka (Chen et al., 1991). This estimation matches well with the orbitally tuned oxygen isotope record from deep sea cores of Martinson et al. (1987). The oxygen isotope record from the ice core from Greenland, on the other hand, shows that the δ18O values higher than the present persisted for about 19,000 years between 133 ka and 114 ka B.P (Dansgaard et al., 1993).

The ice core data from Greenland (GRIP members, 1993; Dansgaard et al., 1993) as well as orbitally tuned oxygen isotope record from deep sea cores (Martinson, 1987) show that there were at least three warm periods separated markedly by two cold periods during the MIS 5e substage lasting 2,000, 1,000 and 3000 years (GRIP members, 1993). The temperature differences between these cold and warm periods would span about 7°C (GRIP members, 1993). Evidence of oscillations within the MIS 5e was also found in the Vostok ice core. However, only two warm periods could be identified (Jozuel, 1987).

The derived evidence from various sea-level indicators, mainly reef terraces, shows that the sea-level across the Pacific during this period was ~6 m higher than present though there are exceptions that suggest that the sea-level was only few meters above present (Nunn, 1999). More than one peak (i.e. warm period/sea level high stand)

can sometimes be resolved from these indicators. The MIS 5e terrace record on Huon Peninsula, Papua New Guinea, for example, can be interpreted as a result of a double high-stand (Chappell, 1974). Though other similar evidence in the Pacific can be found, some sea-level records show only one MIS 5e peak (Nunn, 1999). Evidence of a double MIS 5e sea-level highstand has been reported also from other parts of the world (e.g. in the Bahamas, Carew and Mylroie, 1999). Lambeck and Nakada, (1993) pointed out that the variations of sea-levels with time and location during the MIS 5e highstand can be attributed to isostatic response due to the change of ice-water.

Last glacial and its sea-level stands

After the MIS 5e warm period, the temperature on the planet dropped significantly. However, the cooling was not uniform, and alternating warm-cool periods occurred. The first cool period was MIS 5d with sea level dropping ~45 m below the modern sea level (Waelbroeck et al., 2002) (Figure 4) followed by a warm period MIS 5c. The latter would have two peaks at 103.3 and 96.2 ka B.P. as shown by the evidence of orbitally tuned oxygen isotope data (Martinson, 1987). During MIS 5c, the sea level rose up to between –30 to –13 m below the present, as estimated from oxygen isotope record from equatorial Pacific (Waelbroeck et al., 2002) or coral terraces on Huon Peninsula, Papua New Guinea, equatorial Pacific (Lambeck et al. 2002) (Figure 5). A cold period (MIS 5b) followed, and the sea level dropped to ~50 m below modern sea level ~90 ka B.P. (Waelbroeck et al., 2002)

The following warm period (MIS 5a) caused the sea level to rise to similar elevations, some –30 to –17 m below present, sea level peaking between 82 and 90 ka B.P. (Waelbroeck et al., 2002, Lambeck et al. 2002), though an earlier timing is

suggested by Martinson (1987). The record from Huon Peninsula shows that there might have been two peaks during the MIS 5a (Lambeck, 2002).

The last warm period during the glacial, stage MIS 3, was the longest, with five fluctuations (Lambeck et al. 2002). The oxygen isotope record of Waelboroeck and others (2002), and Shackelton (2000) match very well with the coral record on Huon Peninsula (Lambeck et al. 2002) and the island of Malakula (Cabioch et al., 2001) with the duration of the stage being from ~62 ka to ~32 ka B.P. and sea level ranging between ~75 to ~40 m below modern sea level.

The last glacial maximum reached occurred from ~30 ka B.P. to 19 ka with the sea level about 120 m (Lambeck et al., 2002, Waelbroeck et al., 2002) to 125 m (Peltier, 2002) below present sea level.

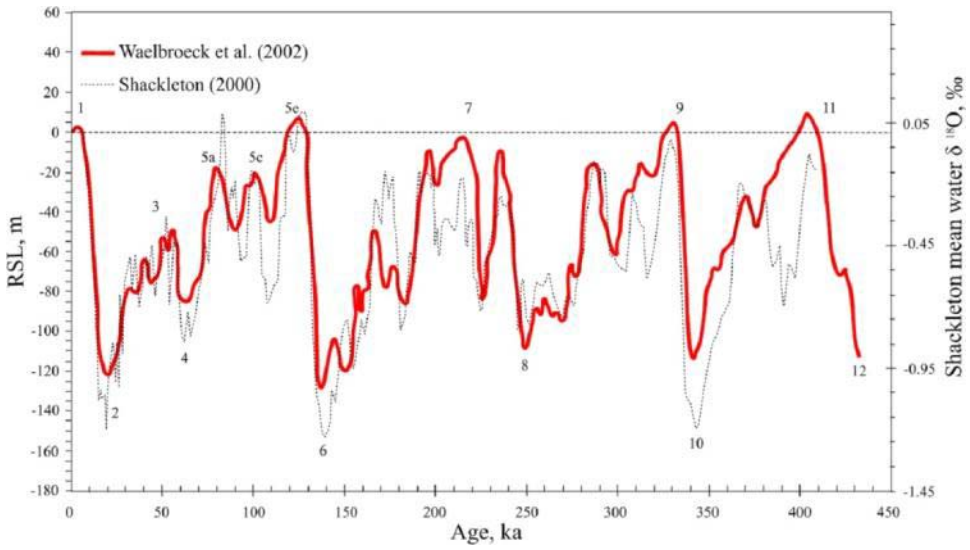

Figure 4 Relative sea-level curves. The Waelbroeck et al. (2002) curve is a composite curve based on benthic foraminifera isotopic record retrieved at one North Atlantic and one Equatorial Pacific site. The Shackelton (2000) curve was obtained by using the oxygen isotope record from atmospheric oxygen trapped in Antarctic ice at Vostok. (From Lascu, 2005.)

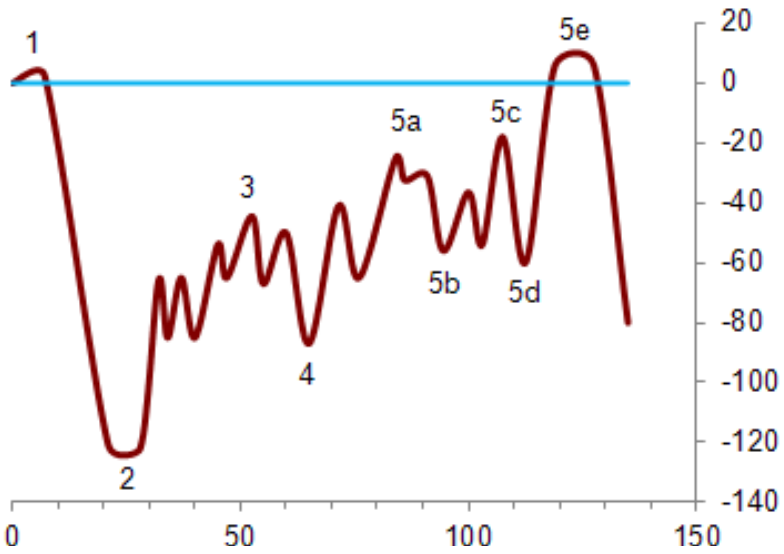

Figure 5 Sea level curve for the last interglacial cycle derived from the study of reef terraces on Huon Peninsula, Papua New Guinea. The red line is the actual sea-level curve while the blue line represents the modern sea level. (After Lambeck, 2002.

Causes of regional differences in duration and differences of the level of sea-level stands as a response to the glacial cycles

General

As stated above the main control on sea-level change in the Quaternary is the change in ocean volume due to ice sheet melting and growing. However, significant differences in the paleo sea-level record as well as in the modern sea level around the planet have been observed. The main reasons for the regional sea-level differences can be attributed to two factors (Lambeck, 2004):

- change in ice-water loading that modifies the planet's surface including the ocean floor and thus changing the sea surface relative to the land,
- change in the gravitational potential of the earth-ocean-ice system due to the redistribution of the ice-water mass and earth deformation.

Change in ice-water loading

During the glacial periods, ice accumulates on continents at high latitudes. Mantle material is displaced outward under the load pressure and broad bulges develop around the loaded area. When the ice sheets melt away, these forebulges subside and after the initial rapid sea-level rise due to the added melt water, the relative sea level keeps rising as the uplifted land bulge subsides (Lambeck and Chappell, 2001).

Away from the ice sheets, the melt water load on the oceans floor causes floor and margin subsidence. The further away from the ice sheets, the more this effect is pronounced. Once the melting has ceased, the relative sea-level keeps falling as the ocean floor subsides.

The deformation of the planet's surface depends on the distribution of the ice sheets and configuration of the oceans. Further it greatly depends on the differences in mantle viscosity.

Change in gravitational potential

An important consequence of the redistribution of the mass within and on the planet and its deformation is the change in gravity field that affects the sea surface which in turn further complicates the local sea-level change (Lambeck, 2004).

A more direct effect is the loss of the gravitational pull of ice caps after their melting causing a lowering of ocean surface proximal to the ice and height increase or the ocean surface in the far field (Milne and Shennan, 2007).

In summary

As evident from above, the factors that influence the sea-level change depend on the distance from the ice sheets, configuration of planet's surface and inhomogeneity of

the mantle. The amplitudes as well as timing of the sea-level stands can thus vary considerably from site to site even if they are located close to each other.

The combination of the deformation-gravitational effects is termed as glacio-hydro-isostatic effect (Lambeck and Chappell, 2001).

Sea level fluctuations in the Holocene in the Pacific (far field)

General

During the last glacial maximum (ca. 21,000 calendar years ago) the sea level was about 120 m below present sea-level (Peltier, 2002). During deglaciation the sea level rose. In the Pacific it reached its maximum in mid-Holocene (~4,000 years ago), and evidence shows that the sea-level was up to ~3 m higher than at present day (e.g. Tracey, 1964; Pirazzoli and Montaggioni, 1984; Bell and Siegrist, 1991; Kayanne et al., 1993; Grossman, 1998; Nunn, 1998; Dickinson, 1999; Dickinson, 2001; Randall and Siegrist 1996; Dickinson, 2004; Zong, 2007). The sea-level drawdown after the peak level at ~4 ka is linked to two mechanisms of glacial isostatic adjustment (GIA) after the ice-sheets melted (Mitrovica and Peltier, 1991; Mitrovica and Milne, 2002). The first is the equatorial ocean syphoning by which the water migrated away from far-field equatorial ocean basins in order to fill the space vacated by collapsing forebulges at the periphery of previously glaciated regions. The second one is ocean load-induced levering of continental margins in which migration of water into offshore regions of subsidence produces global scale drop in the sea surface that induces sea-level fall at sites well away from these margins. The sea-level drawdown and its timing, however, were uneven and differed across the planet, regardless even of its proximity to the continents. In the Atlantic Ocean, for instance, no mid-Holocene highstand has been observed. The

differences are attributed to variations in properties such as mantle viscosity and crust thickness with the viscosity of the lower mantle being by far the most dominant (Mitrovica and Milne, 2002). Differences have been observed also on very local scale (Fleming, 1998). These were attributed to ocean floor and landmass geometry.

Holocene sea-level on Guam

On Guam as well as on Rota the sea level was higher than the present during the mid-Holocene for about 2,500 years, but estimates of the inclusive dates vary: between 5,500 BP and 2,800 BP (Bell and Siegrist, 1991); between 6,000 to 3,200 BP (Kayanne et al.; 1993); between 4800 and 3,100 (Randall and Siegrist, 1996); and between 4750 BP and 2,250 BP (Dickinson, 2000). Kayanne et al. (1993) and Randall and Siegrist (1996) attribute the sea-level drawdown to tectonic uplift. Dickinson (2000), however, links mid-Holocene higher sea level to the *hydro-isostatic* emergence and estimates it to be approximately 1.8 (±0.2) m for the Mariana Islands. His estimate is based on the 1.2 to 2.0 m emergence of the mid-Holocene reef flats and associated paleo sea-level notches on Saipan, Tinain and southern Guam, and the argument that there could have been no systematic uplift that would have uplifted all the islands for a more or less same amount. Observations of the emergent mid-Holocene reef flats on Rota and Guam, nevertheless, show elevations above the estimated mid-Holocene sea-level. Dickinson suggests that these areas were subject to a post-mid-Holocene *tectonic* uplift due to a subduction of a seamount chain right beneath northern Guam and Rota. For northern Guam the estimated tectonic uplift is about +0.8 m (Dickinson, 2000). For the outcrops found in Tarague embayment, however, an uplift of at least +1.9 m would be needed to explain the high elevation of the observed mid-Holocene reef outcrops. (Randall and Siegrist, 1996).

On Yap and Palau (Dickinson, 2000; Kayanne et al., 2002), however, there is no evidence of a mid-Holocene high stand. It is suggested that late Holocene subsidence had a similar rate as the sea-level drawdown (Dickinson, 2000). Given the evidence of recent tectonic activity on Guam, care should be taken when considering the actual height of the sea-level during the mid-Holocene highstand.

Cave formation and Carbonate Island Karst Model (CIKM)

General

The Carbonate Island Karst Model (CIKM) (Jenson et al., 2006) is useful to describe islands with small catchment-to-perimeter ratio composed of young, eogenetic carbonate rocks that have only undergone meteoric diagenesis (Mylroie and Mylroie, 2007). Such rocks are highly porous and have high hydraulic conductivity, promoting diffuse flow. The resulting specific hydrogeology is the reason for a different model of cave formation from that prevailing on the continents, where carbonate rocks have undergone deep burial (mesogenesis) and were later exposed to the surface (telogenetic rocks), as discussed in Vacher and Mylroie (2002).

The fresh water lens and the cave formation

When meteoric water percolates downwards through carbonate rock and reaches seawater within the rock, it accumulates creating a floating body of fresh water in the shape of a lens. This is because freshwater is less dense than seawater. The lens water may be saturated with CaCO3 as it can lose all its dissolutional potential while percolating through the carbonate rock and dissolving it. At the fresh-water lens and seawater interface a mixing zone is created. Even if both waters are saturated with respect to CaCO3, they create an undersaturated water mixture able to dissolve CaCO3 (Wigley

and Plummer, 1976; Dreybrodt, 2000) (Figure 6). The same mixing effect occurs where water percolating through the rock from the surface mixes with the freshwater in the lens. At the margins of the lens these two mixing zones converge, concentrating the dissolutional processes at the lens margin on the flank of the island. Further, the lens water flows towards the island margin and as the vertical cross-sectional area decreases towards the lens margin, the flow velocities increase. This causes faster mixing and reactant exchange at the margin (Mylroie and Mylroie, 2007 and references therein). Last, the top of the lens and the lens boundary with seawater are density interfaces that can trap organic material. Decomposition of organics creates CO2 and possible excess of organics can cause the conditions to turn anoxic; thus promoting bacterial production of H2S (Bottrell et al, 1993). Both of the dissolved gasses promote dissolution of CaCO3 at the density boundaries where these phenomena occur. Because of all of the above, dissolutional potential is the greatest at the lens margin near the flank of the enclosing landmass and therefore the biggest caves are found there (Figure 7). These so-called *flank margin caves* have a distinct morphology: cave chambers are wider than they are high, with curvilinear and cuspate margins, numerous ramifying and dead-end passages near the back of the cave with many cross-links and connections; remnant bedrock pillars are common. They are completely surrounded by bedrock and have no exits/entrances as they form within the diffuse flow system. Therefore they are enterable only when intersected by later vertical or lateral erosion.

Caves are also found where descending surface water mixes with the lens water (Figure 7). These caves are usually smaller and flatter than flank margin caves and are called water-table caves. Where breached and exposed at the surface they are also called banana holes. Recently, banana holes and water table caves have been reinterpreted as

developing as transitory flank margin caves when prograding sands move the shoreline seaward (Mylroie and Mylroie, 2009). Same as the flank margin caves, water table caves are enterable only when breached by erosion.

It should be noted, however, that recent research shows that flank margin caves can form in other environments than just in eogenetic carbonates of small islands. Flank margin caves have been also identified in telogenetic limestones of the coasts of New Zealand (Mylroie et al., 2008) and talus limestone breccia of Cres island (Croatia) (Otoničar et al., 2010). The caves in telogenetic rocks have a different cave morphology that is structure-controlled (e.g. by joints or bedding planes) while the caves in breccia have a similar morphologic characteristics as caves in eogenetic rocks due to similar three-dimensional homogeneous porosity.

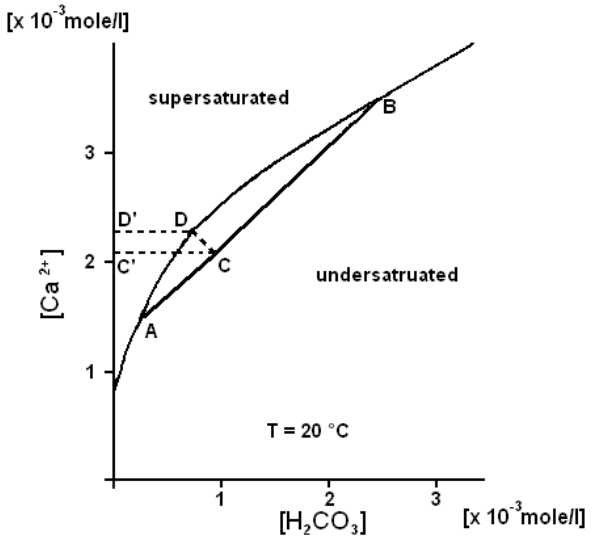

Figure 6 The equilibrium curve divides the $H_2CO_3 - Ca^{2+}$ in two parts. Above the curve, solutions are supersaturated. Below the curve, solutions are undersaturated. Mixing of two saturated solutions A and B leads to an undersaturated solution, i.e. C. The additional amount of Ca^{2+} that can be dissolved after mixing is given by C'D' (after Dreybrodt, 2000).

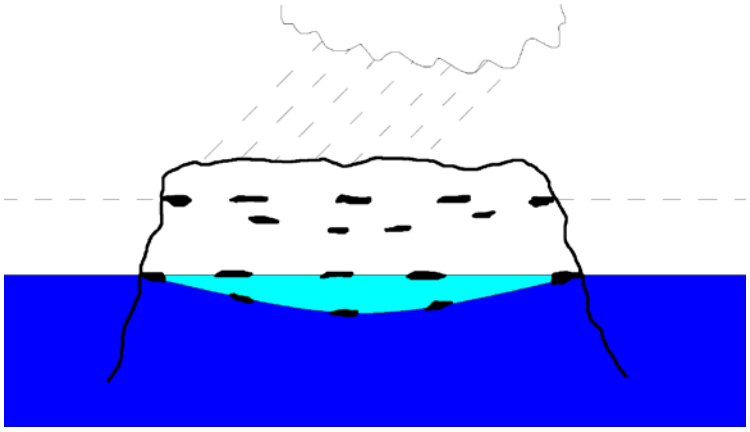

Figure 7 The fresh water lens floating on the sea water and the biggest caves forming in the mixing zone at the margin of the lens near the flank of the enclosing landmass. The caves may also form in the mixing zone at water table. Note the set of caves in the diagram left by a former sea level.

Lithology and glacioeustatic role in the CIKM

Flank margin caves of CIKM fall into the category of syngenetic caves (Mylroie and Mylroie, 2009). Syngenetic caves by definition are caves that formed by dissolution in carbonate rocks that have not yet reached diagenetic maturity. The category is further subdivided into:

- syndepositional caves formed while the carbonate sedimentary unit containing the caves was still being deposited and
- eogenetic caves formed in carbonate rocks after deposition is complete but before diagenetic maturity is achieved by deep burial.

Besides the particular lithology and cave formation, CIKM also takes into account other factors when considering small carbonate islands (Jenson et al. 2006, Mylroie and Mylroie, 2007). Glacioeustasy, for example, has moved the sea level and thus the fresh water lens position up and down over more than 100 m. Each sea-level stand has therefore left a set of caves reflecting the freshwater and seawater mixing position. Sea-level highstands of known duration can give an estimation of the rate of cave formation.

Flank margin caves of tens of thousands of cubic meters of void space in the Bahamas, for example, developed in a time span of 12,000 years (MIS 5e), proving the freshwater lens margin a fast-acting speleogenetic environment (Mylroie and Mylroie, 2009). Local tectonic movement, however, may cause overprinting of dissolutional and diagenetic features developed during different glacioeustatic events.

Based on non-carbonate basement/sea level relationships, carbonate islands can be divided into four categories (Mylroie and Mylroie, 2007) (Figure 8):

1) Simple Carbonate Island (only carbonate rocks are present, meteoric catchment is autogenic).

2) Carbonate-Cover Island (only carbonate rocks are exposed, non-carbonate rocks partition and influence the freshwater lens, catchment is autogenic).

3) Composite Island (carbonate and non-carbonate rocks are exposed allowing autogenic and allogenic catchment, the freshwater lens is partitioned and stream caves develop).

4) Complex Island (carbonate and non-carbonate rocks are complexly interrelated by depositional relationships and/or faulting.

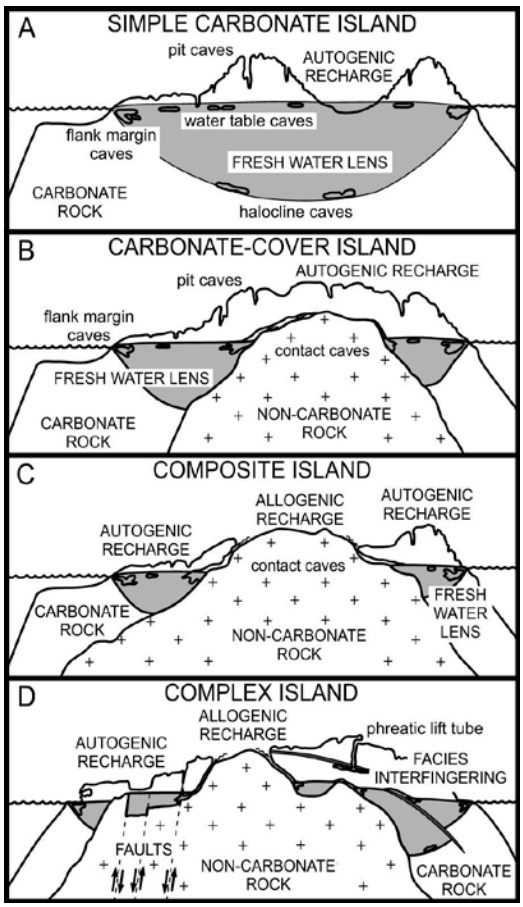

Figure 8 CIKM categories (From Jenson et al. 2006, with permission).

CIKM on Guam

Northern Guam is predominantly composed of carbonate rocks. Locally it exhibits each of the first three CIKM categories (Jenson et al., 2006). As noted by Jenson et al. (2006), approximately 41% of the volcanic basement under the surface plateau has stood below sea level since the carbonate rocks above it were deposited. This portion of the islands fits the simple carbonate island model. Overall, about 58% of Northern Guam has had, however, a volcanic basement lying above sea level during sea-level low stands and can thus fit the carbonate cover island category. One percent of the carbonate plateau surface has volcanic outcrops protruding through the limestone, and therefore falls into the composite island model.

Flank margin caves reflecting ancient freshwater lens position are found around the perimeter of the island where cliff retreat has intersected them. Not many water table caves can be found due to thick carbonate cover above most of the water table levels, which prevents collapse to expose the voids. Or, based on the new banana hole model, Guam did not have a prograding sand environment like in the Bahamas. Discharge from the plateau is via costal springs and coastal seeps, the largest discharge features being associated with fractures and caves. Caves in carbonates formed along streams flowing from non-carbonate rock onto carbonate rocks are found around Mt. Santa Rosa and Mataguac Hill in northern Guam, and in many locations in volcanically-dominated southern Guam (Jenson et al., 2006).

Sea-level indicators

Sea-Level Notches

General

A sea-level notch (marine notch, paleoshoreline notch, bioerosional notch, nip) is an indentation or undercutting a few centimeters to several meters deep left by sea erosion in coastal rocks (Pirazzoli, 2007) (Figure 9; 10). There are three mechanisms reported that can form sea-level notches: mechanical action, dissolution and bioerosion (Pirazzoli, 1986).

Mechanical action involves abrasion by wave-borne sand and gravel. Notches cut in rock have a noticeably rounded and polished appearance which makes them easy to recognize. Pressure induced into pores by crystallizing salt in the midlittoral and supralittoral zone may also play a role in erosion of the coastal rock.

The role of dissolution is rarely debated and its actual role unclear. Alkaline sea-water is supersaturated with respect to $CaCO_3$ and thus at least in principle unable to dissolve limestone or other rock cemented with $CaCO_3$. However, several mechanisms were proposed that could turn sea water into an undersaturated state. The perhaps most probable conditions that could make sea-water an efficient solvent are found where shores are interfringed with mangroves where abundance of organic material and limited water mixing can lead to acidification of the water (Pirazzoli, 1986). A strong correlation between sea-level notches and coastal springs has been reported from Greece (Higgins, 1980), which would allow mixing dissolution to occur.

Bioerosion has been recognized to be by far the most important mechanism in sea-level notch formation in carbonates. Endolithic organisms, primarily algae, penetrate into limestone in littoral zones either through pores or by chemically boring holes. Surface feeders such as gastropods, chitons, sea urchins and parrot fish, graze upon epi- and endolithic organisms simultaneously abrading the surface with their hard teeth or equivalent (Pirazzoli, 1986; Spencer, 1988; Radtke, 1996) (Figure 11). Many genuses such as *Porolithon*, *Clinoa*, *Lithophaga*, *Cyanophyta*, *Clorophyta* etc. are borers that secrete organic acids in order to dissolve or soften the rock.

The research of sea-level notches on Guam showed a correspondence between the density of limpet (*Patella chamorrorum*) population and notch depth in the intertidal zone (Emery, 1962). Also, the pH measurement of the soles of the limpets showed values between 5.7 and 7.2 indicating the ability of the limpets to dissolve limestone rock. Emery (1962) thus suggests that the limpets could play a role in notch formation though a few notches without limpets were also found. Besides the limpets, chitons (e.g.

Achantopleura gemmata) and boring barnacles (*Lithothrya* sp.) are thought to be of a key importance in notch formation on Guam (Taboroši, 2002).

Figure 9 Exposed sea-level notch at low tide. In the background the cora-algal ridge at the margin of the reef flat. Ritidian Point, Guam.

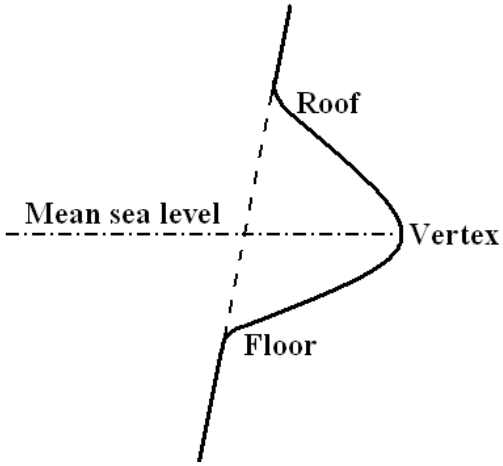

Figure 10 Sea-level notch profile. (Modified after Pirazzoli, 1986.)

Figure 11 Surface of the inner part of a sea-level notch. Note the borers (black dots), algae (pink color) and the grazers (gastropods). Ritidian Point, Guam.

As sea-level indicator, midlittoral notches are by far the most important. The precision of a notch as a sea-level indicator is the highest (Pirazzoli, 1986) where:

- the site is sheltered,
- the tidal range is low and
- the cliff face is vertical.

The vertex (Figure 10) of the notch curve is usually assumed to correspond to the mean tide level; the lower part of the "floor" of the notch extends to approximately the lowest tide level while the edge of the "roof" of the notch is located near the highest tide level (Pirazzoli, 1986; Radtke, 1996). At exposed sites, e.g. at the tip of the headlands, continuous wave action may splash water into the roof of the notch shifting the top of the notch and the vertex above the normal height. It has been recognized that the vertex of the notch can correspond also to the mean neap tide (Pirazzoli, 2007) or mean high water level as it was also observed by Dickinson (2000; 2001) in the Marianas and elsewhere in the Pacific.

Limestone coasts exposed to persistent trade winds and to strong surf and spray develop a surf bench due to organic incrustations (Pirazzoli, 1986). The corresponding surf notch can therefore develop 2 m higher than normally (as a tidal notch). A surf notch is, however, easy to recognize by the presence of an adjacent surf bench.

Erosion rates

The maximum erosion rates are usually less than 1 mm to 1.5 mm/yr. In porous Quaternary coral limestone the rates from two sites (Barbados and Aldabra) were reported to be between 0.2 to 2 mm/yr (Pirazzoli, 1986). Other sources (e.g., Spencer, 1988) report similar values for relatively unconsolidated tropical limestones exceeding 1 mm/yr. A maximum value is found in the littoral zone, and evidently increases mainly with exposure. Where surf and spray are the major factors, erosion rates exceed 1.0 to 1.5. mm/yr, and the location of maximum rate shifts from the midlittoral to supratidal zone.

Influence of the slope

A major influence on sea level notch development is the cliff slope (Pirazzoli, 1986). The most favorable conditions for notch formation occur where the cliff is vertical (90°). With a given erosion rate of 1 mm/yr, a symmetrically undercut 5-cm deep incision can develop in 50 years, while on a 27° slope 1500 years are needed for the same value. On non-vertical slopes, asymetrical notches develop (Figure 12). With the cliff slope lower than 90° and with the same erosion rate, the time necessary to develop a notch depends also on the tidal range; the smaller the tidal range, the shorter is the time needed to form a notch.

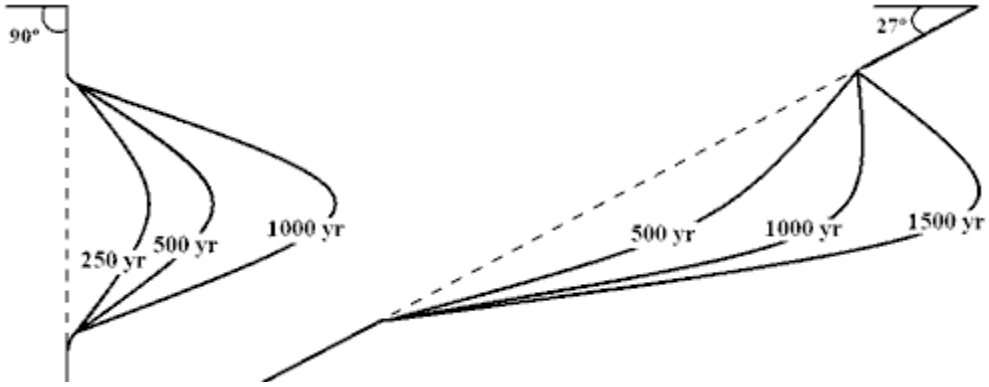

Figure 12 Symmetry and rates of notch formation dependency on the slope angle. Tidal range is assumed to be 1 m, erosion rate at mean sea leve1 mm/yr. The depth of the notch on the vertical slope is 1 m. (After Pirazzoli, 1986).

Modification of the morphology due to sea-level fluctuations

The morphology of the notch is also influenced by the relative sea-level change (Pirazzoli, 1986). If the sea level is stable, a V-shaped sea-level notch will form with the roof and floor of the notch corresponding to the tidal range. Other shapes that develop when sea-level fluctuations occur are summarized in Figure 13.

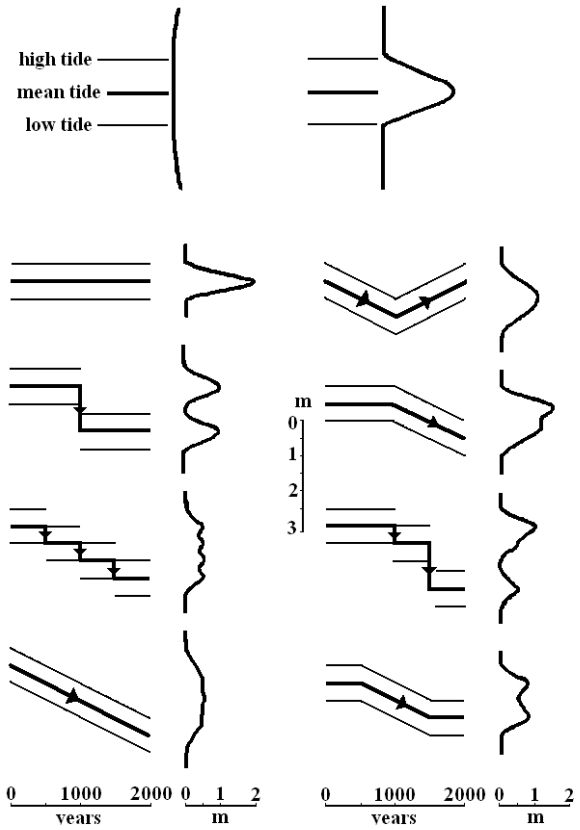

Figure 13 Sea-level notch profiles as a result of different relative sea level fluctuations. The maximum erosion rate is assumed to be 1 mm/yr. (Modified from Pirazzoli, 1986.)

Dating

While sea-level notches are one of the most precise sea-level proxies, they have a distinct downside: they are very difficult to date. In the most fortuitous cases, datable calcareous parts of organisms in their living position are found within the notches. Indirect dating can be made by geomorphic correlation with coeval paleoreef flats with datable coral (Dickinson, 2001) or beach deposits (Pirazzoli, 1986). Dating of beachrock is, however, complicated and mostly unreliable.

Coral Reef Terraces

The reef flat is defined by the upward limit of coral growth where relative sea level is rising or, where sea level is falling, represents a wavecut platform carved at the downward limit of intertidal erosion (Dickinson, 2001). Some reef flats display coral heads in growth position, whereas others are mantled by cemented coral rubble distributed across the reef flat by storm waves. In the latter case, phreatic subtidal cements vs. vadose intertidal cements help discriminate the paleo-low-tide level by petrographic studies. Algae may incrust the corals during a sea-level stand when reef growth has reached equilibrium with the sea level. They can grow upward well into the intertidal zone. Paleo low tide is interpreted to be the contact between the coralline and overlying algal limestone (Bell and Siegrist, 1991).

Only where the paleoreef flat is clearcut and well preserved as an essential horizontal bench, can an emergent terrace be interpreted with confidence as a paleoshoreline indicator (Dickinson, 2001). Microatolls also represent emergent reef flat conditions.

As opposed to the sea-level notches, coral reef terraces are easy to date since they usually (if not too old and recrystallized) have plenty of datable corals in their growth position. Carbon-14 is useful for younger corals, U/Th for older ones.

The record of global sea-level change can be interpreted from the study of ancient terraces that have been uplifted (Pirazzoli, 1993). When interpreting the following assumptions are usually made: (1) the eustatic sea level position corresponding to at least one raised terrace is known, and (2) that the uplift rate has remained constant in each section. Several research efforts have reconstructed the sea-level curve by studying the uplifted reef terraces on Huon Peninsula of Papua New Guinea (e.g. Chappell, 1974).

Beachrock

General

Beachrock is found at low latitudes approximately 30° north and south of the equator and extending just outside the range of modern coral reefs (Hopley, 1986). It appears there is no connection with rainfall since beachrock is found in Arabia with fewer than 2.5 cm of rain per year to the islands of the Pacific and the Caribbean with 150 cm of annual rainfall (Scoffin and Stodart, 1978). The internal structure of beachrock is typical of beach deposits and shows laminations of 1 cm to about 10 cm in thickness (Hopley, 1986; Scoffin and Stodart, 1978). It is composed of fragments of skeletal organisms such as corals, *Halimeda*, calcareous red algae, benthic foraminifera, mollusks, and where present, ooids (Scoffin and Stodart, 1978). It forms in the intertidal zone and is cemented with CaCO3 as calcite, aragonite or Mg-calcite, depending on the cementation environment. Aragonite is associated with precipitation from sea water. The dominating mechanism is believed to be degeassing of CO2 and evaporation of water when the water is perched and trapped in pores during low tides and heated by the sun.

World War II debris found in beachrock proved that beachrock can form in seven years (Scoffin and Stodart, 1978) while exposures on Magnetic Island (Australia) formed as quickly as in six months (Hopley, 1986). Therefore, given sufficient stability of the beach deposits, tidal levels achieved only few times a year may allow cementation to take place above mean high water level. A conservative approach could thus be to correlate the emerged outcrops with the highest astronomical tidal level (HAT), i.e. the highest water level that a given formula can ever predict. But cementation may also occur from a perched water table caused by water being thrown up over the sediment by high storm water. Cement formed from meteoric water percolating through the deposit is calcitic and

therefore easy to identify. The lowest level of cementation corresponding to the lowest tidal level of a given sea-level stand cannot be identified. Thus only the uppermost level of the beachrock can be used as a past sea level indicator.

Dating

Dating of beachrock represents a major problem. Though unexpected, neighboring pieces of loose shingle on beaches were found to be as much as 3000 radiocarbon years apart in age (Scoffin and Stodart, 1978). The cement, on the other hand, can have exchange of carbonate with the water percolating through the rock and therefore a continuous rejuvenation of the apparent age (Hopley, 1986). Unless a skeleton of an organism in growing position is found, an extensive dating program should be followed on both constituent biogenic materials (skeletons) and cementing matrix.

Flank Margin Caves

General

Flank margin caves can be a good sea-level indicator since they form at sea level. For a more extensive description of their formation see pages 34 through 39.

Flank Margin Caves in relation with sea-level notches

When breached, flank margin caves can resemble a sea-level notch and have often been misinterpreted as such (Mylroie and Carew, 1991). Sea-level notches as well as flank margin caves form at a sea level if a sea-level stand was long enough so that significant dissolution and bioreosion, respectively, can occur. Flank margin caves form somewhat behind the sea-level notch, and with lateral erosion they can get breached and as such might actually resemble a sea-level notch (Figure 14; 15) (Waterstrat et al.,

2010). A modern relation between the sea-level notches and flank margin caves can be well observed in Talafofo Bay and Tanguisson (Figures 16; 17) where lateral erosion exposed the flank margin caves that formed just behind the notch.

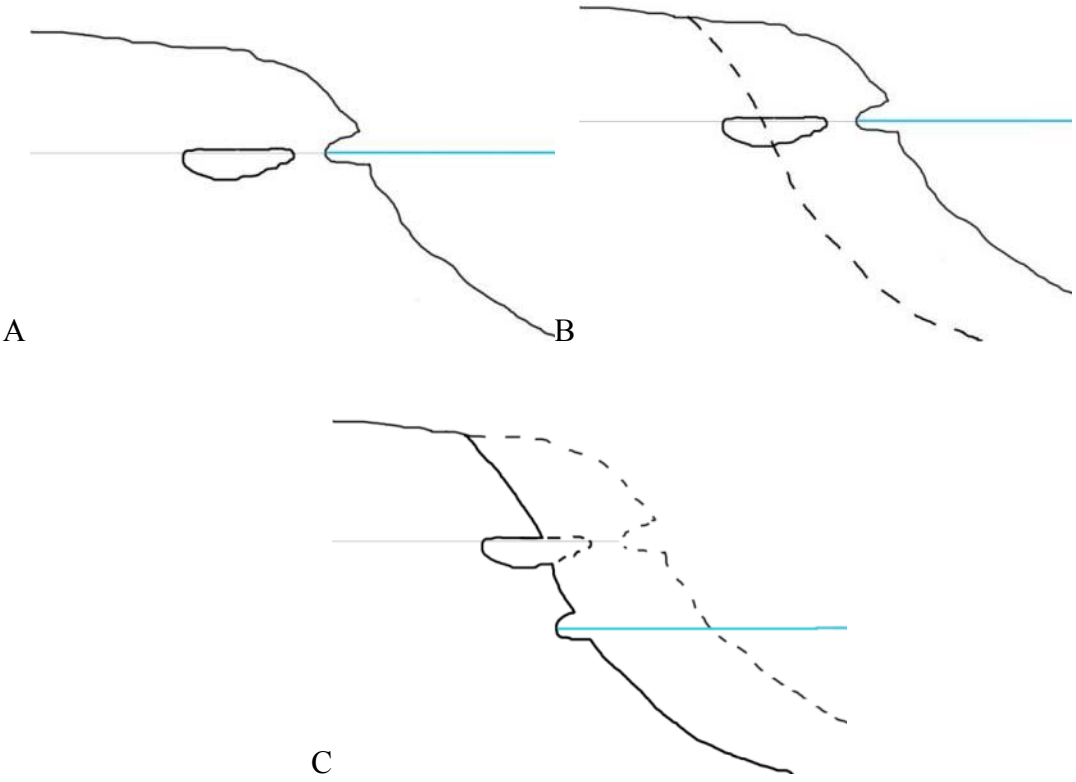

Figure 14 Formation of the sea-level notch and flank margin cave (A), erosion of the sea-level notch and breaching of the flank-margin cave by lateral erosion and formation (B), and formation of a new sea-level notch after the relative sea-level change (C).

Figure 15 A set of breached flank margin caves (above) resembling a sea-level notch (below). Gun Beach, Guam.

Figure 16 Modern and paleo sea-level notch (to the right). Lateral erosion exposed the flank margin caves just behind the notches. Talafofo Bay, Guam.

Figure 17 Modern sea-level notch and caves just behind it in the mid-Holocene Merizo Limestone at low tide. Tanguissan, Guam.

Though similar, the two have some characteristic geomorpic features listed below (Mylroie and Carew, 1991; Reece et al., 2006).

- Breached flank margin cave:
    - Undulating floor or roof.
    - Rounds off or necks down laterally and re-opens into an adjacent reentrant (beads-on-a-string morphology).
    - Smooth, dissolutional walls (if not subsequently altered).

- Sea-level notch:
    - Flat floor and roof
    - Uniform morphology and laterally extensive.
    - Evidence of grazing and boring.

The origin of the notch can be successfully resolved also by the presence of secondary calcite deposits (Taboroši et al., 2006). If these deposits formed as subaeral

calcite deposits, a calcerious tufa, they are usually lightweight, porous and friable with a quite irregular and often crooked shape. Outside surfaces of such deposits generally also feel powdery and earthy and vary from chalk-white to dark colors. They exhibit no visible dissolutional textures or karren features and consist mainly of unorganized microcrystalline CaCO3 with organic material and detrital grains. On the other hand calcite true speleothems form in an enclosed cave environment (by CO2 diffusion and not evaporation) and when later subaerially exposed are composed of homogenously and densely laminated calcite. They have a cylindrical or conical form in vertical orientation, as the speleothems observed in caves. The surface is usually smooth or dissolution pockmarked, though after breaching of the cave it can be altered and superimposed by eogenetic karren (Taboroši et al., 2004) and in some cases can also have thick organic-rich powdery coatings.

Denudation

The theoretical dissolution rate on karst terrain and its application to the Tarague limestone

The theoretical model that links chemical and environmental factors such as temperature, CO_2 pressure and precipitation in solutional denudation is the following (White, 1984):

$$= \qquad (1)$$

where:

= autogenic solutional denudation rate in mm/ka for the system in equilibrium, giving the maximum denudation value.

= the rock density (g/cm^3).

= is the equilibrium constant for calcite/aragonite.

= the equilibrium constant for $H_2CO_3 \leftrightharpoons HCO^{3-} + H^+$.

= the equilibrium constant for $HCO^{3-} \leftrightharpoons CO_3^{2-} + H^+$.

= the equilibrium constant for $CO_2 + H_2O \leftrightharpoons H_2CO_3$.

= the partial pressure of CO_2 (atm).

= precipitation (mm/yr).

= evapotranspiration (mm/yr).

The most important variable of the above is the annual water discharge (P – E), which is also evident from the graph in Figure 18. White (1984) emphasizes that the characteristic time for limestone to reach equilibrium with water is several days and therefore the dissolution of the rock is slow and some of it occurs underground. In addition, it is argued by Purdy and Winterer (2001) that the dissolutional effect of rainwater on the rock surface is instantaneous compared to the time needed for evapotranspiration to take effect, and therefore evapotranspiration should not be taken into account in the above equation.

Of lesser importance, but not negligible, is the CO_2 partial pressure. A factor of 100 in the partial pressure of CO_2 results in only a factor of 5 in the dissolutional denudation rate. CO_2 partial pressure depends mostly on whether the rock is bare or covered with soil containing decomposing organic material that raises the CO_2 levels in the soil through which the water percolates before getting in contact with the rock.

The least important is the temperature reflected in the constants. The equilibrium dissolutional denudation rate increases only about 30% when temperature drops from

25°C to 5°C. Beacuse the mean high and low temperatures in the tropics stay within a 5°C difference, temperature variation has little effect.

Last but not least, a controlling factor that should be taken into account is also the density of the rock, which depends on mineral density and porosity of the rock and is inversely proportional to D_{max} (Purdy and Winterer, 2001). High porosity results in less carbonate mass that has to be dissolved for the same surface lowering compared to a dense limestone rock (Figure 19). High porosity also offers larger surface area for dissolution reactions.

According to White (1984) the theoretically calculated lines for denudation rate versus climate are in compliance with the empirically obtained lines of Smith and Atkinson (1976). It should be also pointed out, however, that the constants used in the above equations are valid for the equilibrium state but in reality the system is almost never in equilibrium and therefore the true dissolutional denudation rates are actually smaller than the theoretically based estimates.

In order to estimate the theoretic dissolutional denudation rate on Guam for young limestones (Tarague and Merizo), various lines were calculated for different and temperature values on a D_{max} vs. precipitation graph (Figure 18). In the calculations, aragonite has been assumed to be the sole mineral component of the rock, as the Tarague Limestone is young (125 ka). Therefore the density and equilibrium constant for aragonite (K_A) were used, though the resulting differences in D_{max} are really small (Figure 19). For the density of the rock, 30% porosity was taken into account, which is comparable to the porosities reported for the reef limestones on Guam, or to the porosity expected in primary (eogenetic) carbonates (Ayers and Clayshutle, 1984; Mink and Vacher, 1997; Reale et al., 2004). Considering the mean annual precipitation minus

evapotranspiration, i.e. ~1400 mm of water passing through the rock annually, the maximum possible dissolutional denudation rate for the atmospheric CO_2 values (i.e., bare rock) and constancy of these values through time, the dissolutional denudation rate should be ~30 mm/ka which would amount to a total of ~3.5 m since the end of the last interglacial (~116 ka). However, if we consider the objections to this model (Purdy and Winterer, 2001) and the average annual rainfall for northern Guam (~2350 mm), the maximum dissolutional denudation rate would be ~50 mm/ka (Figure 18) and the total dissolution since MIS 5e ~6 m. Considering higher values because of a soil cover, surface lowering from ~8.5 m for normal soils and ~18 m for CO_2 -enriched soils is calculated with evapotranspiration considered. Values of ~14 m for normal soils and 30 m for CO_2 -enriched soils are obtained if evapotranspiration is not considered. In conclusion, the maximum theoretic values for solutional denudation in conditions analogous to those of the research area on Guam span from 3.5 m to 30 m, mostly depending on the and the amount of water involved in the dissolution of $CaCO_3$. It should be pointed out that these calculations are all based on the assumption of and rainfall constancy since MIS 5e, though at least the latter probably varied through the Last Glacial Cycle as suggested by evidence from some other islands in the Pacific Basin (Nunn, 1999).

These calculated values for the conditions encountered on Guam are consistent with reported values from other sites in the tropics. In Vanuatu, with the mean precipitation of about 4000 mm/yr, the reported denudation on MIS 5e reef limestone since its exposure is 12 to 15 m (Strecker et al., 1986), which would be roughly 6 to 7.5 m equivalent on Guam considering the rainfall difference. Of the same order of magnitude is the estimation of the average dissolution rate of Lincoln and Schlanger

(1987) for reef limestones in the tropics which would account for ~4 m since the end of the MIS 5e. Considerably higher rates but still within the above calculated range are the estimations for denudation of atoll islands by Purdy and Winterer (2001) and Dickinson (2004) of 15 to 20 m since MIS 5e.

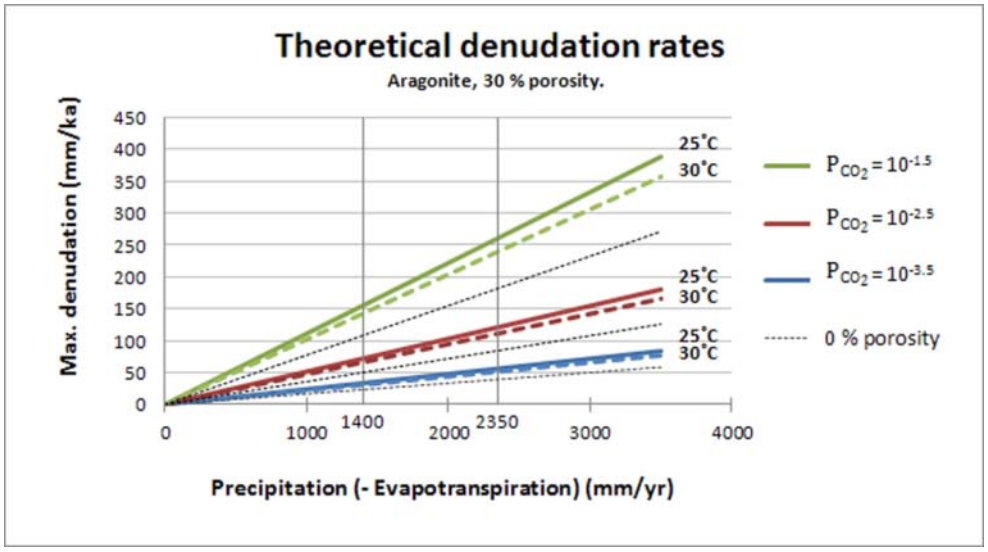

Figure 18 Denudation rate dependence on the water flux at different CO_2 partial pressure ( ) and temperature values for aragonitic rock with 30% porosity. The thin black dashed lines represent the same dependence for aragonitic rock with 0 % porosity at 25ºC for the same values of the adjacent lines. The x-axis are marked the values of the average rainfall (2350) and the average rainfall minus the evapotranspiration (1400) in northern Guam. The values of $K_{A/C}$, K_1, K_2 and K_{CO2} are from Ford and Williams, 2007. values for soils are from White, 1984.

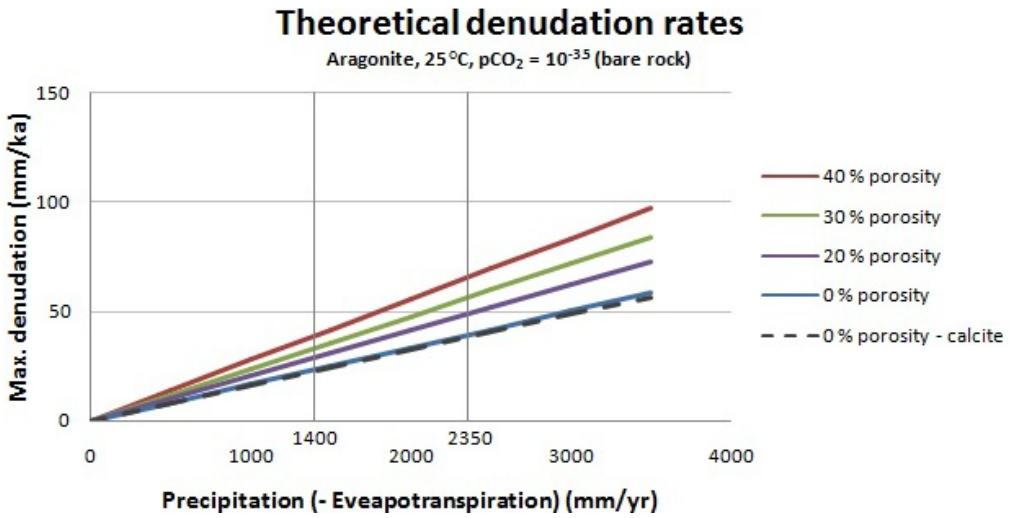

Figure 19 Denudation rate dependence on the water flux for different porosities of aragonitic rock at 25ºC and for atmospheric values. The black dashed line shows the denudation rate dependence for calcite with 0 % porosity at the same conditions for comparison. The x-axis are marked the values of the average rainfall (2350) and the average rainfall minus the evapotranspiration (1400) in northern Guam. The values of K_A, K_1, K_2 and K_{CO2} are from Ford and Williams, 2007. values for soils from White, 1984.

Surface lowering estimation from field observations on limestone terrains

Tropical Karrentische

Dissolutional rates of surface denudation can be estimated from the height of the limestone pedestals that were protected from dissolution by a boulder sitting on such a pedestal. The pedestals with the boulder on top are also called *Karrentische* (singular *Karrentisch*, means "karren table") and were extensively studied in glaciated areas where glaciers have left non-carbonate boulders on glacially scoured limestone rock surfaces after glacial melting (Figure 20) (Ford and Williams, 2007). Dissolution by rainwater has lowered the rock surface around these boulders while the rock just beneath the boulder has been protected from the rain. The height of the pedestal is thus a measure of the dissolutional denudation since the glacier melted, i.e. some time after thelast glacial

maximum (Ford and Williams, 2007). A similar approach can be used non-carbonate components of limestone such as chert nodules and quartz veins. Because the solubility of chert and quartz in rainwater is negligible compared to the solubility of carbonates, they start to stick out of the rock as the surrounding carbonate gets dissolved with time (Figure 21). As for the *Karrentische*, the time constraint is represented by the retreat of the glaciers that leveled the heterogeneous rock surface and allowed the onset of the differential dissolutional denudation after they melted away.

Figure 20 A classic *Karrentisch*. A granite boulder sitting on a marble pedestal. The height of the pedestal represents the amount of denudation since the area was deglaciated. Norway. (Courtesy of J.E. Mylroie.)

Figure 21 Quartz vein sticking out of the marble bedrock. The height of the vein above the surrounding rock rapresents the amount of surface denudation since the area was deglaciated. Norway. (Courtesy of J.E. Mylroie.)

An analogous approach has been also applied in the tropics where boulders can roll off the upper portions of slopes. However, the time at which the boulders fell on the observed surface is difficult to determine and any estimation of denudation rates isthus more uncertain and must thus represent minimum values (Figure 22).

One possibility of constraining the time at which the boulders were placed on the ground is by dating the speleothems formed in the voids between the boulders and the ground (Kindler et al., 2010, and references therein). However, the dates obtained from such speleothems give only a minimum age because the actual start of their formation is uncertain. Further, only under some of the boulders can the right conditions be established for the growth of the speleothems, and thus the selection of suitable speleothems for U/Th dating is very restricted.

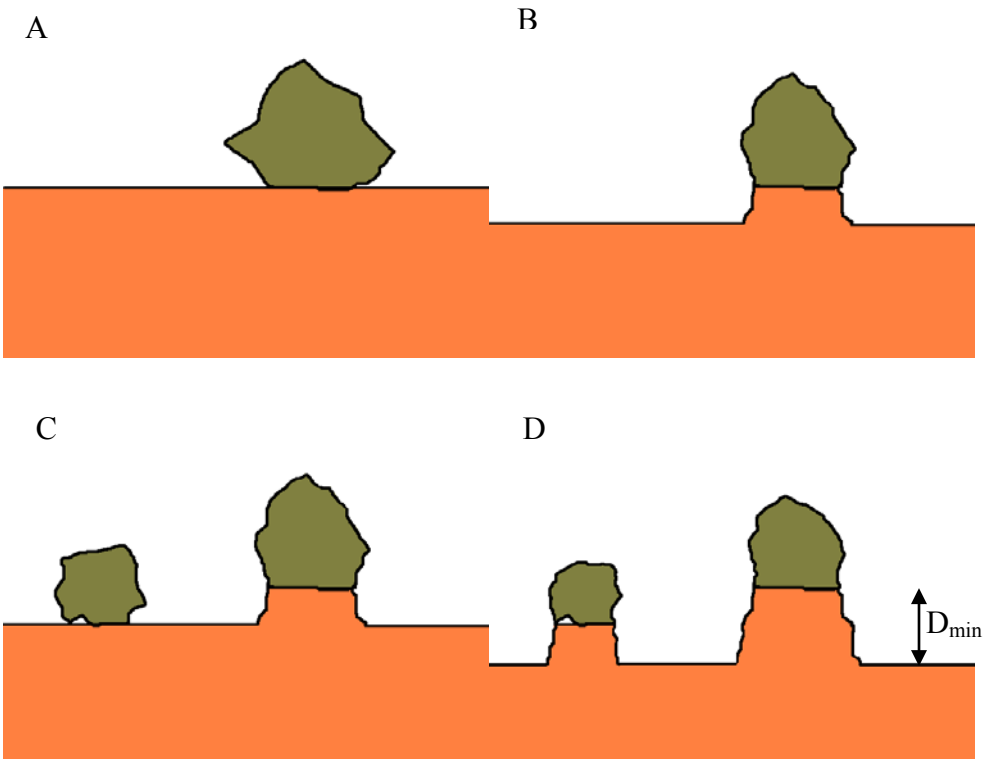

Figure 22 Formation of the *Karrentische* in the tropics. Part of the ground becomes protected from denudation once a boulder falls on it (A) while the surrounding ground gets lower (B). With time, other boulders fall on the ground (C) and as a result we get *Karrentische* with pedestals of different heights (D). The height of a pedestal represents the denudation since the boulder fell on the ground or the minimum denudation (D_{min}) since the limestone ground became exposed to denudation. Note that the boulders dissolve as well, if they are made of limestone.

Surface relief

Another proxy for minimum denudation rates in the tropics can be karst relief such as cockpit karst, pinnacle and or tower karst. Such landforms are also a consequence of differential dissolution that concentrates along specific flow paths (Ford and Williams, 2007). For example, concentrated flow along fractures will dissolve more rock along them while the blocks between the fractures will not keep pace (Figure 23). Further, when depressions are formed along the fractures, organic-rich material will preferentially accumulate in the fractures rather than being evenly distributed across the surface. The

water percolating through the fractures will thus be even more enriched with CO_2 and thus even further enhance the dissolution along the fractures, which will become even more permeable and drain even more water which will wash even more organic material from the surface into the fracture, a positive feedback effect. If gorges along the fractures form this way, the intervening blocks will develop into cone and tower karst. If dissolution concentrates at the fracture intersections, the surface will take form of the cockpit karst (White, 1984). The top of the ‘’towers’’ and ‘’cones’’ therefore represent the elevation that is the closest to the original surface elevation while their height represents the minimum denudation since the beginning of the dissolutional denudation. For young limestones, the time constraint can be a known sea-level highstand during which limestone was formed and after the end of the highstand, subsequently exposed. The time of the sea-level fall can be also determined by dating the skeletons of the organisms present in the rock if they have not been re-crystallized (Pirazzoli, 2007).

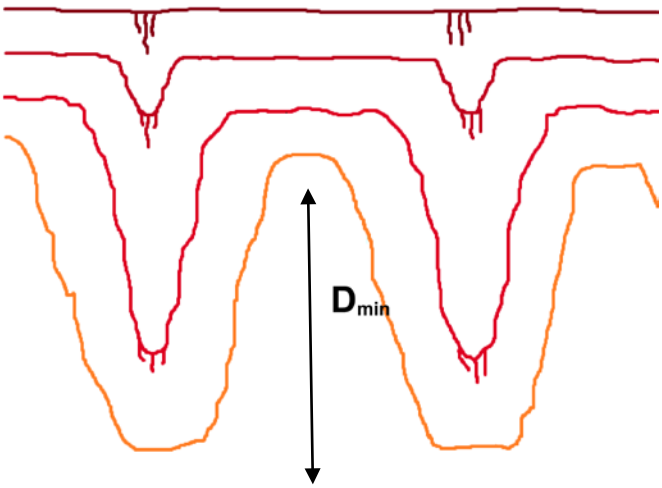

Figure 23 Formation of karst pinnacles because of preferential dissolution along fractures. From the initial flat surface (dark red) a pinnacle karst surface develops (orange). The height of the pinnacles represents the minimum denudation (D_{min}) since the limestone ground became exposed to denudation. (Modified after White, 1984.)

CHAPTER III

METHODS

Field analysis

A field survey was done in the area around Ritidian Point and Tarague embayment at the north end of Guam (Figure 1). Initially the coastal areas were walked with the aim to identify any geomorphic features associated with sea-level stillstands, especially flank margin caves and sea-level notches. Special attention was paid to the lithology and the lowermost limestone deposits were explored. After potential cave entrances were identified they were dug with hand tools such as pick and spade, and finer tools such as a flat hammer, hoe, dust pan and a steel bucket. In order to remove big rock blocks from the entrance, hammers and chisels were used to break these blocks into smaller and more easily removable pieces. A hammer and chisel were also used to enlarge a narrow cave passage that was too narrow for a human to pass. Many volunteers were involved in this part of the field work. Due to high CO2 levels in one of the caves, a scuba tank was used for exploration and sample collection. Subsequently, areas further from the coast were also explored.

Most of the research field is located on the Guam National Wildlife Refuge and so a permanent permit for the purpose of the research was obtained. For the areas on Anderson Air Force Base (AAFB) a permit was obtained for each field day and a person from the military was needed as an escort. For the exploration along the Ritidian cliff and

the elevation measurements in the Tarague embayment a person from the Environmental Office of the AAFB was always present.

Cave mapping

Caves were surveyed in accordance with current international standards for cave cartography and mapping established by National Speleological Society (e.g. Dasher, 1994). Sunnto compass with inclinometer and metric tape were used for measurements. To enter into some of the caves, the entrance had to be excavated. For some parts, hammer and chisel needed to be used to enlarge the passage to make it enterable for surveyors.

Geologic mapping

The boundaries of the stratigraphic units were walked and the key points were recorded with a GPS unit. For the Tarague area the previous map (Randall and Siegrist, 1996) was used and modified for this purpose. The GPS points were imported to a GIS and overlaid onto a LiDAR-derived hillshade of the area. The data were further elaborated in the GIS and individual polygons were created for each stratigraphic unit. An analogous approach was used for recording and elaborating the geomorphic features.

GPS

A Garmin Colorado300 receiver was used for recording stratigraphic and geomorphic points of interest. The typical accuracy (95%) of the device is <10 m, depending on the satellite availability and strength of the signal.

Spatal relaitionship and morphology analysis

GIS spatial analysis was used to determine the range of elevations occupied by the selected geomorphic features and to obtain general elevation characteristics of the surface morphology of the studied area. A digital elevation model (DEM) was used to visualize the relationship between stratigraphic units and geomorphic features of interest.

Elevation measurements

The elevation of the selected points was measured by differential leveling using SOKKIA 3000C level. As a reference point, a survey landmark was used (survey landmark number 0146, order 2, class I). The local mean sea level is used as a datum and is based on the tide gauge record in Apra Harbor between 1983 and 2001 (National Geodetic Vertical Datum (NGVD) 29). Its precision in elevation is ±10 cm. For control, the values of the measured points located at easily identifiable landmarks were compared with elevation that can be read from 1:5,000 topographic maps and digital elevation model (DEM). The measurements of all the stations were done with the accuracy to a millimeter, while the final results were rounded to a decimeter accuracy, which is the accuracy of the initial survey station, i.e. the survey landmark.

The elevation of the vertices of the notches was measured with the help of an aluminum rod with a mounted bubble level. Three points of each vertex were measured (where applicable) and the average considered as the elevation of the vertex at the measured site. The rod was placed between the notch vertex and the measuring staff in order to read the value on the scale of the staff. In Ritidian-east area (Figure 24) the same datum was used as for the other stations in the area. For the modern notches in Pago Bay two nearby benchmarks were used. These have the mean low low water (MLLW) as a datum though based as well on NGVD 29. The elevations reported from this site are

corrected for the difference in the selected datum, i.e. the mean sea level was used as a datum just as for all the other measurements.

The elevation of the vertices of the inland notches was measured indirectly by using DEM with tape and inclinometer due to the remoteness, difficult terrain, thick vegetation, and presence of the talus under the notch. The oblique distance between the elevation of the vertex of the notch and the flat part of the terrace beneath was measured together with the angle between the oblique line and the horizontal. The vertical distance between the terrace and the notch vertex could this way be calculated. The location of the measured point on the terrace was then recorded with a GPS unit and the elevation of that point determined with DEM. While the tape could be held straight, the inclination could be measured only to about ±2° accuracy. The error of these measurements was thus estimated to be ±0.5 m.

The elevation of cave ceilings was measured with the help of the measuring tape and inclinometer from the surveyed elevation points near the cave entrances or, depending on the conditions, with the help of the surveying staff that could be extended up to 7.6 m high. The ceilings of caves below the tops of cliffs were measured with a tape from a survey point on the ground just below the cliff and corrected for the angle if the tape could not be extended vertically to the measured point.

The highest elevation of the fossil reef remnants was measured where there was a stable enough spot on the often very jagged surface to place the measuring staff. If such a spot was not at the very highest spot of the surface, the difference was measured with the help with aluminum rod in the same way as the notch vertices were measured. In one case the difference had to be estimated.

A more general elevation analysis of the tops of the terraces was done by GIS digital elevation model (DEM) analysis. The accuracy of the elevation method was tested by comparing the DEM elevation to the known elevation of a survey landmark on a flat parking lot (at Ritidian Point) and to other points of known elevation, such as topographic peaks and mountain tops found on the 1:5,000 topographic map of the studied area. The accuracy proved to be within the accuracy of the survey landmark, i.e. ±0.1 m. However, when estimating the elevation of inland paleo-notches, the exact location of the reference point on the terrace below the notch is uncertain due to GPS location determination uncertainty, the uneven surface of the terrace and its gentle inclination in some areas. When estimating the elevation of the inland notches an error of ±1 m was taken into account.

Feigl test

To distinguish aragonite from calcite in field samples, stain testing with Feigl's solution according to Ayan (1965) was used. The stained samples were always >0.5 cm in diameter and samples of known calcite and aragonite (fresh corals) were added as a control. The Feigl solution was prepared in the WERI chemical laboratory.

X-ray diffraction (XRD)

The qualitative and quantitative mineral composition of the bedrock samples was done by using X-ray powder diffraction (XRD) with the X-Pert PRO with α1 from 10 to 90°C 2Θ. To quantify the individual mineral phase, the samples were then spiked with Al2O3 and refined with the Rietveld method. An agate mortar was used to grind the samples. The analyses were done at the National Institute for Chemistry, Slovenia.

Optical microscopy

Optical microscopy was used to characterize the bedrock in thin section with special attention to the stage of diagenesis. Some of the thin sections were stained with the Feigl's solution to distinguish aragonite from calcite. Aragonite could be distinguished from calcite also by the texture in thin section as described in Sandberg (1985) and McGregor and Abram (2008). Thin sections were examined by a Truevision M1 petrographic microscope.

U-Th dating

U-Th dating of the speleothems was done according to the technique of Edwards et al. (1986) and Cheng et al., (2000), at the University of Texas at Austin. U and Th isotope analyses were conducted on thermal ionization mass spectrometer (TIMS). Because the site specific initial 230Th/232Th ratio is unknown the age was calculated for two initial ratios; 4.4 ppm (the bulk value of the continental crust) and 15 ppm (the bulk value for ocean water). The reported $\pm 2\sigma$ uncertainty is a mean of tens to hundreds of isotope ratio measurements plus systematic errors (Cheng et al., 2000).

The collected speleothems were cut into halves with a diamond saw and a translucent bottom layer that showed no visible signs of detrital contamination was drilled with a 0.5 mm drill. After chemical analysis showed that non-translucent calcite was clean of 234Th, these were also drilled for dating. A clean bottom-layer-flowstone core was drilled with a dental hand drill. Sample preparation and dating was done at the University of Texas at Austin.

CHAPTER IV

RESULTS

Research area

The coastal area around Ritidian Point, northern Guam was chosen as research site. The area south-east of Ritidian Point (further referred as "Ritidian-east"), east from the Guam National Wildlife Refuge facilities to the north-west end of Jinapsan Beach, was field surveyed and examined in detail. Three other areas were examined for comparison; the adjacent area around Ritidian Point (further referred as "Ritidian-central"), the area south-west from Ritidian Point to approximately Achae Point (further referred as "Ritidian–west") and the Tarague embayment (Figures 1; 25) area between the south-east end of the Jinapsan Beach (Mergagan Point) and Scout Beach. The area further south was not examined. Access was restricted because of the firing range facilities. The Tarague embayment was examined for comparison since it is the continuation of Ritidian-east and a detailed geologic survey has been done previously (Randall and Siegrist, 1996). All the areas were examined between the shoreline and the Ritidian cliff, which is the main, 150-m high cliff that separates the northern Guam plateau from the coast (Figure 26). The Jinapsan Beach area was not examined since it is privately owned and permission for research was not obtained. Finally, the rim of the Ritidian Cliff was also examined for potential faults and as an overview of the Ritidian-east and Ritidian-west areas from above.

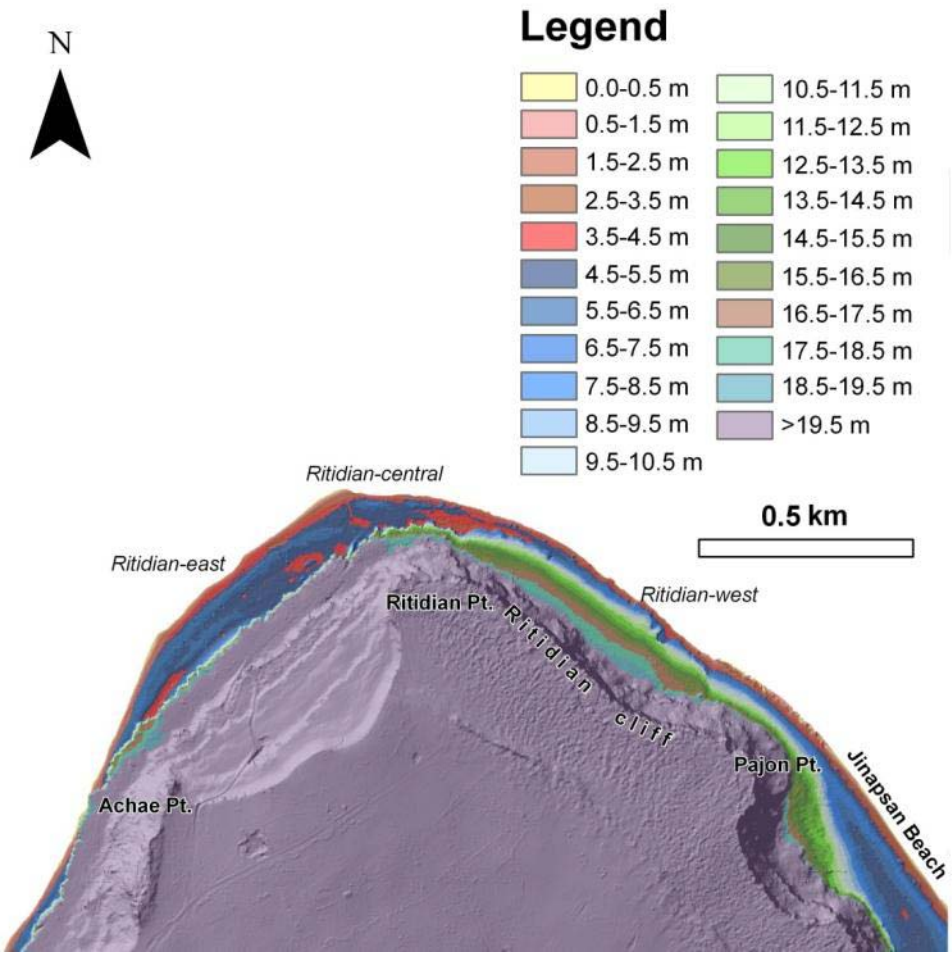

Figure 24 DEM of the research area. Achae Point is at the extreme south-west part of the map and Pajon Point at the extreme south-east part of the map.

Figure 25 Ritidian cliff. Note the terrace covered with the vegetation above the frontal plain.

Geomorphic and geologic description of the examined areas

Ritidian-east

The examined area can be divided into the following areas, from coast to inland: sandy beach, low, flat limestone terrace (fossil reef, Merizo Limestone), backbeach deposits, first terrace above the backbeach deposits. These physiographic zones are defined and described below.

The area is bounded on the southeast by the boundary between the Guam National Wildlife Refuge and private property. The boundary between Ritidian-east and Ritidian-central is marked by the change in elevation of the first terrace above the backbeach deposits. The low cliff present in Ritidian-west and Ritidian-central area ends abruptly right at the boundary between the two research areas.

The beach is relatively large in the northwest part, with extensive beachrock deposits (Figure 26). Immediately followed by the backbeach deposits. Further

southeast it becomes very narrow and interrupted by the headlands of the adjacent low terrace and sometimes thus forming small bays (Figure 27). In the southernmost part of the area the beach is not present. It stretches up to ~3 m above the sea level and it is represented within the light brown area near the sea on the DEM map (Figure 24). Beachrock is common on these beaches.

The low terrace, interpreted as Merizo Limestone by Randall and Baker (1989), is not present in the NW part where it could be buried under the modern backbeach deposits as also noted by Randall and Baker (1989). It is well observed in the central part of the area where it occasionally forms small headlands interrupting the beach or forming small bays (Figure 27; 28). At the sea-ward side it usually ends with a small elevated rim made of predominantly fossil algae and associated biota (Figure 28). In the southernmost part it stretches to the sea forming the shoreline. Commonly it is covered with a thin layer of backbeach deposits. On the DEM map (Figure 24) it is represented by the dark brown and partly by the red color as it extends up to 3.5 – 4.0 m in elevation.

Figure 26 The beach in the northwest part of Ritidian-east area. Note the prominent beachrock outcrop by the sea. In the background on the right side of the picture there is the Ritidian cliff.

Figure 27 Beach reentrants at Ritidian-east. The low terrace is visible on the left forming a headlands while in the front there is a beachrock outcrop.

Figure 28 The low terrace along the coast interpreted as the Merizo Limestone (Randall and Baker, 1989). The standing feature stands on the elevated rim of the terrace made of predominantly fossil algae and associated biota. Note a beach reentrant in the back and the the Ritidian cliff in the background on the right side.

The backbeach deposits are the most abundant in the NW part of the area where they extend across a ~80 m broad plain (Figure 24, the blue and red areas; Figure 25, the front part of the picture) that narrows to a 50-m wide strip of land adjacent to the beach where there is a road. The plain slopes gently downward inland. The thickness of the deposits is unknown. These deposits form a narrow storm berm parallel to the beach that stretches all along the area where backbeach deposits are abundant. The berm reaches the elevation of up to ~6 m and it is well visible on the DEM map as a narrow dark to light blue line (Figure 24). The rest of the backbeach, however, has an average elevation range between ~3 and 5.5 m and are represented by gray, red and blue color on the DEM map (Figure 24).

The first terrace above the backbeach deposits emerges out of the backbeach deposits as a few meters-high scarp (Figure 25; 29) in the northwest part of the area. The

scarp, however, gets gradually lower towards the southeast and can pinch out and reappear at several places. It can rise as much as ~5 m high above the ground in the small reentrants in the terrace. The surface behind the scarp slopes gently upward inland, and near the cliff the slope becomes even gentler forming an almost flat area (Figure 30), which is well shown by the brown and light blue elevation band on the DEM map (Figure 24). However, a gentle break of slope has been observed within 10-30 m inland from the scarp along most of the terrace in the examined area. The elevation of the top of the terrace varies and ranges between 16.5 and ~20 m above sea level.

The rock of this terrace has compositionally and texturally well-preserved fossils (Figure 31) and in general the limestone has a yellowy color and high primary porosity (Figure 32). Corals and fossil remains of *Halimeda* are in most cases predominantly (> 60 %) still aragonitic as confirmed by XRD analysis. Especially in areas along the scarp, the coral reef can be remarkably well preserved. Most of the terrace, however, is covered with rubble and only occasional outcrops of bedrock are visible. These outcrops can be made either of well-preserved fossils that have not undergone much diagenesis or of well-recrystallized rock. Outcrops of well-recrystallized rock tend to be more common closer to the cliff. Along the scarp in the middle part of the Ritidian-east area, however, there is an extensive outcrop of detrital facies limestone (Figure 29), predominantly made of fossiliferous detritus, similar to that found in modern beach sand (Figure 26). The part made of this biocalcarenite has low porosity and has a distinct morphology (Figure 29). Such biocalcarenite appears in many parts of the outcrop. The outcrop of detrital facies does not end abruptly and can appear in other parts of the scarp as well. In the northwest part of the Ritidian-east, such biocalcarenite is covered with coralline facies.

Above the first terrace above the backbeach deposits there is a discontinuous and dissected and sloping ledge of very uneven elevation (Figure 24). Behind this ledge, there is the Ritidian cliff (Figures 24, 25 and 26) above which there is the northern Guam plateau. All the limestone above the first terrace above the backbeach deposits is white and well recrystallized limestone, assumed to be the Marianas Limestone. However, individual predominantly aragonitic (>90%) corals were also found.

Figure 29 The scarp separating the low terrace with the backbeach deposits and the first terrace above the backbeach deposits. The detritial facies limestone of the scarp has a rounded morphology. Note the roots growing in the joints of the rock contributing to its physical weathering.

Figure 30 The nearly flat areas of the first terrace above the backbeach deposits found in the proximity of the Ritidian cliff.

Figure 31 An example of a well preserved coral on the first terrace above the backbeach deposits.

Figure 32 The scarp of the first terrace above backbeach deposits. Note the high primary porosity of the reef facies limestone.

Ritidian-central

This area can be subdivided, going landward, into:

- sand beach,
- backbeach deposits,
- cliff,
- first terrace above the backbeach deposits.

The area can be considered as a subdivision of Ritidian-west since it is in large part similar to the Ritidian-west area that is discussed in detail bellow. It is limited to the west by the road that descends to the National Fish and Wildlife Refuge area. The main feature that characterizes this part of the research area is a rather narrow and relatively steep first terrace above the back beach deposits that ends seaward rather abruptly with a low cliff that continues to the Ritidian-west area but continues as a low scarp into the Ritidian-east area. The low cliff, however, is interrupted north-westwards with another

low scarp made of a well preserved fossil reef made of ~100 % aragonite corals. The low cliff itself is made of well-recrystallized calcitic white calcitic rock.

Similarly as in Ritidian-east, a well preserved coral reef facies is found near the edge of the terrace where the rock is almost entirely bare. In Ritidian-central there is the best preserved examples of buttress and channel reef morphology (Figure 33). This indicates that the area near the edge of the terrace was once part of the forereef while the reef flat must have been higher up. All the corals are well preserved and at least partly aragonitc. In the area near the Ritidian cliff, however, there are also outcrops of recrystallized rock and usually of algal facies. Right next to the Ritidian cliff the terrace is mostly covered with rubble, talus material, boulders and also a thicker layer of soil.

Figure 33 Inherited ridge and channel morphology of the surface. On the picture a ridge is well visible in the middle of the picture. Note the abundance of coarse rubble in the surroundings due to the ridge physical weathering.

Ritidian-west

This area can be subdivided, going landward, into:

- sand beach,
- backbeach deposits,
- cliff,
- first terrace above the backbeach deposits.

The broad sand beach stretches all along the area. It slopes up from the sea at an angle of about 20-30º, forms a flat area above 2.5 m above sea level, and is immediately followed by backbeach deposits. It is represented by a brown area on the DEM map.

Backbeach deposits initially slope up inland and form a wide storm berm about 6.5 m in elevation. The berm is continuous all along the beach and in some parts there are two such parallel berms. The surface of the deposits gently slopes down behind the berm(s) inland towards the cliff. The storm deposit area forms a flat (Figure 34) that is approximately 230 m wide and it thins out near Achae Point. A surface test pit made by the archaeologists showed the elevation to be 4.4 m, so the reef buried under the backbench deposits is ~1.8 m above the sea level. A reef limestone outcrop with a ~3 m pinnacle (Figure 35) was found rising out of these deposits not far away from the cliff. The pinnacle is predominately made of at least partly aragonitic corals.

The low cliff rises abruptly ~16 m above the backbeach deposits and > 20 m above the sea level. Its elevation comprises what would be the whole gentle slope of the terrace at Ritidian-east. It is made of entirely recrystallized dense calcitic limestone of various facies.

The first terrace above the backbeach deposits behind the low cliff is almost flat with a slight upslope inland. It is about 150 m wide and has an average elevation of

between ~20 and 25 m. It extends from the Ritidian Point to Ache Point where it thins out. At the seaward edge of the terrace just above the cliff there are several outcrops of well-preserved coral reef facies (Figure 36) with corals being from partly to almost entirely made of aragonite, as confirmed by XRD analysis. These reef deposits are no more than ~2 m thick near the very seaward edge of the terrace. Near the inland edge of the terrace, in the proximity of the cliff of the next terrace, hardly any aragonitic fossils were found. More than 90% aragonitic corals were, however, found attached to the cliff notches.

This terrace is followed by four other terraces of a comparable width up to the top of the plateau (Figures 24; 34). These terraces were used in the uplift rate study by Bureau and Hengesh (1994). The limestone of these terraces is well recrystallized; aragonite can be found only in traces, especially as fossil fragments within the detrital facies.

Figure 34 The backbeach deposits forming a wide plain at Ritidian-west. From the plain emerges the ~20 m cliff (covered with thick vegetation) above which there is the first terrace above the backbeach deposits. In the background there is the Ritidian cliff at Ritidian Point. Note other terraces between the first terrace and the Ritidian cliff.

Figure 35 The 3 m pinnacle in the background hidden in the vines. In the foreground the continuation of the same reef limestone outcrop emerging from the backbeach deposits.

Figure 36 Remarkably well preserved corals at the seaward edge of the first terrace above the backbeach deposits.

Tarague embayment

The examined area can be subdivided the same way as Ritidian-east:

- beach sand,
- low terrace and the reef "knobs",
- backbeach deposits,
- first terrace above the backbeach deposits (Tarague Limestone).

The beach sand is similar to that at Ritidian-east. Beachrock is less common and there are no beach reentrants.

The low terrace is similar to that at Ritidian-east but with the difference that it can be dissected in many places and can extend into the sea where it can form small patches or "knobs". Further southeast, a bit off the searched area, a well preserved buttress and channel reef morphology emerges from the sea. Based on ^{14}C dating these outcrops were assigned as the Merizo Limestone by Randall and Siegrest (1996).

The backbeach deposits follow the beach or the low terrace and form a narrow berm. It formed an about 80 m wide flat in the northern part where there is a parking lot and up to 50 m at Scout Beach.

The first terrace above the backbeach deposits begins with a scarp just as at Ritidian-east and has about the same slope angle. It is about 300 m wide at Scout Beach and it slowly pinches out near the parking lot at the northern side. Its maximum elevation is ~20 m. Near the seaward edge of this terrace, a coral reef facies is well preserved with corals being at least partly aragonitic. The two entirely aragonitic corals were dated to be ~126 ka and ~132 ka placing the formation of this terrace during the MIS 5e sea-level rise (Randall and Siegrist, 1996) and the area mapped as the Tarague Limestone (Siegrist and Reagan, 2008). The measured elevation of the two dated *Goniastrea* corals in this research was ~9 m, which is about 4 m higher than that reported by Randall and Siegrist (1996). The comparisons of the location of the corals with the contours on the 1:5000 topographic map and the read elevation value on a DEM are in excellent agreement with the 9 m elevation.

Most of the terrace behind the scarp, however, is covered with rubble and soil cover and few bedrock outcrops are found. The bedrock crops out on the road along the powerline near the coast show well-recrystallized rock..

A slope break was observed in the middle of the terrace. This break of slope is also visible on DEM map. Pinnacles about 2 high were observed immediately behind the scarp near Scout Beach.

Figure 37 The Tarague embayment. In the far background there is the Ritidian Point.

Ritidian cliff top

Genereal

The edge of the limestone plateau, i.e. top of the Ritidian cliff, is potentially the best place where vertical displacement could be observed. The top of the cliff of the Ritidian Point from the beacon along the cliff edge towards Pajon Point was walked and the terrain observed (Figure 38). Special attention was paid to possible evidence of faulting.

Figure 38 Walked route along the edge of the Ritidian cliff.

Observations

The cliff edge is higher in elevation than the immediate interiors. The limestone rock, under the weathered patina, is snow white, well recrystallized, consisting of a reef facies and is strongly karstified. Many pits, vadose shafts, sinkholes and karst pinnacles were encountered along the cliff line. At many places relict caves were observed. Clear evidence of former caves was the flowstone on the rock surface together with truncated stalagmite bases (Figure 39). A more evident cave notch, i.e. a breached cave that resembles a sea-level notch, was found near the end of the explored territory (Figure 40).

The joints seen from the coast were also found at the cliff edge (Figure 41). No evident vertical displacement could be observed at the very edge, in part due to the intensely karstified surface. At some places the joints were dissolutionally enlarged (Figure 42) but they could not be tracked far away from the cliff edge. A wider view of the key areas was also obstructed by thick and low vegetation. At some places a small, vertical displacement of about a meter could be argued (e.g. Figure 43).

Other joints were also observed. These joints seem to have two preferential angles at which they dip towards the coast and most likely cause small rock collapses from the cliff edge since many parts of the cliff edge are not flat but have a slope of the same angles (Figure 42; 43).

Figure 39 Exposed truncated stalagmite on the top of the cliff surface. Note the concentric texture typical of speleothemes.

Figure 40 Breached cave just below the edge of the cliff. Note the cave formations hanging from the ceiling.

Figure 41 Joint with a possible minor vertical displacement or just a piece of rock fell of on one side of the joint.

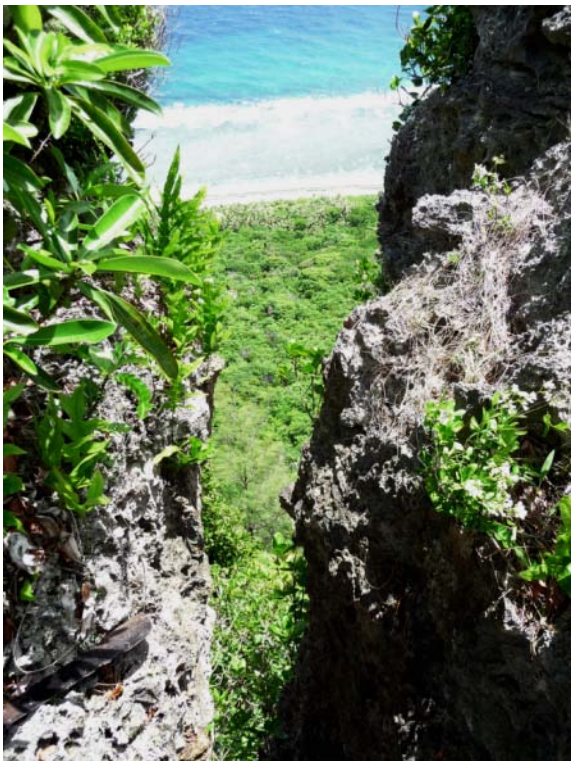

Figure 42 Dissolutionally enlarged joint at the edge of the cliff.

Figure 43 Low angle joints that may cause cliff edge rock collapses.

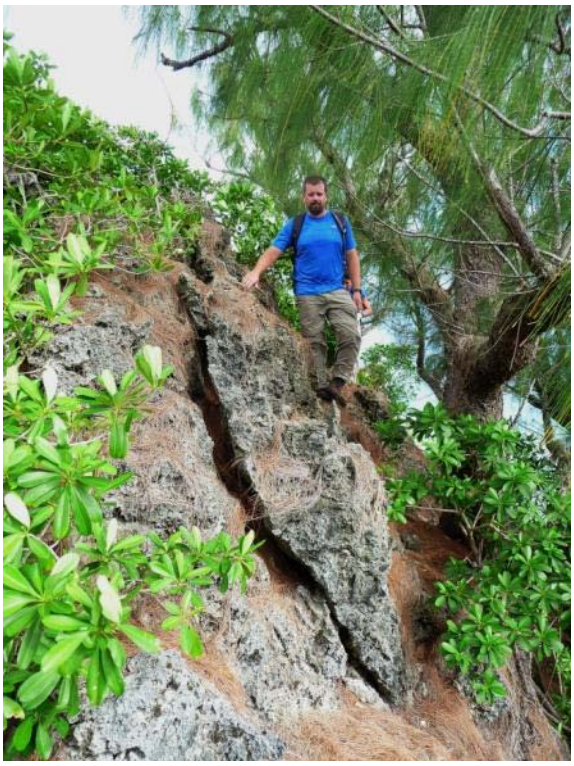

Figure 44 High angle joints responsible for rock fall from the cliff edge.

The observed denudation indicators in the research area

General

Pinnacles, pedestals and notches can be used as denudation indicators. They are described and compared in separate paragraphs for all the study areas.

Surface relief

Rock features that stand out above the surrounding area were found in all the studied areas though in general they are rare everywhere and the first terrace above the backbeach deposits is predominantly flat and covered with rubble (Figure 30). Most commonly these upstanding outcrops occur at the margin of the terraces, either near the scarp-end of the terrace or near the Ritidian cliff, just away from the talus area.

Rock build-ups up to 1 m high are quite common in Ritidian-west area where they appear as small isolated knobs on top of the first terrace above the backbeach deposits. An isolated conical outcrop standing just above the backbeach deposits 20-30 m from the cliff of the first terrace above the backbeach deposits at Ritidian west was also observed. The outcrop is made of mainly aragonitic coralline limestone which suggests that it is of young age. It was measured to be 3 m high and its base lies above the backbeach deposits (Figure 35). The surface of the backbeach deposit in this area was measured to be ~4.2 m above sea level so the top of the pinnacle is ~7 m above sea level.

Less common are the "knobs" in the Ritidian-east (Figure 45) and Tarague embayment. The more common upstanding outcrops in Ritidian-east occur as irregular rocky "mounds: (Figure 46). In Ritidian-central the upstanding outcrops occur near the terrace scarp in blocks typically 1 to 1.5 m high and approximately as much wide, that tend to be aligned perpendicularly to the terrace scarp/cliff line (Figure 47, see also Figure 33). These vague rows are separated from each other by relatively flat and low areas. Similarly, aligned pinnacle-shaped outcrops were observed elsewhere (Figure 48). Higher and pinnacle-shaped outcrops are less common. They were observed in a relatively small area in Tarague embayment where they occur ~10 to 20 m apart from each other and are typically 2 to 2.5 m high near the seaward edge of the terrace (Figure 49). Very similar outcrops, but less common are found also in Ritidian-east area near the talus under the Ritidian cliff (Figure 50).

The highest pinnacle was found in the Ritidian-central area at the eastern margin of where the aligned upstanding bedrock blocks can be found. The pinnacle is 6.1 m high measured from the top to the ground at its side (not the upslope or the downslope side) (Figure 51). The whole pinnacle is made of two pinnacles of which one is made

predominantly of coral reef facies while the smaller is made of both corals and crustose algae. The limestone at the very top of the highest pinnacle is very dense and mainly composed of fossil detritus. In the space between the two pinnacles, the limestone is mainly composed of fossil corals that are not *in situ* and are rounded which suggests that they were transported (Figure 52).

Figure 45 A ~1 m pinnacle (front) and a "knob" (back). Note the otherwise flat area around.

Figure 46 A rocky “mound” near the edge of the first terrace above the backbeach deposits at the sout-east end of Ritidian-east area. The area around is flat.

Figure 47 Aligned bedrock outcrop at the seaward edge of the first terrace above the backbeach deposits, Ritidian-central.

Figure 48 Aligned bedrock upstanding outcrops near the seaward edge of the first terrace above the backbeach deposits. The dashes outline the direction of the alignment. Note the destructive effect of the vegetation.

Figure 49 A 2-m pinnacle at Tarague embayment near the seaward edge of the Tarague Limestone terrace (equivalent of the first terrace above the backbeach deposits in Ritidian area).

Figure 50 A ~3 m pinnacle at Ritidian-east near the talus area of the Ritidian cliff. Note the porous nature of the reef facies limestone.

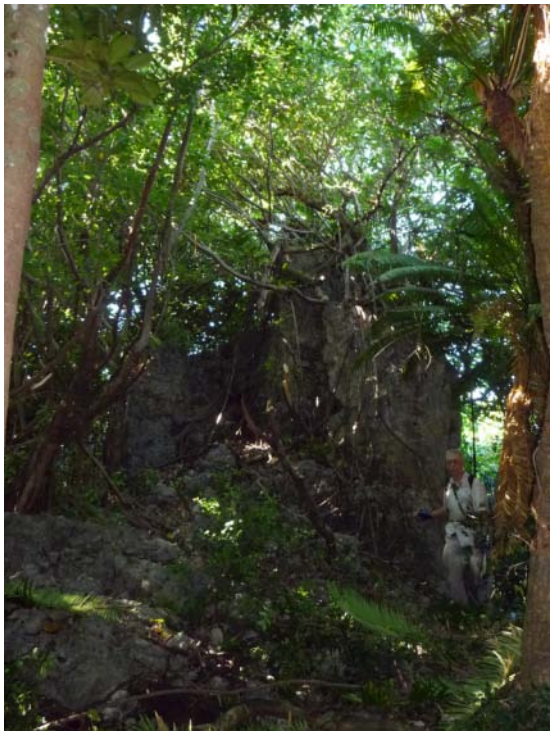

Figure 51 The highest found pinnacle ~6.1 m high, Ritidian-central. The picture is taken downslope.

Figure 52 The same pinnacle as in Figure 51. Note the channel between the dashed lines infilled with rounded fossil corals.

Pedestals (tropical *Karrentische*)

The *Karrentische* kind of geomorphic structures are found everywhere under the Ritidian cliff. Because they are analogous in the mechanism of pedestal formation to the *Karrentische* observed in the glaciated areas, but still different in how the boulders were placed to their position, they are referred further in the text as "tropical *Karrentische*". By far the most abundant are in the Ritidian-east area where we find boulders of sizes ranging from 0.5 m in diameter to the size of a multiple-storey house. They are all found in the area adjacent to the Ritidian cliff together or next to the talus pediment. The boulders lay on flat surface or pedestals of decimeters up to several meters high. Typically the pedestals do not exceed 2 m of elevation above the surrounding ground

(Figure 53) though pedestals up to ~5 m were observed. Examination of the rock of the tropical *Karrentische* revealed that the pedestals consist of different lithology than the boulder. The rock of the pedestal consists of beige coraline limestone with corals with well preserved fine texture that also comes out on the surface of the rock by weathering (Figure 54, 55 A). Stain test showed that this rock is mainly made of aragonite. The rock of the boulder, on the other hand, is nearly snow white with poorly preserved texture of the found fossil corals (Figure 55 A). Hand specimen has visible crystals and stain test showed that the boulder rock is entirely composed of calcite (Figure 55 B). The difference, however, is not obvious or noticeable if no corals are present and the limestone of the pedestal is made of crustose and other algae, which precipitate white calcite. Nevertheless, in older limestone rock, the calcite crystals tend to be bigger and visible with the naked eye as myriads of small reflecting faces when exposed to the sun In one case the fossil corals found on the pedestal's surface were recrystalized into calcite while the fossil corals found ~5 cm beneath the surface were still at least partly aragonitic as shown by stain tests.

The highest pedestal was found near the cliff at the top of the first terrace above the backbeach deposits in the northwest side of the Ritidian-east area and was named “Maipi Fina’ Mames” (Figure 56). The surrounding ground is nearly flat. The pedestal has steep sides that after 4.8 m measured from the top of the pedestal, gently grade into the more or less flat surrounding terrace. From the ground to its highest position under the boulder, the pedestal is more than 5 m high. It mainly consists of limestone of the coral-algal facies. The fossil corals of the pedestals are well preserved and are only partially recrystallized (Figure 55). In comparison, the boulder on the top consists of highly crystalline calcite and completely recrystallized corals with strongly obliterated

texture (Figure 55A). Stain tests confirmed, as for other tropical *Karrentische*, that the pedestal is made of at least partly aragonitic fossil corals while the fossil corals of the boulder are made of calcite (Figure 55 B). In the void spaces between the boulder and the pedestal, a breccia that appears to be talus exists. Within the voids of this talus, secondary calcite deposits can be observed (Figure 57). Because of the visible alteration by corrosion, and other weathering processes also observed on broken surfaces, their suitability for dating to get a minimum age of the placement of the boulder on to this location is questionable.

Figure 53 A tropical *Karrentsich* (named Kawaii) in Ritidian-east area. The 2-m pedestal is made of reef yellowy limestone with well preserved aragonitic corals while the boulder is made of well recrystalized white limestone.

Figure 54 A close-up picture of Kawaii. The difference in lithology can be recognized already by the rough weathered surface of the pedestal with well visible corals (arrow) and a more smooth of weathered surface of the more homogeneous recrystallized boulder. Note also the roots growing through the various voids in the rock which accelerate the physical weathering of these outcrops.

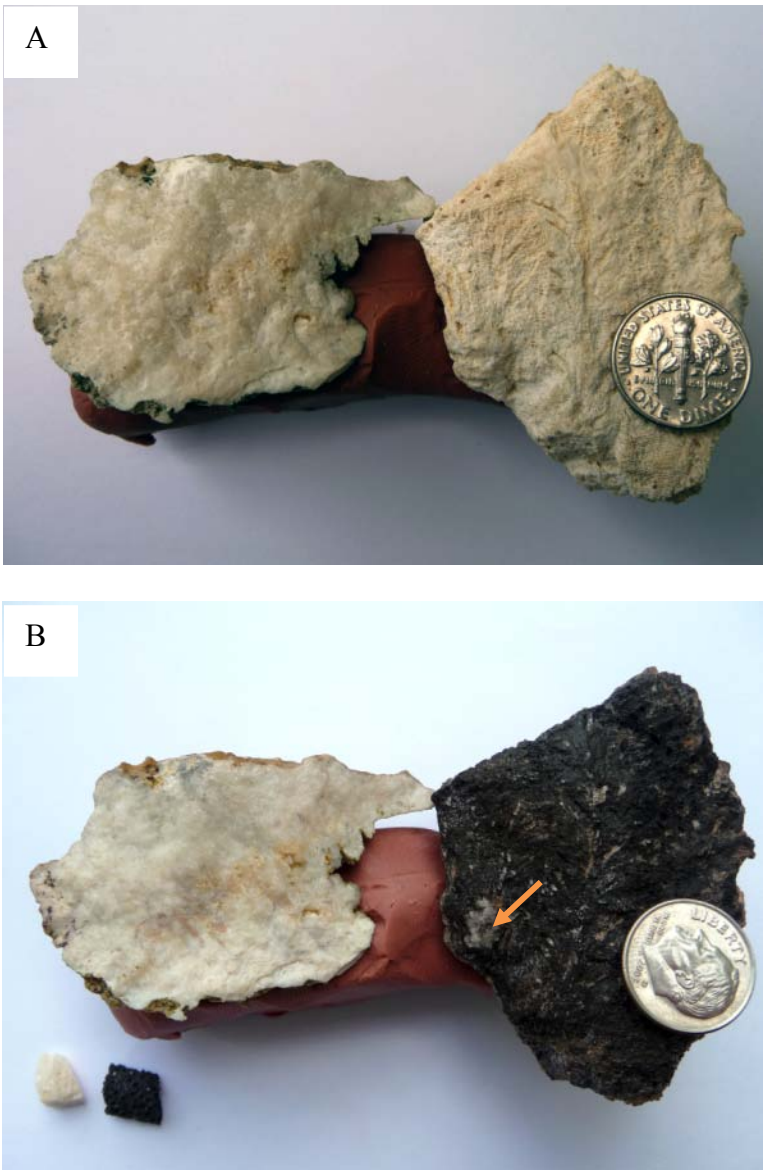

Figure 55 Rock samples from the Maipi Fina' Mames *Karrentisch*: A rock sample from the boulder (left) and from the pedestal (right) before the stain test (A). Both of the samples are fossil corals; a *Goniastrea* sp. (left) and a *Porites sp.* (right). Note the finely preserved texture of the *Porites* sp. and the barely visible texture of the recrystalized *Goniastrea* sp. Stain test revealed that the *Porites* sp. is at least partly aragonitic while the *Goniastrea* sp. is entirely made of calcite (B). Note a recrystallized calcitic area within the *Porites* sp. (arrow). The two small samples in the lower left corner are probe samples, a known sample of calcite (white) and a known sample of aragonite (black).

Figure 56 Maipi Fina' Mames tropical *Karrentisch*. The height from the feet of the explorer on the right side to the contact between the pedestal and the boulder is ~4.8 m. The height from the terrace flat to the contact between the pedestal and the boulder is >5 m.

Figure 57 Speleothems between the boulder and the pedestal of the Maipi Fina' Mames tropical *Karrentisch*. The rightmost stalagmite has been strongly affected by weathering thus revealing the typical layered inner texture of the speleothems. The inner stalagmites look better preserved.

Cave descriptions

Ritidian-east

In the same area, six small caves up to ~5 m in diameter were found. All the caves are dissolutional in origin and fit the criteria for flank margin caves. From northwest to southeast, the first one is Mayulang Cave. It is a breached cave lying in the steep slope at the edge of the Tarague Limestone terrace (Figure 58). The cave entrance opens behind a storm berm deposit and the cave itself is filled with Holocene beach sand mixed with organic matter. Though mainly breached, the intact part as well as the remnant cave wall on the S side suggest that the cave was elongated with the long axis having roughly a NE-SW direction which is perpendicular to the shoreline. The outer cave wall seems to have a collapse surface (Figure 58) while the cave walls of the intact part of the cave are smooth and have cusps characteristic of dissolutional caves (Figure 59). The collapse

surface indicates reef facies of limestone bedrock. The cross section (Figure 60, profile A – A' and C – C') of the caves shows a narrow and irregular upward elongation. No joint was observed. The cave narrows abruptly in the vertical dimension all around its rim at the bottom just above the sediment and it gets pinched out by the sediment fill (Figure 60, profile A – A', B – B'). The cave has a narrow horizontal branch that extends at the southwest end of the cave. The branch is wholly in the bedrock. There are also a few short and narrow vertical branches in the ceiling. The cave had dry walls during mapping (November) and only one speleothem is present in the cave. The observed stalactite is inactive, with its lower point extending into the sediment fill. It also appears to be in good, unweathered condition.

As the maximum elevation of the ceiling, the "vertex" of the ceiling arch was measured, rather than the top of the narrow vertical extension.

Figure 58 The entrance of Mayulang Cave. The sand on the ground is sloping down from a storm berm. Note the collapse walls.

Figure 59 The interior of Mayulang Cave with smooth and cuspate ceiling. Note the sand mixed with organic matter that fills up the cave and the possibly datable speleothem on the left side of the picture.

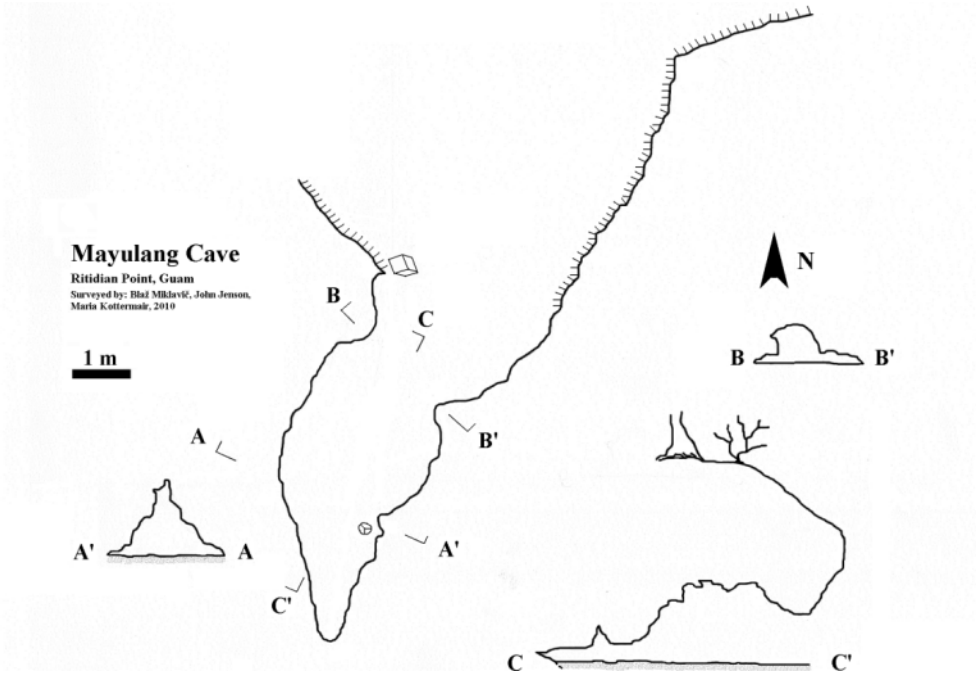

Figure 60 Map of Mayulang Cave.

Further southeast is Pepe Cave which lies on a gently dipping part of the terrace where the Tarague Limestone merges with the Merizo Limestone without any

topographic change. It is a low cave with a collapsed ceiling and narrow and elongated collapse opening (Figure 61). The cave formed at the interface between the *Halimeda* facies (ceiling) and coralline reef facies (Figure 62, profile B-B', Figure 63). The cave walls are very irregular with speleogens and other forms of embossments and hollows and short and small dead-end ramifications, especially in the lower part where the bedrock is composed of coralline limestone with individual corals partly isolated from the bedrock (Figure 63). The southward-oriented branch pinches out slightly upward in the bedrock (Figure 63, upper left part of the figure) while the northeast oriented branch has rubble and organic sediment on the floor. Because the ground beneath the rubble cannot be seen a narrow vertical passage may lead further down, similarly as in Tokcha Cave (see below) (Figure 63, profile B – B').

The maximum ceiling elevation (~7.5 m) was measured from a survey point just above the cave entrance.

Figure 61 The entrance of Pepe Cave.

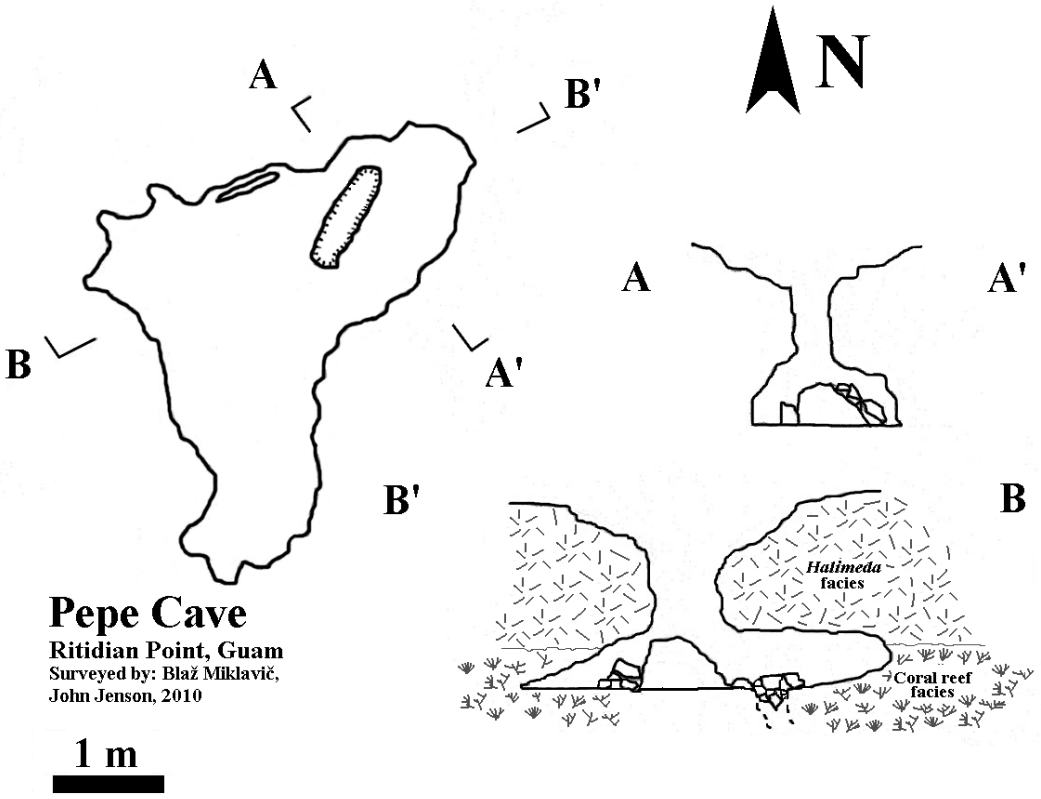

Figure 62 Map of Pepe Cave.

Figure 63 The interior of the Pepe Cave. Note the *Halimeda* facies limestone of the ceiling (upper arrow) and the coral reef facies limeston in the lower part of the cave (lower arrow). Beneath the rubble there could be a continuation of the cave.

Tokcha Cave has a collapse entrance on the top of the terrace about 20 m from the terrace's scarp (Figure 64). The entrance was buried at the time of discovery. During digging various materials in the rubble were observed besides the collapse rock, including pieces of apparently Holocene rubble such as corals and various shells as well as shards of ancient indigenous ceramic. Fine beach sand was also observed in small pockets. The bedrock on the top of the cave is partly to predominantly aragonitic (23 to 97 %, Appendix B) as shown by XRD quantitative analysis. At the bottom of the collapse depression the cave begins with a narrow horizontal passage followed by a 2-m drop leading to the main chamber, which has three ramifying passages (Figure 65). They all have a general NE-SW direction perpendicular to the coast. The bottom of the cave is entirely covered with beach sand (Figure 66), predominantly composed of fragments of the *Halimeda* algae. Just below the vertical drop that connects the main chamber with the

surface there is organic-rich sediment with rubble forming a mound that is the highest elevation of the cave floor.

The northern of the two passages leading in the direction towards the coast gradually narrows to the point that makes further exploration impossible (Figure 66). The possible continuation seems to be blocked with the beach sediment. The wall rock along this passage is flowstone free, very irregular with speleogens and fine cusps cut into the fossil-coral-rich bedrock (Figure 66; 67). The southern of the two passages is, in contrast, entirely coated with flowstone forming thick flowstone deposits and speleothems. The passage is vertically elongated and narrows laterally, partly due to flowstone deposits which also make it impossible to determine if this passage is joint controlled. At the beginning of this passage a 50 cm pit was dug reaching the bottom of dense flowstone, which uncovered many smaller stalagmites that had been buried (Figure 68).

The main chamber has a very irregular cave wall. At the southeast side the cave wall is covered with irregularly shaped speleothems and flowstone (Figure 69). The cave wallon the northwest side is predominantly composed of bedrock with of small niches, cusps and embossments that give the wall a rugged appearance. An elongated bedrock pillar is also present in this part. The ceiling extends in a NE-SW narrow line with several ramifications but any possible structural control over the cave morphology was impossible to determine due to the abundant cave deposits (stalactites and flowstone). The passage at the southwest end of the main chamber with a NE-SW direction is low and full of speleothems. The bottom is covered with the *Halimeda* sand with stalagmites sticking out of the sand. Digging in this area revealed that the sand deposit is about 30 cm thick.The rock beneath the sand is as well thick flowstone.

Along the southeast cave wall and especially as a rim around some of the speleothems, a crust of cemented beach sand often occurs. This crust is found at higher elevations than the present sediment (Figure 70). Also, a glass Coca-Cola bottle was found in one of the side pockets.

The speleothems in this cave are abundant, well developed and seemingly actively growing. They are in good condition and suitable for dating and stable isotope analysis which can be used to interpret paleoclimate. The bottom part of two of these speleothems were U-Th dated, and giving ages of 36,570 ±0.220 ka and 36.220 ±0.290 ka (Appendix C).

As a maximum, ceiling elevation of the roof of the entrance passage was measured. This ceiling also coincides approximately with the "vertex" of the ceiling arch of the main chamber (Figure 65, profile B – B').

Figure 64 The collapse entrance of Tokcha Cave. The fossil coral head just above the head of the explorer is at least partly made of aragonite.

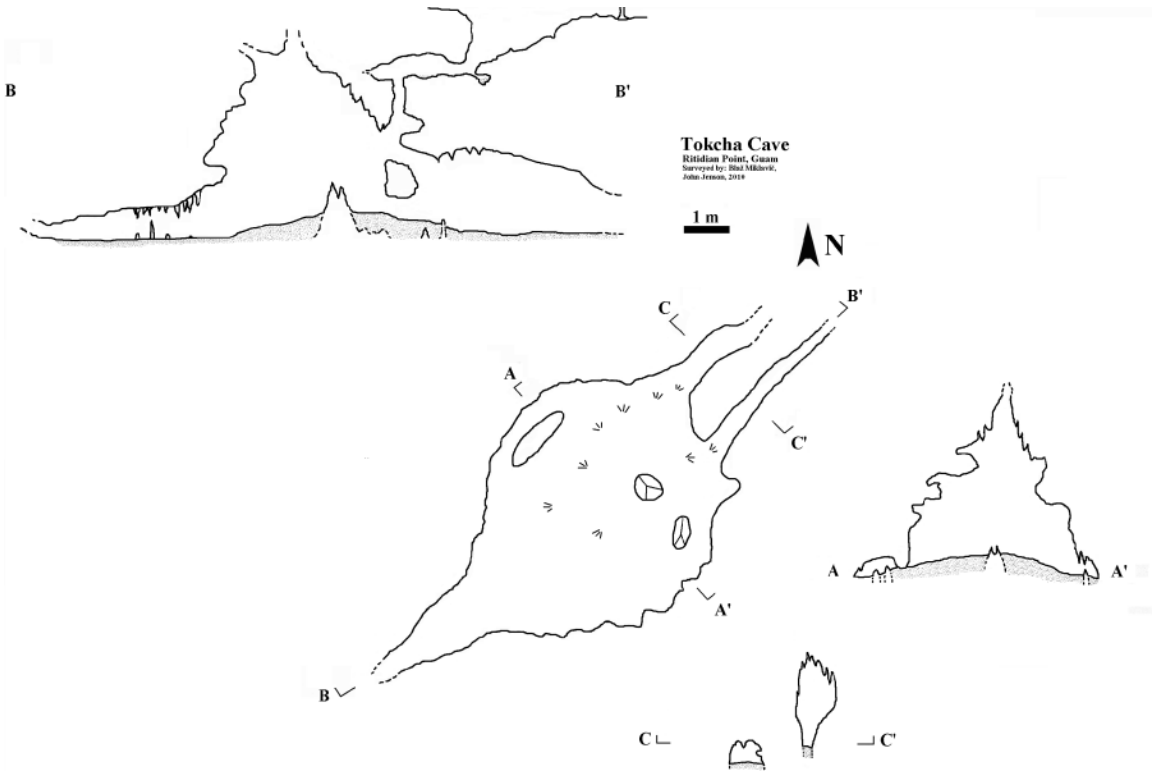

Figure 65 Map of Tokcha Cave.

Figure 66 The northern of the two passages leading towards the coast. Not the fossil coral reshaped into a speleogen hanging from the ceiling.

Figure 67 Fossil corals, a speleogen and dissolutional cusps (background) in the ceiling of the northern passage.

Figure 68 A pit in the sand revealed buried stalagmites. The bottom of the stalagmite folded in silver tape on the right side of the picture was dated.

Figure 69 Southeast part of the main chamber and the south-west oriented passage.

Figure 70 Sandstone rim along the north-eastern part of the south-east wall.

Alietai Cave is just 10 m east from Tokcha Cave. The entrance is buried and could not be successfully excavated (Figure 71). Therefore it was not included in the study. The surrounding bedrock is coral reef facies. Thin section analysis showed that the fossil corals are undergoing diagenesis with aragonite being inverted into calcite (Figure 71 A). The presence of aragonite was confirmed also by staining of the thin section (Figure 71 B).

Figure 71 The Alietai Cave with the partly dug out entrance. The surrounding bedrock is coral reef facies with the corals predominantly or partly aragonitic.

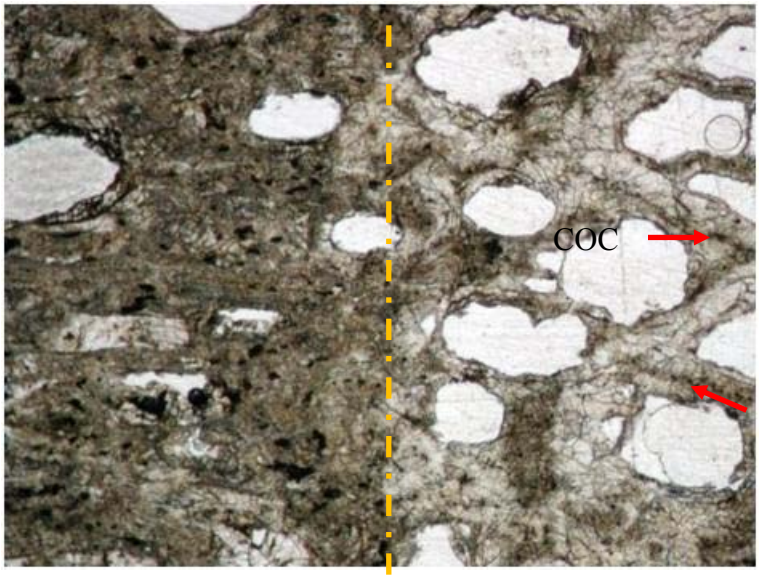

Figure 72 An image of a typical diagenetic texture of a coral with a well-developed neomorphic front in the middle of the picture (yellow dashed line) undergoing diagenesis in thin section. On the right side of the picture we see neomorphism (replacement of original aragonite by calcite while preserving the coral structure) with relics of the original aragonite (darker areas marked with red arrows) mainly along centers of calcitization of the coral (COC). The pores in the in the neomorphic zone became jagged. The aragonitic "chalky" zone on the left side (darker area) is typical for neomorphic fronts (McGregor and Abram, 2008). Plan polarized light, 4×.

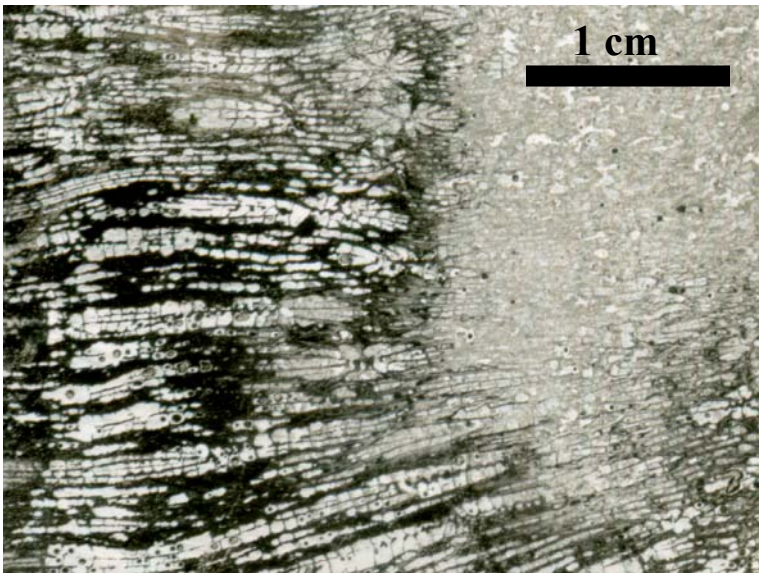

Figure 73 Stained thin section of a coral undergoing diagenesis. The black-stained right side with well-preserved coral texture is aragonitic while the unstained right side with obliterated texture is calcitic.

From Alietai Cave further southeast along the coast two voids formed along joints in a wall of a reentrant in the Tarague Limestone (Figure DEM, locations) are too narrow for exploration but still valuable for the research purposes. The first one, Batingting Void has formed along a junction of three joints (Figure 74). It has smooth walls and continues and ramifies further into the rock. The vertical of the three joints has another small enlargement further up and small niche with speleothems. The elevation of the top part of the ceiling is 7.5 m.

Figure 74 The triangularly shaped Batingting Void developed along the joint of two joints in the scarp of the first terrace above the backbeach deposits (Left of the explorer, at his shoulder height.). Note the high porosity of the rock.

The second one, Sesgao Void, has a bigger opening with smooth walls (Figure 75). Observations from the outside suggest that it has considerable continuation in a slightly down sloping direction. The elevation of the top part of the void is 6.8 m.

Figure 75 Sesgao Void. It formed where a vertical and horizontal joint merge.

The two entrances of Old Cove Cave were found in a 3 m scarp of the Tarague Limestone terrace (Figure 76). The lower entrance, that is big enough for human exploration begins with a downsloping oblique passage of NE-SW direction that ends with a ~1 m step and continues where it widens into a small chamber (Figure 77). This chamber has a down sloping continuation in the southeast that slowly thins out and fills up with rubble. To the more southerly direction the chamber continues and splits into sub-chambers, separated from each other by ~40 cm steps, giving a step shape form of the cave (Figure 77, profile A –A' and C – C'). Smooth cusps are observed on several places of the cave wall (Figure 78). In the central area there is a large flowstone formation (Figure 79).

The cave has another entrance that is ~1 m higher and has more or less the same NE-SW direction as the lower entrance. It is too low to crawl through though it widens and slopes down to the central part of the cave.

The bedrock of the cave is entirely coral reef facies limestone. Later cemented infills with fossil Gastropod shells can be observed in the cave.

The measured elevation was the ceiling of the higher entrance (7 m) (Figure 76), which also shows dissolutional features such as a smooth and cuspate ceiling.

Figure 76 The upper entrance of the Old Cove Cave.

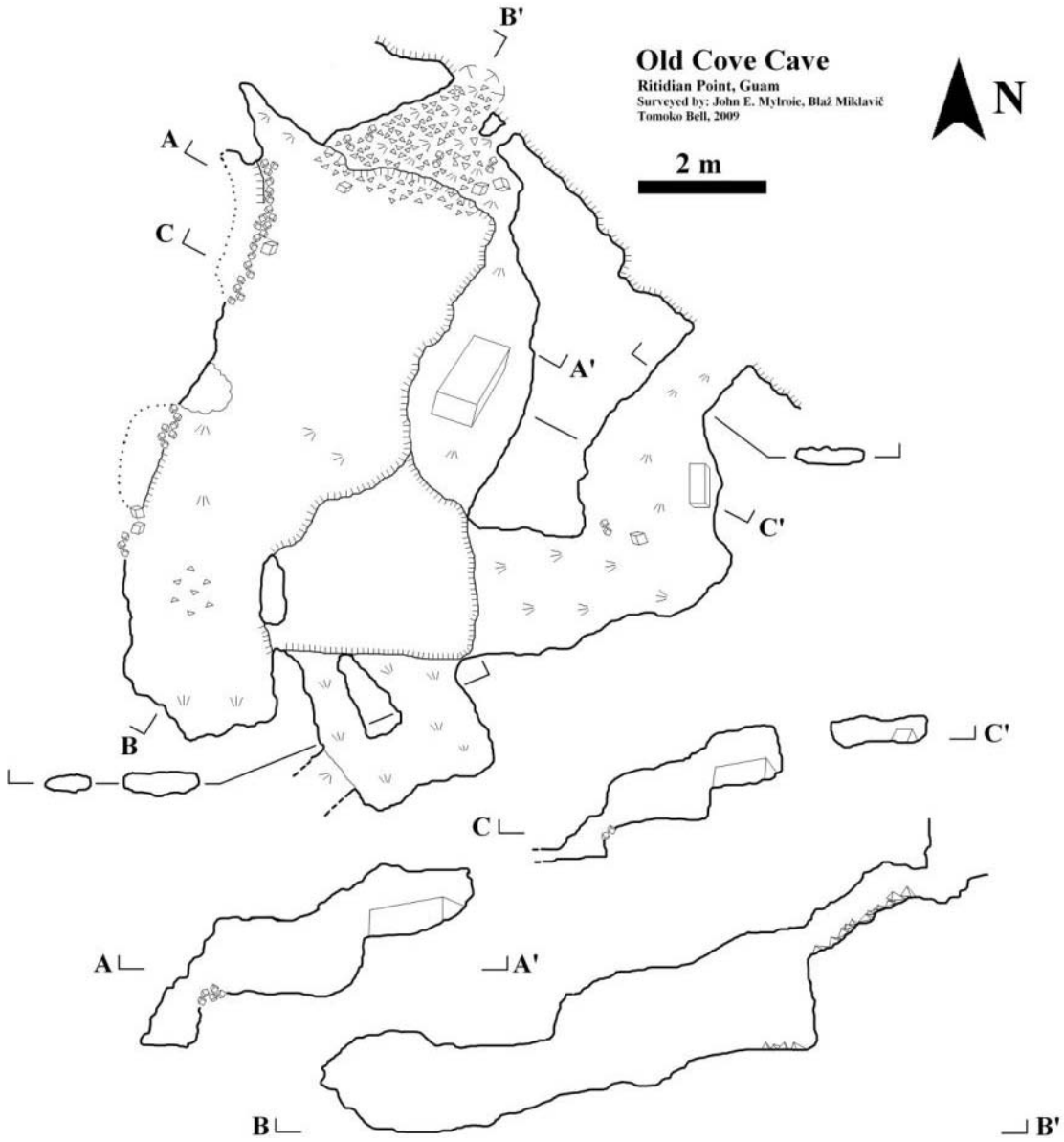

Figure 77 Map of Old Cove Cave.

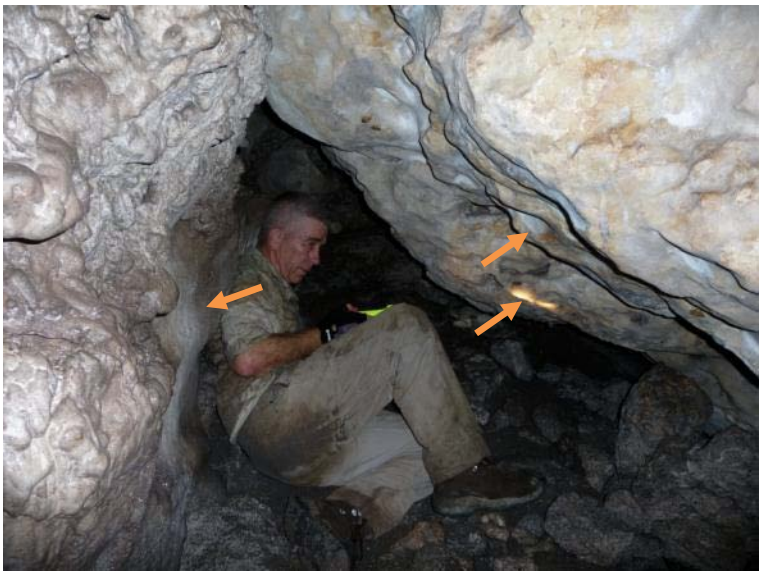

Figure 78 The interior of the Old Cove Cave. Note the smooth and cuspate (arrows) walls.

Figure 79 Flowstone formation in Old Cove Cave. The dates from the drilled cores (arrows) suggest an age older than 18 ka.

Similarly as for Tokcha Cave, Old Cove Cave entrances are followed by subhorizontal to oblique narrow passages that lead to the main chamber. No other caves were found further southeast along the coast to the Jinapsan Beach.

In none of the above caves was there any evidence of re-flooding of the caves, e.g. dissolved speleothems or other flowstone surfaces, actively dissolving cave walls etc.

The previously reported Jinapsan Cave and Ritidian Cave (Taboroši, 2006) are found at the top of the terrace near the base of the cliff. The entrances to both of the caves are ~20 m above the modern sea level and both caves extend down below to the fresh water lens. No signs of dissolution are observable on the bedrock or submerged speleothems at the lens level. Almost all the ceiling and walls in Jinapsan Cave are covered with flowstone so that the original bedrock cannot be observed. In a small part of the cave wall near the bottom of the cave the original rock is partly exposed. This rock is made of well-recrystallized coralline limestone. In Ritidian Cave there are more bedrock exposures but all are collapse surfaces. Because the original ceiling and cave walls cannot be (sufficiently) seen to determine their speleogenesis, the caves were not included in the study. They appear to be progradational collapse features from dissolutional voids at some depth below modern sea level.

Two cores were drilled in a flowstone deposit (Figure 79) and one of them was successfully U-Th dated to be 18,160 ±0.790 ka old (Appendix C). One sample had too much common Th (i.e. 232Th) for reliable dating. It should be noted, however, that none of the cores reached bedrock so that the actual age of the onset of that flowstone deposition must have begun prior to 18 ka.

Another cave with a buried entrance, Futon Cave, was found above Old Cove Cave. The cave occurs along an oblique crack and follows it for about 5 m and then pinches out. It has some speleothems but was found dry when entered. One of the speleothems grew over a gastropod shell. Joints similar to the one in the cave are found in

the surrounding area and seemingly follow the reef shapes. They do not show signs of dissolutional origin typical of flank margin caves.

Tarague embayment

For comparison, research was done also in the Tarague embayment where two caves were found in the research area. One cave (Well # 5) was previously described by Taboroši (2006) and revisited for the purpose of this research. The cave is almost entirely filled with rock blocks and a part of the cave extends down to the fresh water lens. An exploration of the cave from the top of the lens with mask and snorkel revealed that the cave continues under the water vertically and laterally and that there are plenty of angular blocks and rubble. The original dissolutional ceiling could not be observed anywhere in the cave so that the cave, was not included in the study. As with Ritidian Cave and Jinapsan Cave, it appears to be a progradational collapse.

The other explored cave is actually almost entirely breached. It has a semicircular shape and was hence named as Crescent Moon Cave. Only the ends of the semi circle are still preserved as a cave while the ceiling in the middle has collapsed. The floor is covered with beach sand mixed with organic matter and collapse rubble. In the north end of the cave there are plenty of stalactites. While the ceiling at the south end is clearly original dissolutional ceiling, the ceiling of the N end is a bit more ambiguous because of the speleothems. The maximum elevation of the ceiling of the south end of the cave was measured to be 7.3 m above sea level while the north end was measured to be 8.6 m above sea level. The original elevation of the ceiling between the two ends is unknown but it is safe to assume that it was not significantly different.

Ritidian-central and Ritidian-west

Caves in the cliff of the first terrace above the backbeach deposit in Ritidian-central and west area were also examined for comparison. These caves except for one were described and mapped by previous research in the area (Taboroši, 2004; Taboroši, 2006). Here only the details important for this research are pointed out together with the results of the elevation measurements.

In the Ritidian-central field area only one cave is present and was named Ritidian Gate Cave by Taboroši (2004). This cave located in the cliff nearby the NWR facilities, is known to be an archaeological site. Its interiors stretch high up beyond direct measureable height. This vertical extension is really narrow and could be of a vadose nature. Because of the above, no measurements were done at this cave.

A new cave, not previously reported, was found near the top of the cliff and was named Monitita Cave. One of the entrances is from the top of the terrace that is made predominantly of aragonitic limestone. A bigger entrance is from the cliff side, just below the top of the terrace and explorers can climb down along the trees that grow around the entrance, which were probably the reason the cave was previously overlooked. The floor and the ceiling of the entrance are connected with many pillars made of secondary calcite deposits. The cave ramifies inland and has small niches and dead-end passages and it continues to neighboring small caves in the cliff through small openings, typically for beads-on-the string type of flank margin cave pattern. The cuspate walls and ceiling have some speleothems and most of them show signs of re-dissolution as do all the caves in this cliff. The top of the ceiling was measured with a tape from a surveyed point on the backbeach deposit and found to be ~21.4 m above sea level.

In Ritidian-west area several caves are present in the cliff. The measured survey points on the ground below the cliff were between 4.2 and 6.0 m where talus was present. The ground material is mainly beach sand enriched with decomposing organic matter. Ritidian Beach Cave has the ground in front of it at the elevation at 5.9 m. The speleothems found in the cave show signs of dissolution. The ceiling of the cave is cuspate and shows no signs of collapse and was measured to be ~13.5 above sea level.

Another unnamed breached cave ~1 m below the top of the cliff also reported by Taboroši (2006) is found further southwest along the cliff. The elevation of the ceiling was measured to be ~18 m. Because only a small part of the cave survived the erosion care should be taken to consider that the elevation of the ceiling of the intact cave could have actually been higher.

The roof of an overhang just northeast from the Pictograph Cave (also named Star Cave, Carson, person. commun.) has the elevation ~12.8 m above sea level. The Pictograph Cave lays on the southwest side of a larger reentrant that is rimmed with small overhangs connected with the ground by secondary calcite columns. All of these columns are in an oblique position and only one column is truly vertical. The elevation of the ground in and around the remnant is anomalously high and exceeds 9 m. The ceiling of Pictograph Cave was measured to be 12.9 m but since the remaining cave is just a fraction of a once much larger cave that probably existed here and its ceiling has collapsed, the maximum elevation could have been higher.

Paleonotches

Paleo sea-level notches were observed along the coast and inland of the researched areas. Paleo notches in the coastal area were observed in the Ritidian-east

area, where they were also studied most extensively, as well as in the Tarague embayment while Ritidian east is mainly beach except for Achae Point. Inland notches were only studied in the Ritidian area. No inland exploration was done in the Tarague embayment. While the paleo notches near the coast are relatively uniform, the inland paleo notches are more complex and deserve a more thorough description.

Inland paleo notches

Inland notches were observed across the whole Ritidian area. All these notches are incised into the cliff wall and lay a few meters above the underlying terrace, which can be accessed by climbing the talus accumulated just beneath the cliff.

In the Ritidian-west area a double notch was observed on two sites. The southwestern most site (RWC-N1) has both of the notches well expressed, with the upper one being better expressed and deeper than the lower (Figure 80). Both stretch 20-30 m sideways. At the northwestern-most end, the lower intersects with small caves (Figure 80; 81). The distance between the notches measured from vertex-to-vertex is ~3 m. The upper notch is ~1.5 m high measured from the floor to the roof and ~1.5 m deep measured from the vertex to the edge of the notch with a very smooth surface. The lower notch is, on the other hand, typically >1 m high and ~0.5 m deep. In the upper notch, an aragonitic coral was found accreted in growth position to the inner part of the notch (Figure 82). Columns of either bedrock or flowstone, but most probably tufaceous deposits connecting the roof and the floor are also present in the upper notch.

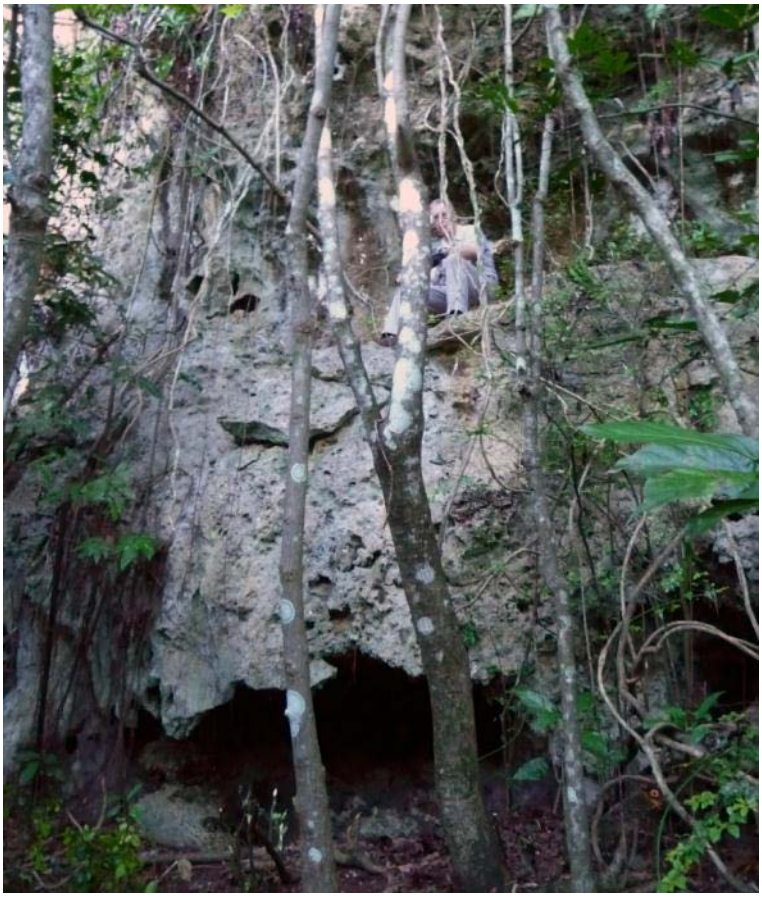

Figure 80 The upper and the lower notch RWC-N1. The lower notch at this point merges with a breached cave. The explorer in mimetic clothes is sitting on the upper notch for scale.

Figure 81 The lower notch at RWC-N1 extending 20-30 m laterally (arrows) and intersecting caves (where the explorer rests).

Figure 82 An aragonitic coral attached on the inner side of the upper notch at RWC-N1.

The second notch (RWC-N2, which was also named the Bedte Cave notch) in this area is a continuation of the RWC-N1 and there is just a short discontinuity between the two. The notches look alike and have similar dimensions as the notches at RWC-N1, and

the distance between the upper and the lower notch is as well ~3 m (Figure 83). Accreted corals, some in growth position and some not, were also found in the upper notch, which has as smooth a surface as observed at the upper notch at RWC-1. Stain tests showed that these corals are at least partly aragonitic. The elevation above the terrace could be measured at this site. The lower notch was ~5.5 ±0.5 m above the terrace and the upper notch thus ~8 m above the terrace. The elevation of the terrace, estimated with the help of DEM, is ~25 ±1 m above modern sea level implying a ~30 ±1.5 m elevation above the modern sea level of the lower notch and ~33 ±1.5 m elevation above the modern sea level of the upper notch.

Figure 83 The upper and the lower notches at RWC-N2. The upper notch is deeper than the lower.

Both of the notches are interrupted by the vertical entrance of the Bedte Cave, which is a cave that extends vertically about 15 m. North along the cliff, only the upper notch can be observed. It, however, disappears at the cliff promontory that is present there and then reappears after it. Closer examination revealed that though apparently

discontinuous, these two elevation-equivalent notches on both sides of the cliff promontory are actually connected by a narrow intricate cave passage, in one part barely wide enough for an explorer, that goes through the promontory. The notch on the northern side of this cliff angle has many columns of either bedrock or secondary calcite deposits (tufa/flow stone) connecting the floor and the roof and it is infilled with cobbles, some of them being rounded corals (Figure 84).

Figure 84 The continuation of the RWC-2 notch on the other side of a tortuous passage. Note the rounded coral cobbles on the floor.

The deepest notch is observed in Ritidian-central area (RWC-N3, "Babui Batku" notch, Figure 85). It is ~20 m long and has a more complex plan view morphology; while the part limited by the cliff end is pretty much a straight line, the inner part (the back/vertex of the notch) is very curvilinear with many indentations or niches (Figure 86). As a consequence of this uneven back-notch morphology the depth of the notch varies and is ~4.5 m at most, while the height is ~1.8 m and rather uniform since the floor and the roof are relatively flat. The roof and the floor are connected by several pillars and

other apparent speleothems were also observed. Hammering revealed that at least some of them are actually speleogens and only appear to be a true speleothems because of a calcite coating. The second notch was not clearly visible and only a speculative shallow notch could be observed below the “Babui Batku”. The elevation above the terrace was measured to be 6.6 ± 0.5 m while the terrace is ~20 ±1 m above sea-level by DEM estimates. The elevation of the notch is thus ~26.6 ±1.5 mabove sea level. In the wall below the northern end of the notch are many aragonitic corals.

Figure 85 Babui Batku cave notch from the side.

Figure 86 The inside of the Babui Batku. The explorer is looking at the coral cobbles on the floor. Note the uneven backnotch morphology with a small niche.

A prominent notch (RE-N1) is also observed in the Ritidian-east area in the surroundings of the Ritidian Cave (Figure 87). The notch looks analogous to the upper notch at RWC-N1 and RWC-N3 (Babui Batku) having columns connecting floor and roof and have the general characteristics of the tufa formations (Figure 87; 88). Inside the notch are true, and sometimes massive, speleothems that are potentially datable (Figure 85). The distance between floor and roof is ~2.8 m, and maximum depth of the notch is ~2.6 m. It extends laterally about 20 m though not with the same depth and its vague continuation can be seen with interruptions even further. No notches have been observed above or below. The notch is ~7 m above the immediate ground made of talus that (Figure 84) is ~1 m above the elevation of the terrace flat on which the talus lays. This terrace flat is deduced from DEM with the location determined with a GPS unit, ~20 ±1 m above the modern sea-level. The notch is therefore ~28 ±1 m above the modern sea level.

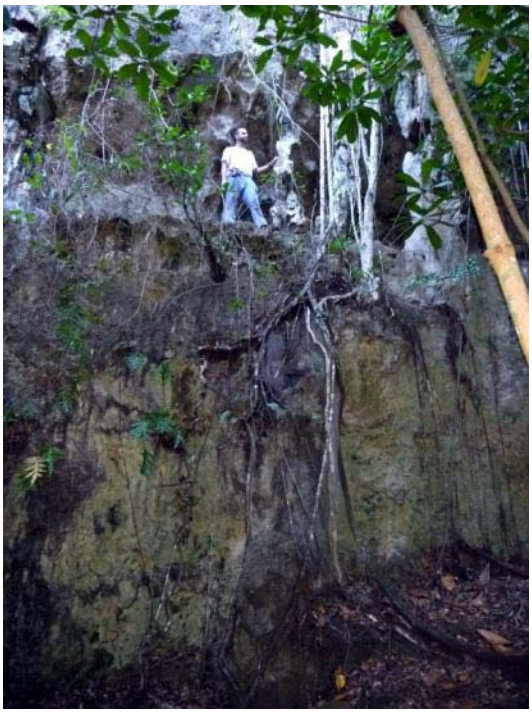

Figure 87 The RE-N1 notch ~7 m above the immediate tallus ground and ~8 m above the terrace. The explorer (for scale) is leaning on a tuffa column.

Figure 88 The inside of the RE-N1 notch. Note the tuffa columns and the true speleothem on which the hammer is laying.

Coastal Paleonotches

In the Ritidian-central area a set of paleo sea-level notches was found in a ~9 m cliff emerging from backbeach deposits about 80-100 m from the coast. The cliff is made of solid, dense, and well recrystallized limestone. The exposed notches were found at the southeast end of this cliff where it changes into a 1 to 2 m scarp with at least partlyaragonitic corals as shown by the stain tests. Because the notch is cut deep in the rock, measurements were possible only where fractures cut the notch and vertical indentations exposing the cross section are present (Figure 89). The vertex of the notch around these fractures, however, was somewhat elevated to the vertex elevation away from the fractures. Three points were measured, two of them near the fractures with elevations of 4.88 and 5.08 m. Measurement away from the fractures was possible only at one site. Elsewhere, the deeply cut notch made it impossible to set the measuring staff close to the vertex. At this one site, the elevation of the vertex was at 4.47 m. The elevation of the backbeach deposits in the area is 4 to 4.5 m (Figure 24), so any lateral extension of this notch to an elevation lower than this is covered by these deposits.

Figure 89 Different vertex positions, the highest being near the vertical indentation delineated by the fracture (right side of the picture). A vertical indentation into the notch exposing its cross section on the right side of the picture.

Three notches were found in the Ritidian-east area in the scarp of the first terrace above the backbeach deposits.) The first notch (RE-N1) is a ~25 m long notch in a ~1.5 m scarp sticking out of the backbeach deposits (Figure 90). Because the scarps are far enough from the storm berm, the elevation of the backbeach deposits drops below 4 m allowing the notch to be exposed. The scarp is also not parallel to the modern beach and field observations suggest that it must have formed a sheltered, southeast side of a paleo reentrant. Measurements were made at three sites approximately 5 to 8 m one from the other and three to five measurements at each site. The values spanned from 4.03 to 4.41 m above sea level, with the average of the site being 4.23 m, rounded to 4.2 m.

Figure 90 Notch RE-N1. Note the retreat of the roof of the notch evidenced also by the rubble on the ground.

The second notch (RE-N2) is located at the inner edge of the southeast side of a small reentrant and is 2-3 m long. The notch is cut into a coral limestone (e.g. Figure 32; 36) with at least partly aragonitic corals as shown by stain tests and its roof has evidently undergone some erosion. In spite of the coralline facies the notch surface is very smooth. Just below the notch there is a young limestone deposit, which is, by facies comparison, the mid-Holocene Merizo Limestone. The vertex of the notch is quite uniform and givien the small notch, only one measurement was taken (4.14 m, rounded to 4.1 m).

The last measured notch (RE-N3) in Ritidian-east area is located just above another Merizo Limestone deposit (Figure 91). It is located at the inner side of what it appears to be a paleo headland and is ~3 m long. Measurements were made at two sites along this notch, two measurements at each site with the span between 4.14 and 4.33 m and average 4.21

Figure 91 RE-N3 notch – a classic notch.

For comparison, coastal paleonotches were also measured in the Tarague embayment. One paleonotch (Tg-N1) was measured on the northern side of Mergagan Point. The notch is located above an exposed Merizo Limestone deposit (according to Siegrist and Reagan, 2008) and extends laterally several tens of meters, but the elevation of only one site at its southern- most end was measured. The three measurements span from 3.83 to 3.92 m, with the average being 3.88 m, rounded 3.9 m.

The second measured notch (Tg-N2) is located on the southern side of Mergagan Point in a cliff few meters above the ground with no Merizo Limestone (reef deposit) in front of it. Two measurements were taken at one site with values 4.46 and 4.58 m and average 4.52 m, rounded 4.5 m. As a peculiarity, a notch was observed also around a boulder at Mergagan Point which was ~1 m higher on the side facing the ocean than on the side facing the land. The lower of the two notches was measured to be 3.2 m above sea level, so the upper notch was 4.2 m above sea level. Similar occurrence was observed

in modern mushroom rocks in Haputo and Tanguissan. Because of the unknown relationship of these notches to sea level, they were left out of the notch analysis.

In Ritidian West all the measured points on the ground along the cliff, which is also the lowest part of the area with the storm berm near the coast being the highest, exceeded 4 m in elevation (from 4.2 to ~6 m where talus was present), so if there are notches of mid-Holocene origin, they are covered. No other notches were observed in the land-surveyed area but there is a paleonotch in the cliff just where the road connecting the Guam National Wildlife Refuge facilities with the rest of the island descends this cliff. The elevation of the ground here is ~4.2 m (from DEM analysis) and the top part of a roof of a paleonotch can be observed just above the ground (Figure 92) while a more evident notch is 5.5 m above the ground measured with a tape, making the total elevation of the notch ~10 m above sea-level. This notch is considerably high (floor to roof) and mostly obliterated.

Figure 92 The top of a probable notch buried below the backbeach deposits (lower arrow) and a notch 5.5 m above the ground (upper arrow) or ~10 m above the modern sea level.

Prominent sea-level notches about 2 m higher than the present notch are observed all around Guam. These are the most prominent and well preserved notches on the island. For comparison, one of these notches was measured in Pago Bay.

Figure 93 The modern (lower arrow) and paleo (upper arrow) sea-level notch in Pago Bay.

Modern sea-level notches

In order to fully understand the relation between the modern sea-level and sea-level notches, the notches in the research area at Ritidian-east (Figure 9, Table 3) and Pago Bay were selected for study (Figure 93, Table 4). The latter were selected to test a potential variation in elevation with the distance, because the site is in a sheltered area and should thus give the most representative results (Pirazzoli, 2007,) and because of convenience of the nearby benchmark network. Because the shore is a cliff in Pago Bay, the modern notch and the near paleo sea-level notch are one above the other and comparison of the elevation of the two was possible at the same site. Here all the measured sites were within 30 m of the shoreline. At Ritidian-east notches at headlands

were avoided. The measured sites were along ~1 km of coast. Sites that have the same number but different letter in the table were measured from the same initial station/reference point and are thus relatively close to each other. The results are summarized in the tables below.

Table 4 The measured elevations of the modern notch at Ritidian-east.

Site	Measured pt. (m)	Average (m):
104c	A: 0.60 B: 0.61	0.61
103b	A: 0.66 B: 0.68 C: 0.73	0.69
103a	A: 0.73 B: 0.77 C: 0.78	0.76
104a	A: 0.80 B: 0.76 C: 0.77	0.78
104b	A: 0.71 B: 0.68 C: 0.66	0.68
35	A: 0.56 B: 0.52	0.54

Table 4 (Continued)

34b	A: 0.60	0.60
23a	A: 0.49	0.49
23b	A: 0.35	0.35
Tot. avg.		0.61

Table 5 Measured elevations of the modern notches in Pago Bay.

2	A: 0.35 B: 0.36	0.36
3	A: 0.54 B: 0.51	0.53
4	A: 0.40 B: 0.47 C: 0.43	0.43
5	A: 0.35 B: 0.37 C: 0.39	0.37
6	A: 0.61 B: 0.47	0.54
Tot. avg.		0.45

Reef outcrops

The highest points of the most prominent and accessible outcrops of the fossil coral reef form the lowest terrace in the Ritidian-east area. The highest outcrops are always composed of fossil algae and were previously described as the coral-algal ridge of the Merizo Limestone (Randall and Baker, 1989). The analogous facies are observed today at the reef margin and are visible above the sea level, even at high tide.

The highest point of a beachrock outcrop was also measured for comparison with similar outcrops in the Tarague embayment. The elevation of this outcrop was measured to be 1.85 m, rounded 1.9 m above the sea level.

Table 6 Measured elevations of the Merizo Limestone algal-ridge facies limestone ioutcrops.

Site	Measured value	Rounded value
28 (AR1)	3.575	3.6
38 (AR2)	3.862 + ~ 0.15	4.0
39 (AR3)	3.749 + 0.134	3.9
41 (AR4)	3.670 + 0.445	4.1

CHAPTER V

DISCUSSION

Geomorphological comparison of the examined areas

Ritidian areas and Tarague embayment

A brief comparison of the areas east and west of Ritidian Point (Fig. 24) reveals a notable difference. While on the western side there is a well-developed set of wide terraces, there are only three barely distinguishable terraces on the eastern side. The MIS 5e terrace at Ritidian-east is separated from the Holocene backbeach deposits by a small scarp while at the Ritidian-west the terrace adjacent to the Holocene deposits (and the presumed underlying Merizo Limestone) is separated from the MIS 5e terrace behind it by a ~20 m cliff.

Further, at Ritidian-west a broad storm-deposit flat with two well-developed storm berms is present while at Ritidian-east a relatively narrow storm-deposit flat with a narrower and lower storm berm in the northwest part occurs. Both thin out and disappear towards the southeast.

Counterintuitively, the prevailing trade winds and the waves associated with them come from the northeast, and so backbeach deposits would be expected to be more abundant in the Ritidian-east area. Further, the wind coming from the typhoons, even if variable from typhoon to typhoon, would be expected to be in general more powerful on the east rather than then the west side of the Ritidian Point (Lander, person. com.). It could be that the more exposed side has a more erosional nature while the western,

leeward side, has a more depositional nature. However, the waves that can deposit more than 6 m high sand deposits must be sufficiently strong and high. Similar logic applies to the terraces because they cut into the cliff more significantly on the western rather than eastern side. Another possible reason could also be a different uplift/subsidence history of the two sides. However, no measurable displacement was observed at the top of Ritidian cliff where a fault was mapped by Tracey et al. (1964) and Siegrist and Reagan (2008).

Regardless of the reason for the east-west disparity, the contemporary situation seems to be analogous to the MIS 5e condition. There is just a narrow Holocene (mid-Holocene) flat and low terrace at Ritidian-east, just as it is narrow at the top of the MIS 5e terrace. In some areas the almost continuous slope ends in the sea. On the Ritidian-west, on the other hand, the Holocene flat is wider and completely comparable with the width of older terraces. It could be that the abundant backbeach deposits play a key role in terrace formation as they protect the underlying fossil reef flat from erosion. As it is today it might have been in the past as well.

The Tarague embayment area has the same morphology as Ritidian-east. A notable detail, present on both sites, Ritidian-east and Tarague embayment, is the steep break of slope on the MIS 5e terrace. The slope break is probably remnant of a later sea-level stand. The same sea-level stand should have left a sea-level signature in the 20 m cliff at Ritidian-west.

Ritidian cliff

The displacement along joints observed in Ritidian Cliff cannot be determined with confidence because of intense karstification, thick vegetation, rock collapses along the edge of the cliff and considerable dissolutional erosion evidenced by relict caves of

which mainly just the cave floor is observable today. All the above factors obscure the evidence of any possible displacements that could have occurred in the observed area. At the same time, however, all these processes give an insight into the cliff retreat mechanisms and explain phenomena such as talus and boulder accumulation at the foot of the cliff.

Since the cliff is vertical from the bottom to the almost the very top it means that the lateral erosion or cliff retreat is more or less equal vertically along the cliff. If the erosion was more concentrated along the top of the cliff, the cliff would tend to deteriorate into a steep slope.

The low terrace (fossil reef)

Interpretation of the geology

By facies comparison with the dated locations of the mid-Holocene Merizo Limestone, e.g. in the Tarague embayment, it can be concluded that the fossil reef observed along the the Ritidian-east coast that forms the lowest terrace and is often covered with backbeach deposits is also the Merizo Limestone as also concluded by Randall and Baker (1989). The elevation of the exposures are, however, anomalously high.

The first terrace above the backbeach deposits – Ritidian-east

The first terrace above the backbeach deposits in Ritidian-east is completely analogous in morphology and its elevation to the terrace in Tarague embayment where two corals were dated to be of MIS 5e age (Randall and Siegrist, 1996). On both terraces the corals are made of at least partly if not mostly aragonite as confirmed by stain tests and quantitative XRD analysis. In contrast to the fossil corals found at higher elevations

where aragonite is rarely present. In addition, the rock has a relatively unaltered and just partly recrystallized appearance with a distinct yellowy color as opposed to the older limestones' snow white appearance. Therefore it can be concluded that the rock forming the first terrace above the backbeach deposits at Ritidian-east is also the MIS 5e Tarague Limestone (Figure 94; 95).

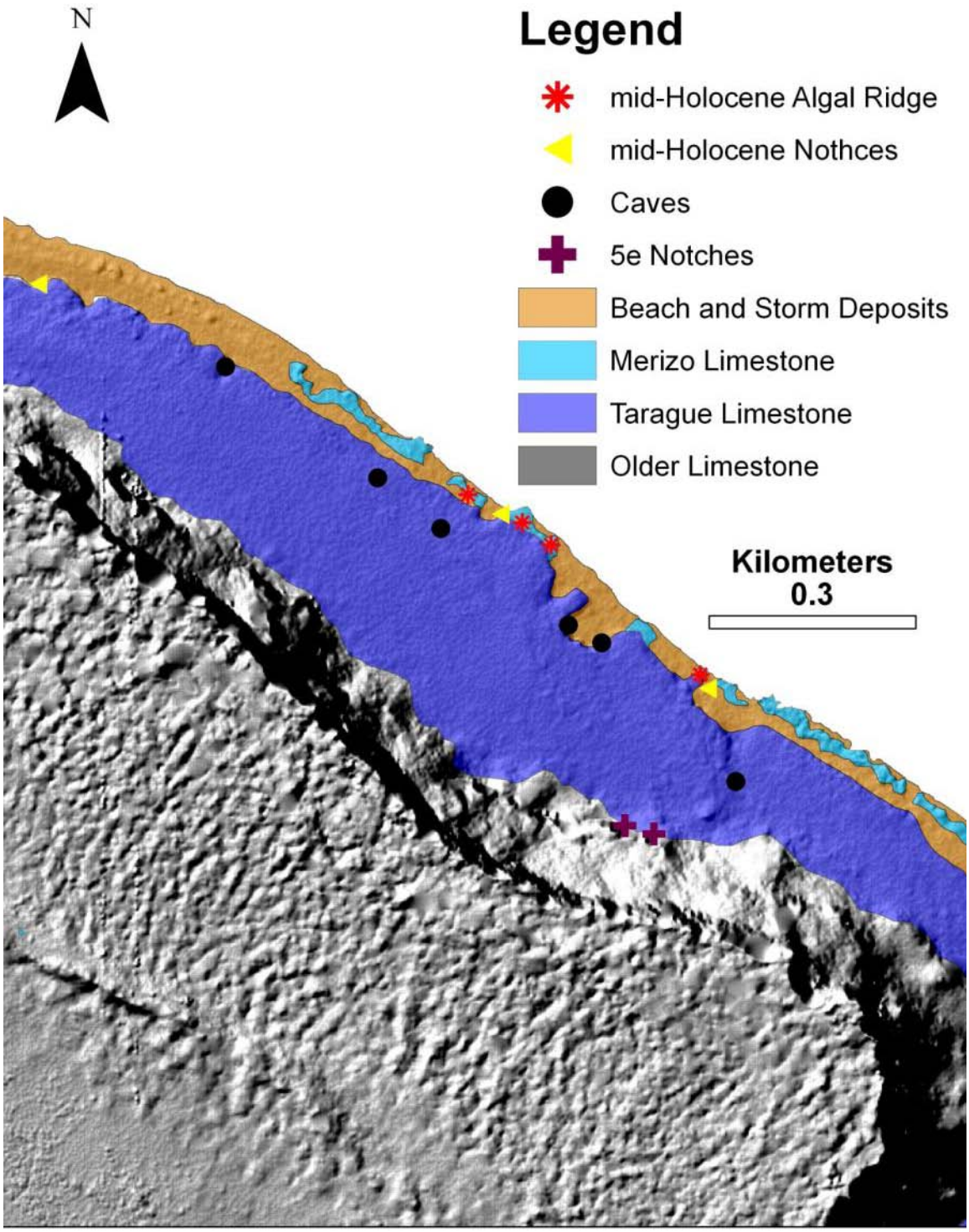

Figure 94 Geologic map of Ritidian-east.

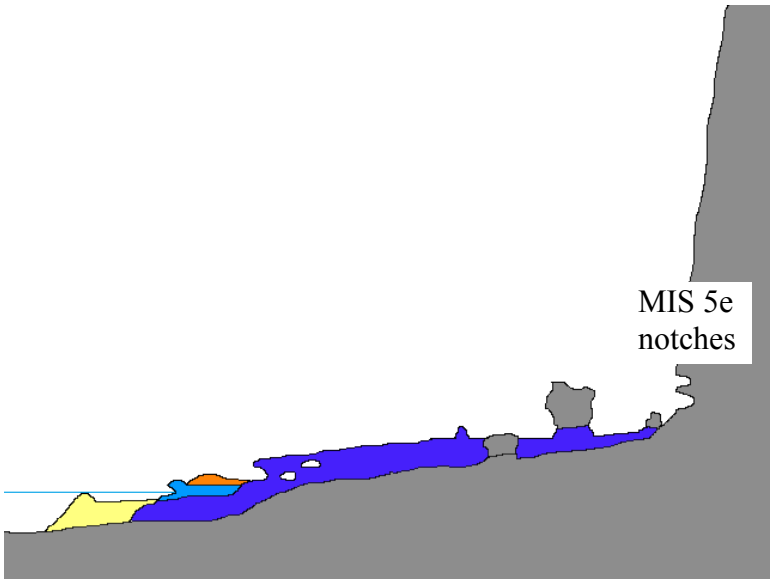

Figure 95 A schematic profile of the Ritidian east profile. The profile is not in scale and the thicknesses of different geologic units are arbitrary/interpretative.

The seemingly anomalous outcrops of well recrystallized rock that are found near the Ritidian cliff can be interpreted as exhumed pre-MIS 5e topography of the older Mariana Limestone. Typically reef deposits are thin near the shoreline (cliff) and can be thus eroded faster there when exposed to the surface. This outcrop occurs near the cliff where plenty of boulders have been falling off the cliff, some of them very big. Such boulders had been almost certainly falling off the cliff during the MIS 5e reef deposition, and were partly to completely buried by its growth and latter exhumed by surface erosion.

The first terrace above the backbeach deposits – Ritidian-central and –west

Although the cliff of the seaward edge of the terrace is interpreted to be made of the Mariana Limestone, the limestone above shows all the distinct features of the Tarague Limestone mentioned above. The 3 m pinnacle observed below the terrace that sticks out of the backbeach deposits (Figure 35) is also most probably made of Tarague Limestone.

The terrace, however, on this side of the Ritidian Point was preexisting and a reef veneered the top of it when the terrace was submerged during the MIS 5e. So did the corals that form the 3 m pinnacle that grew right below the terrace, perhaps on the pre-existing Pleistocene terrace mentioned by Randall and Baker (1989) which the modern reef laps on. The lack of the well preserved reef deposits containing aragonitic corals on the first terrace above the backbeach deposits in the area near the Ritidian cliff could be solely due to erosion that entirely stripped away the Tarague Limestone veneer. Such an outcome could not occur in the Ritidian-east area because at this locality the terrace is constructional, i.e. formed by carbonate deposition while in the Ritidian-west area there was probably only a thin veneer on the preexisting erosional terrace (i.e. formed by the sea eroding into older rock). Further down slope on this terrace the Tarague Limestone deposits could be thicker and they could actually be preserved.

Interpretation of surface denudation indicators

Inerpretation of the surface relief

The origin of the highstanding features (e.g., Figures 45 to 52) is not completely clear. Their significance as indicators for dissolutional denudation is also not clear. Those with more or less pinnacle-shaped geomorphic structures that are a consequence of higher dissolution along preferential flowpaths and higher dissolution rates in depressions where organic rich material accumulates are interpreted as karst pinnacles. The initial reef topography could have provided the initial depressions that would serve as traps for organic material and preferential drainage through these depressions or parts of the reef with higher porosity. This could well be the case of Ritidian-central and some parts of Ritidian-east where such features are evidently aligned and separated by depressions

(Figure 47; 48). These aligned features could be remnants of reef buttresses or spur and groove reef morphology. In some places the erosion might have totally obliterated the initial morphology, leaving behind just isolated pinnacles or knobs that appear to be random as a consequence. This would also explain why pinnacles tend to occur near the sea-ward edge of the terrace. The isolated 3-m pinnacle at Ritidian-west standing above the backbeach deposits could also be at least a remnant reef structure though its isolated occurrence is difficult to explain.

The pinnacles and other highstanding features found near the base of the cliff could be pedestals which recently lost the covering boulder by dissolution. This would explain why pinnacles tend to occur near the cliff but not immediately under the cliff where the tropical *Karrentische* usually occur. The oldest boulders would in fact lay the furthest from the present cliff since they must have fallen before the cliff retreat moved the cliff to its present position. If the boulders had fallen from the cliff while a possible sea-level stand was at or above the present terrace; level, the boulders could have been moved seaward by storm waves.

A contributing reason for the overall scarcity of pinnacles and their total lack in most part of all the areas could be the enhanced physical weathering owing to the activity of the thick vegetation (Figures 29; 33; 48; 51; 54) present in nearly all the studied field areas. The growing roots of the trees following moisture and soil along fissures and other small depressions could contribute to the disarticulation of the bedrock and leveling of the surface.

The anomalously high pinnacle (Figures 51; 52) found at the eastern margin of Ritidian-central area can be explained in many ways. It could be a tropical Karrentsich of

which the boulder totally dissolved away or crumbled. Evidence of the cap-rock, however, was not found in the surrounding area.

The fossil assemblage of the rock at the very top of the pinnacle suggests that this rock was deposited as a detrital facies in the algal ridge zone. It is very dense with very low porosity compared to the surrounding rock and as such it could have slowed down the denudation. If we take into account the mean rainfall for northern Guam without evapotranspiration, assuming zero porosity for the top rock of the pinnacle and 30% porosity of the surrounding rock, and considering that both rocks are bare and aragonitic, the denudation rate for the top rock would thus be 39.3 mm/ka while the surrounding rock would dissolve at a rate of 56.2 mm/ka, resulting in ~2 m difference in denudation in 116 ka or ~3 m if the porosity of the surrounding rock was 40%. If we consider that all the decomposing organic detritus is washed away from the top parts and is accumulated on the ground, higher can be considered for the surrounding rock and therefore higher dissolutional denudation rates can be expected. Though at a glance, the surface has no soil cover, there is plenty of decaying organic detritus under the bare rubble seen on the surface. For a rock with 30% porosity and of normal soils (= 10-2.5 atm) the denudation rate would be 121.1 mm/ka resulting in ~9.5 m difference in denudation in 116 ka compared with the top rock of the pinnacle (0% porosity) and 7.5 m with a rock with 30% porosity with all other conditions being the same (rainfall, temperature, mineral composition). Therefore, pinnacles ~6 m high are theoretically possible.

Another possibility is that this pinnacle evolved from a predisposed reef morphology, e.g. that it was formed as a pinnacle-shaped coral build-up and that the subsequent denudation just enhanced the predisposed form. Its fossil biota, however, suggests that if the initial morphology played a role, it was not decisive. The initial rock

seems to have been made of two reef ridges about a meter from each other (possibly two buttresses or spurs) such that the channel between them was filled with corals torn from their substrate (Figure 52; 96). This rock that formed out of this infill channel was subsequently eroded giving a truncated appearance to the fossil channel infill indicating that the initial form did not play a major role in the formation of the present pinnacle (Figure 97). Also, the outcrop is also truncated in the front, i.e. on Figure 52 we see a cross section of the ridge-channel configuration while its longitudinal continuation is also truncated.

Given all the above and the model of pinnacle formation presented in Figure 23, it can be concluded that the initial topography can compensate the difference between the actual and minimum denudation. The 6.1-m pinnacle on Figures 51 and 52 would thus represent the actual denudation since MIS 5e maximum. It is difficult, however, to estimate the initial topography, neither is the actual denudation of the pinnacle relative to the surroundings certain. Thus it is safe to assume that the denudation as evidenced from the pinnacle in Figures 51 and 52 in the range between 4 to 8 m. In case the pinnacle is formed as a pedestal of the former *Karrentisch*, its height represents the minimum denudation since MIS 52, i.e. 6.1 m.

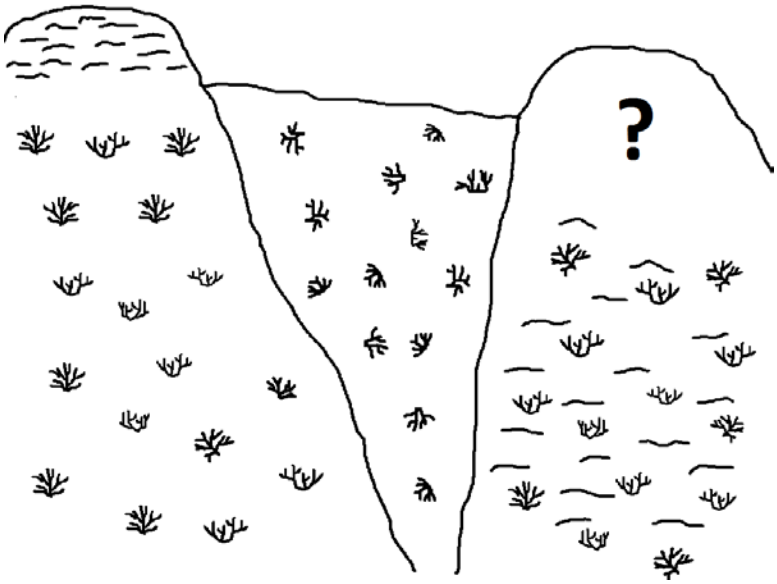

Figure 96 A sketch of a possible reconstruction of the pinnacle in Figure 52.

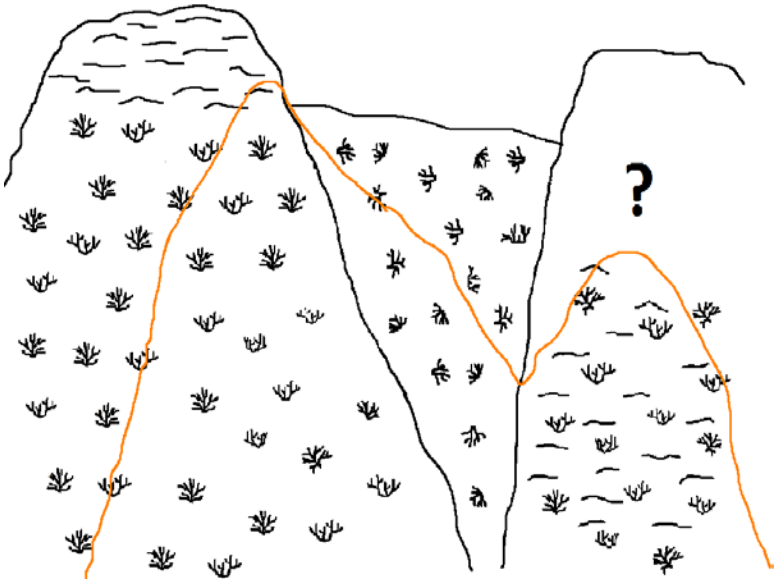

Figure 97 In orange there is the outline (schematic) of the present pinnacle in Figure 52. In spite of the probably predisposed morphology of the pinnacle the present shape is a result of considerable differential denudation.

The 3-m pinnacle emerging out of the backbeach deposits at Ritidian-west just off the cliff of the first terrace above the backbeach deposits (Figure 35) is not easy to

interpret either. Because the corals that dominate it are still at least partly aragonitic and because of its elevation, it is probably coeval with the higher limestone on the first terrace above the backbeach deposits. It was probably part of the reef that accreted to the preexisting terrace. The reasons why it is so isolated and remained preserved are fewer in this case. Given its position and elevation, it is unlikely that it was a pedestal from which the boulder was dissolved or fell off, though this interpretation cannot be totally excluded. No difference in lithology was observed between the top and bottom of the pinnacle though the existence of a denser layer of limestone on the top cannot be totally ruled out since such a layer could have been dissolved away already. A coral build-up that was later modified by erosion, however, seems to be the most plausible explanation. What and how much was denuded is difficult to estimate since the original morphology is not known.

In conclusion it can be said that in spite of a variety of possible interpretations, the highstanding features can give a rough estimate for denudation since the subaerial exposure of the limestone surface. Considering all the field observations of the highstanding features, it is safe to conclude that there has been at least ~6 m of denudation though the described evidence allows this value to be much higher.

Interpretation of the tropical *Karrentische* as denudation indicators

From the observation of the lithology of the *Karrentische* it can be concluded that the boulders originate from the Ritidian cliff made of the Mariana Limestone, while the pedestals are most probably the MIS 5e Tarague Limestone. The boulders fell off the cliff onto the MIS 5e terrace, and protected it from dissolution at the expense of the dissolution of the boulders themselves. It could be argued that the existing boulders have

been recrystallized by meteoric water, while the pedestals beneath were in relative hydrologic "shadow" and therefore the digenetic processes would be faster in the boulder rather than in the pedestal. But the unprotected surrounding rock is just as aragonitic and diagenetically immature as the pedestal rock. Therefore the diagenetic state of the boulders almost certainly reflects their original condition prior to their falling off the cliff. This advanced diagenetic state, relative to the underlying Tarague Limestone, helped to accentuate the difference in denudation of the boulder, versus the Tarague Limestone. The morphology of some smaller *Karrentische* indicate that the capping boulder could not have lost as much mass or it would no longer exist; a larger boulder would have resulted in a different pedestal morphology.

The fact that the date at which the boulders fell on their present position could not be older than the underlying limestone gives a time constraint to the pedestal formation. Because they lay on the top of the terrace, the limestone beneath must have formed around the peak of the MIS 5e highstand, approximately 125 ka ago. The boulders could have also been placed at their current position while the limestone was still forming on a shallow reef flat. In such case, they could have been at least partially overgrown and later exhumed by surface denudation of the surrounding rock. In such case, the actual denudation would be even higher than that reflected in the height of the pedestal.

Though the typical height of the highest pedestals is ~0.5-2 m, one pedestal (Maipi Fina' Mames, Figure 56) is ~5 m high and is probably the best estimation for the denudataion since MIS 5e. The reason why no other pedestals that high are found in the area could be in the composition of the boulders; these are made of limestone as well as the pedestals and therefore subject to dissolutional erosion as well. Hence, if not especially big, they would get dissolved away or become unstable and even crumble and

fall off the pedestal. Such pedestals would then be reshaped by dissolution and without a boulder they would look like a karst pinnacle. This outcome would be progressively expected on the terrace the farther from the Ritidian cliff.The top of the Maipi Fina' Mames pedestal would, given its position on the top of the MIS 5e terrace, represent the best approximation to the original surface of the MIS 5e while the height of the pedestal would be the best approximation for the denudation since the MIS 5e. It is not known, however, when the boulder was placed on its current position, whether it was before the MIS 5e peak and the boulder was exhumed or at the maximum of the MIS 5e, or sometimes later. From the observation of the tropical *Karrentische* it can be concluded that the denudation since MIS 5e highstand has been at least ~5 m.

Interpretation of the sea-level notches

Modern notches

The elevation of the vertices from most of the measured sites at Ritidian-east seem to reflect the Mean High Water (MHW) or Mean Higher High Water (MHHW) though notches reflecting mean sea-level are also present. The maximum difference between the measured sites is 0.43 m, which covers the range from less than the average MSL to higher than the MHHW. The notch vertices in Pago Bay, on the other hand, seem to cluster around mean sea level. The reason for the difference between the two sites could be in the configuration or combination of the coast and sea dynamics. While Pago Bay is a well-developed and protected bay, the Ritidian-east coastline is generally straight; the measured notches were located in small reentrants. Moreover, wave attack at Ritidian Point is much stronger–even though the shoreline is protected by the reef flat, the effect of the waves is pronounced along the shoreline during high tide.

Another explanation for the difference in elevation between the Ritidian-east notches and Pago Bay notches could lay in the tectonics; since the evidence shows that the northern most part of the island has been rising at a relatively high rate compared to other parts of the island, the somewhat higher notch vertices could have been already uplifted, though no consistent specific notch morphology that would support this interpretation was observed. The measured notch in Pago Bay has a low scatter (0.18 m), owing to fewer measurements and smaller spatial distance between the measured sites. The distance between the modern and the paleo sea-level notch is ~2 m. The vertex of the observed part of the paleo sea-level notch appears to be very uniform, which was confirmed by field survey.

The elevation of the vertices from most of the measured sites at Ritidian-east seem to reflect the Mean High Water (MHW) or Mean Higher High Water (MHHW) though notches reflecting mean sea-level are also present. The maximum difference between the measured sites is 0.43 m, which covers the range from less than the average MSL to higher than the MHHW. The notch vertices in Pago Bay, on the other hand, seem to cluster around mean sea level. The reason for the difference between the two sites could be in the configuration or combination of the coast and sea dynamics. While Pago Bay is a well-developed and protected bay, the Ritidian-east coastline is generally straight; the measured notches were located in small reentrants. Moreover, wave attack at Ritidian Point is much stronger–even though the shoreline is protected by the reef flat, the effect of the waves is pronounced along the shoreline during high tide.

Another explanation for the difference in elevation between the Ritidian-east notches and Pago Bay notches could lay in the tectonics; since the evidence shows that the northern most part of the island has been rising at a relatively high rate compared to

other parts of the island, the somewhat higher notch vertices could have been already uplifted, though no consistent specific notch morphology that would support this interpretation was observed. The measured notch in Pago Bay has a low scatter (0.18 m), owing to fewer measurements and smaller spatial distance between the measured sites. The distance between the modern and the paleo sea-level notch is ~2 m. The vertex of the observed part of the paleo sea-level notch appears to be very uniform, which was confirmed by field survey.

Inland sea-level paleonotches

Field study of the double notch present at two sites (Figure 80; 83) at Ritidian-west suggests that they had different origins as paleo-shoreline indicators. The upper—and always the better expressed—paleo-notch appears to be a set of coalesced, "beads-on-a-string", breached flank margin caves. All of the better expressed notches were probably formed by the same sea level, and the differences in elevation between the notches at Ritidian-west and Ritidian-east probably reflects error in the elevation measurements (especially of the reference points on the terrace) or/and due to the Ritidian fault. The relative elevation above the terrace shows less variation, as would be expected if the latter is true.

Evidence in support of the flank-margin-cave origin of the upper notch is the uneven back-notch morphology, especially at the Babui Batku. Other very convincing evidence of a flank margin cave origin of the notch is the connection of the two apparently separated notches by an intricate passage at the Bedte Cave notch. Last but not least, speleogens and true speleothems were found in Babui Batku and at the Ritidian-east notch, which is also a clear indicator of a flank margin cave origin. The caves must have

been breached during a sea-level stand that was at approximately the same level as the caves, as evidenced by the rounded ancient coral cobbles found in Babui Batku and Bedte Cave notch. These cobbles must have been washed into the breached caves by extant

wave action. It is possible that the caves were breached during the same sea-level stand during which they were formed, and that the prolonged lateral erosion or inland progradation of the sea-level notch during the stand breached the caves, as we observe along modern Guam's shoreline (Figure 16; 17). In such cases, the cliff retreat after the sea-level drawdown must have been minimal, perhaps only few meters, in order for these caves to be partially preserved today, at least in the area of these breached caves. The relatively low talus accumulation near Babui Batku and the near absence of talus below the Ritidian Cave Notch supports such a hypothesis. Ancient shoreline in which there is no notches observed could reflect either complete removal by erosion or burial under high talus deposits, which would also indicate a faster cliff retreat. Cliff retreat is faster, of course, when the sea is present at the pediment, undercutting it with the sea-level notch. Once the sea level moves away from the cliff, the cliff retreat slows down as the undercutting ceases.

On the other hand, the notch observed *below* the *cave notch* (i.e., coalesced breached flank margin caves appearing as sea-level notches) in Ritidian-west exhibits characteristics of bioerosional sea-level notch; it has a more uniform morphology, and no speleothems. Such notches are more prone to lateral erosion, which would explain why it was found only at two sites relatively close together.

Because this set of notches is the only ones observed above the reef terrace, it probably formed during the same sea-level stand. That the notches do not lie immediately above the terrace, but rather some 6.5 to 8 m above it, must be due to the terrace surface

having been lowered by denudation of the reef. The theoretic estimations discussed in section 2.7.1 as well as field evidence for the amount of denudation (karst pinnacles and *Karrentische* pedestals) since MIS 5e is in good agreement with the elevation difference between the notch and the terrace.

Another question is why there are two notches, and why one is actually a cave notch, while the other is apparently a true sea-level notch. One possibility is the hydroisostatic response of the Pacific Basin to the previous refilling of the ocean after the penultimate glacial cycle (MIS 6 to MIS 5) was identical to the most recent one (MIS 2 to MIS 1). Just as there was a sea-level drawdown after the mid-Holocene maximum, the same drawdown could have, indeed most likely did, accompany the rise of the sea level to the MIS 5e level, leaving two notches, just as observed all across the Pacific today . The ~3-m difference between the observed set of MIS 5e notches is comparable to the ~2 m difference between the modern and the mid-Holocene sea-level notches. The presence of ancient coral cobbles in the MIS 5e notches suggest that the highstand persisted long enough for lateral erosion to breach the newly-formed caves and wash in the coral cobbles. Breached mid-Holocene caves with washed-in material can be seen in Talafofo Bay (Figures 16; 17).

An alternative explanation for the double sea-level stand would be a double temperature peak during MIS 5e which is also suggested e.g. by the $\delta^{18}O$ record from the Vostok ice core (Jozuel, 1987) and from sea-level indicators across the Pacific (Chappell, 1974, Nunn, 1999) and Atlantic (e.g. Carew and Mylroie, 1999). The difference in the origins of the two notches, i.e. one being a cave notch and the other being a bioerosional sea-level notch, would thus be explained by the difference in duration of the two warm periods. However, the $\delta^{18}O$ record from Greenland (Dansgaard et al., 1993, GRIP, 1993)

and from deep sea floor (Martinson, 1987) point to *three* warm periods separated markedly by colder periods during MIS 5e. A triple notch would be expected in such case. The possibility that such a third notch exists above the two observed remains to be verified or excluded, since the view to the cliff above the two observed notches is strongly obscured by the thick vegetation.

It is also possible that the upper notch was reoccupied by a later sea level which would also explain why it so well expressed. Other evidence in support of re-flooding of the upper notch is the aragonitic corals found attached at to the notch at RWC-1. Finally, it should be noted that the notches could have well formed during some older, non-MIS 5e sea-level stand and, as noted before, the formation of the caves might not have coincided with the time of the notch formation. Dating of the speleothems would actually constrain the time of cave formation, while dating of the coral cobbles found in these breached caves would constrain the time of their breaching or the time when the sea level was close enough to the notch to wash in the cobbles.

Interpretation of the coastal paleonotches

The coastal paleo-notches have more or less the same elevation as the dated mid-Holocene algal ridge reef remnants (Figure 98), and because both tend to form around Higher High Water, they are most probably coeval. Another line of support is that paleo sea-level notches ~2 m above the modern notches are the most prominent and widespread sea-level paleo-notches on Guam, the higher and older notches being somewhat scarcer due to longer exposure to erosion.

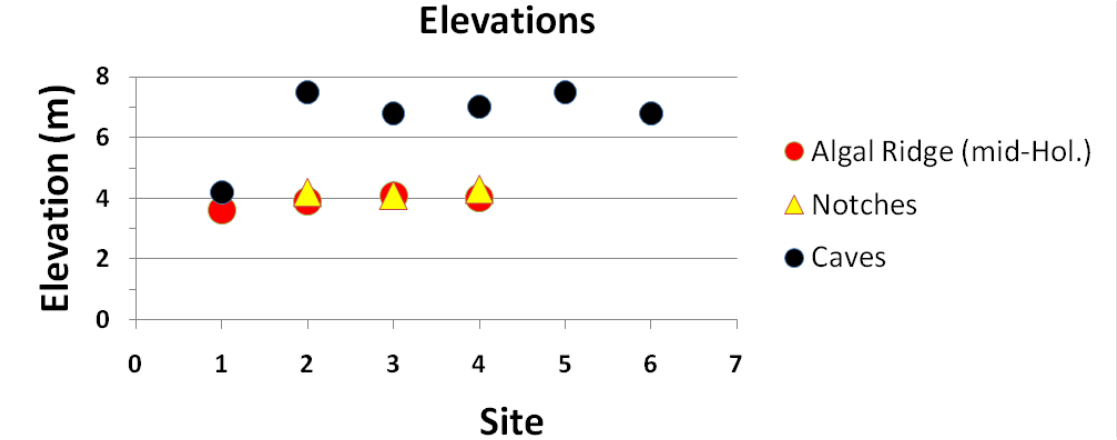

Figure 98 Ploted elevations of the coastal paleonothces, caves, and Merizo Limestone algal ridge facies outcrops.

According to Dickinson (2000), the emergent sea-level notches and mid-Holocene reef and are a remnant of the Pacific mid-Holocene sea-level highstand, which he estimates was 1.8 m above present sea-level. He also posits 0.8 m of uplift since the end of the mid-Holocene in northern Guam. The difference in the average elevation of the modern sea-level notches (0.6 m) and mid-Holocene sea-level notches (4.2 m) measured at Ritidian-east in this study is 3.6 m. If Dickinson's estimation of the mid-Holocene sea-level is correct, then the difference between notch elevations points to at least 1.8 m of post mid-Holocene uplift. The elevation of the measured coastal paleo-notches in the Tarague embayment is similar to that of have a similar elevation as the Ritidian-east notches and though no modern sea-level notch was measured in Tarague area it is reasonable to assume that their elevations do not depart significantly from the elevation between the Mean Sea Level and Mean Higher High Water. Therefore the same difference in elevation and thus the same uplift can be deduced for the Tarague embayment. The inferred 1.8 m of post mid-Holocene uplift is also in agreement with the second tectonic uplift (~1.9 m) suggested by Randall and Siegrist (1996) that coincides with the post mid-Holocene uplift of Dickinson (2000).

Dickinson's (2000) estimations of the uplift are based on a measurement of a paleo-reef flat in Tarague embayment and a sea-level notch comparison near Achae Point. Randall and Baker (1989) report more complex history of the sea-level notches at Achae Point because they found relatively recent corals attached to the lowermost sea-level notch that they found to be considerably above the average Mean Higher High Water. The notches in this area thus seem to have a more complex tectonic history and are thus not suitable for comparison with other notches. For the same reasons, the comparison of the reef flat elevations here with counterparts elsewhere could be problematic.

Interpretation of the cave formation

Ritidian east

Morphology and set-up

Only the caves that showed phreatic dissolutional features and typical flank margin cave features such as speleogens, ramifying and dead-end passages, cuspate walls and ceilings, and dissolutional niches were used for more detailed research. Mayulang, Pepe, Tokcha and Old Cove Cave in plan view all have a clear SW-NE orientation (Figures 60; 62; 65; 77), perpendicular to the coast which suggests that they all formed along freshwater discharge flowpaths since the water flows radially from the land to the sea. Where these caves formed, the underground water flow must have been relatively concentrated. That would also explain the well-expressed SW-NE oriented passages that formed especially in Tokcha Cave. Though jointing of similar direction has been reported from the south-most part of the research area, no joints were observable in the sureveyed caves. Mayulang and Tokcha Cave are analogous in that they both have inland low

passages that extend into bigger chambers towards the coast, which have narrow and tortuous and ramifying vertical dead-end extensions. These chambers could have formed where the mixing of the fresh and sea water at the margin of the fresh water lens was most efficient in forming a CaCO3-undersaturated mixture. The vertical extensions, on the other hand, could have evolved along vadose water pathways that confluenced with the fresh water lens.

An unusual feature of Tokcha and Old Cove Cave is the rather narrow upward extending passages that are actually the entrance passages of both of the caves. They could have developed along some more permeable passage within the rock during extreme events, during which the overflow of water would have forced the water upwards. In Tokcha Cave, however, the entrance passage is at more or less the same elevation as the top of the main chamber, so it would have formed within the lens and was probably just one of the freshwater discharge passages that developed where there was higher permeability in the rock. Another possibility not to be totally excluded is rapid relative sea-level change, e.g., because of a rapid tectonic uplift while the cave was forming, causing a shift of the fresh water lens position and a multilevel cave formation.

Of all of the caves, Tokcha Cave seems to have the most complex history. Its bottom is entirely covered with beach sand that must have come into the cave predominantly if not entirely through the northernmost of the two passages that extend to towards the coast. Below the sand were plenty of stalagmites that must have been growing for a considerable amount of time before they got buried and their growth interrupted. This suggests that during the growth of these stalagmites the cave was closed, and that the sea level was considerably lower than the exit of passages of the cave. The poorly lithified sandstone that occurs only around some of the speleothems and

cave walls probably formed by precipitation of cements out of the dripping water that was splashing and flowing around the stalagmite on which it was dripping, and near the cave walls down which the water was flowing. Such lithified sandstone rims occur considerably above the present level of the sand indicating that the sand deposits were once higher, were subsequently washed out, and were preserved only where cemented. This leads to the conclusion that the cave is episodically flooded, probably during storm events, with the sand being brought in and out of the cave as the entrance/exit is opened and closed during different storms. This lateral entrance probably formed as sea level rose in the Holocene and attacked the side of the outcrop containing the cave, breaching into it. Since then, beach sediment has entered the cave by this pathway. The Coca-Cola bottle found in the cave supports such mechanism since it is unlikely that it came from the surface given that the surface entrance was found buried.

Pepe cave is the smallest of all of the caves and also the lowest, measured from the floor to the ceiling. This cave seemingly formed along the boundary between the *Halimeda* and coral reef facies perhaps because the permeability was higher at this boundary. Because it has a rather flat shape and is also rather small, it could be a water-table cave, though it is found at a similar distance from the coast as the other caves and its elongated shape might suggest that it has also formed in the sea water-fresh water mixing zone rather than phreatic-vadose water mixing zone. Another possibility is that the explored cave is only a part of a bigger cave, because there is a chance of continuation of the cave vertically. In such case, this part of the cave would be only a discharge passage, such as the entrance passage in Tokcha and Old Cove Cave.

All of the examined caves formed in the coral reef facies or at its upper boundary (Pepe Cave). The bedrock in these caves is predominantly made of recrystallized calcite

with well-developed crystals, as would be expected in a rock experiencing fresh water submergence. In Tokcha cave, however, small, up to few millimeter-wide areas of aragonite within the recrystallized rock were found. The *Halimeda* facies rock in Pepe Cave, however, is predominantly aragonitic as shown by the stain test. These observations raise the question of how long did these caves actually stay within the freshwater lens or was the water only occasionally occupying this area and dissolving the rock.

All the observed voids (Sasgao and Batingting) formed along joints, and since they have dissolutional ceilings they must have formed in the phreatic zone. In spite being too small for exploration, they are considerably big and therefore most probably formed in the mixing zone.

None of the caves shows signs of a prolonged re-flooding, such as. by a later sea-level stand. Tokcha Cave, as mentioned above, has been at least partly filled with water during Holocene, but only occasionally, i.e., during storms, perhaps more often so during the mid-Holocene when the sea level was higher as well as the land lower. Given that the sand has cemented to the speleothems, but that the speleothems show no dissolution, seawater (and therefore mixed water) invasion was episodic and of short duration.

Timing of the formation of the caves at Ritidian-east

All the observed caves were formed in the MIS 5e Tarague Limestone, so they formed during a sea-level stand between the MIS 5e and the present sea level. The U/Th dates of two of the stalagmites collected in Tokcha Cave (Figure 68) and the date of the core drilled in the flowstone in Old Cove Cave (Figure 79) places the formation of the secondary calcite deposits between 36 and 18 ka BP. The dates of secondary calcite

deposits, of course, give only a *minimum* age of the cave formation, so the actual age of the cave can be any age between the age of the speleothem and the age of the bedrock., i.e., MIS 5e.

The age of the speleothems suggests the formation of the caves during one of the sea-level stands of MIS 3 or earlier, up to the rock age of ~125 ka. If the caves were formed during MIS 3, then there should be at least a few sets of other caves at elevations between the elevation of the observed caves (~7-8 m, Figure 98) and the top of the MIS 5e level, at ~28 m, or the top of the present MIS 5e terrace, at ~20 m. No other caves were found above the elevation of 8 m.

Further, the caves are located ~20-21 m below the MIS 5e level, or what would be ~14-15 m below the modern sea-level, assuming the MIS 5e sea level was ~6 m higher than the modern one. Eustatic sea-level curves and the local sea-level curve from Huon Peninsula suggest that only two sea-level stands could have been high enough to reach the level where the caves are found: MIS 5a and MIS 5c. If we consider tectonic uplift, however, the sea-level stand that formed the caves must have been even higher than ~14-15 m below the present sea level. For example, if assuming the MIS 5e sea-level stand was ~6 m above the modern sea level but its indicators are found at an elevation of 28 m above the modern sea level, there must have been ~22 m of uplift in the ~125 since the MIS 5e maximum. That implies an average 0.176 mm/yr of uplift, or rounded 0.2 mm/yr, which is in perfect agreement with other estimates for the long term average uplift for northern Guam. Such a rate further implies that by MIS 5c, i.e. ~100 ka BP, there would have already been ~4 m of uplift in the 25 ka time span from MIS 5e to MIS 5c, thus making the *apparent* difference between the sea-level stands MIS 5e and MIS 5c, based the sea-level indicators incised in rock, about 4 m apart. Therefore, if we assume the MIS

5e sea level was 6 m higher than the modern sea level, and allow for 4 meters of uplift between MIS 5e and MIS 5c, the actual sea level of MIS 5c would have been ~16-17 m below the MIS 5e level and ~10-11 m below the modern sea-level.

As mentioned above, MIS 5a sea level might also have been high enough so that the caves formed at that time could, given the average uplift, be found above the modern sea-level today. If we assume that MIS 5a sea level was more or less at the same elevation as MIS 5c, as indicated by the sea-level record from Huon Peninsula (Lambeck, 2002, Figure 5) or oxygen isotope record (Waelbroeck et al., 2002, Figure 4), then during the ~20 ka between the two stands there would be again ~3.5 to 4 m of uplift that would appear in the flank margin cave record as a 3.5 to 4 m sea level elevation difference. Mayulang Cave, as a matter of fact, is ~4 m lower than the rest of the caves, so thus could have formed during the MIS 5a stage.

But because the actual sea-level curve is unknown, there are other possibilities. The MIS 5a sea-level stand could have been higher than the MIS 5c as also suggested by the eustatic sea-level curves (e.g. Waelbroeck et al., 2002, Figure 4)) and the sea-level curve in Huon Peninsula (Lambeck, 2002, Figure 5). In such a scenario and using the same logic as above, the MIS 5a should have been 8 m higher than the MIS 5c to place the bulk of the caves ~4 m above Mayulang cave, which would have been formed during MIS 5c in such a case. That would imply a MIS 5a sea level being ~12 m below the MIS 5e and ~6 m below the modern sea-level. MIS 5c, on the other hand, would in such case have to be ~20 m below the MIS 5e and ~14 m below the modern sea level.

If either of the two highest expected sea-level high stands after the MIS 5e was considerably higher, even higher than the modern sea level (e.g. Shackelton et al., 2000,

Figure 4), then the caves formed during such a sea-level stand could have been placed to near the MIS 5e level and thus already eroded by now.

Because Mayulang Cave has more or less the same elevation as the mid-Holocene reef and related sea-level notch it is not excluded that it could have formed during the mid-Holocene sea-level highstand. The cave is, however, a bit bigger than it would be expected for the mid-Holocene, especially if compared to the caves that were observed behind the mid-Holocene sea-level notch in Talafofo Bay and Tanguisson (Figure 16; 17). At Tanguisson, small flank margin caves are found in the Merizo Limestone, demonstrating that the mid-Holocene sea-level highstand generated flank margin caves, and did so in a few thousand years. Giving the high porosity of the rock and possible preexisting large voids in the reef and given the large caves that formed during a sea-level stand in considerably more arid places like the Bahamas, such a possibility cannot be completely ruled out.

The implication for the sea-level curve

Given that the actual sea-level curve for the Guam area is unknown, reliable inferences regarding timing of sea-level stands can only be made when the trends documented by the indicators are big and distinctive. Even the sea-level curve from the relatively nearby Huon Peninsula is too uncertain to be used as a reliable comparison. It should also be kept in mind that there are important regional phenomena that could be locally important, and which significantly affect the timing and magnitudes of local sea levelS. Guam lies along a plate convergence zone and the deepest oceanic trench in the world. This setting doubtless has an influence on many variables that might affect the sea-levels, such as the gravity field, mantle properties influencing the isostatic effects,

and the water dynamics due to a very high nearby water column, in addition to local tectonic effects.,

From the examined sea-level indicators, an important conclusion can be inferred; the sea level stands that could have formed the caves at Ritidian-east are MIS 5c and MIS 5a. As can be deduced from the sea-level record (whichever interpretation is selected), MIS 5c as well as MIS 5a were relatively high, even if less so than the MIS 5e sea-level highstand (Shackelton, 2000, Figure 4; Waelbrock et al., 2002, Figure 4; and Lambeck 2002, Figure 5).

Another piece of evidence that the notch(es) above the Tarague Limestone terrace were formed during the MIS 5e sea-level highstand is the observed and dated reef facies near the seaward margin of the Tarague Limestone terrace in the Tarague embayment. The fossil reef observed there and elsewhere along the edge of the Tarague Limestone terrace, shows a lush species variety that can only be found down to ~20 m depth (Wells, 1967, Cabioch et al., 1999). This in principle does not help in constraining the sea level unless we have a date from the observed facies at a measured elevation. For example, if the reef growth follows the pace of the sea-level rise (a catch-up reef) we can, theoretically, get a shallow-reef deposit sequence of infinite thickness. At any given point of the sequence, the sea level would result up to 20 m above the chosen point and if that point was an erosional surface we would get an erratic value of the maximum sea level of the reef growth period. But if we have that point dated, we can then at least say that at *that given time* the sea level was *within* 20 m of that point. In Tarague embayment, the two corals were dated to be ~126 and ~132 ka old (Randall and Siegrist, 1996) and measured to be ~9 m above the present sea level. That means that approximately between 126 and 132 ka ago the sea level was within ~20 m above these corals, i.e., within ~29 m

above the present sea level, or less, which is in excellent agreement with the estimated elevation of the cave notch found above the Tarague Limestone terrace in Ritidian-east area. The age of the corals is also close to the MIS 5e maximum, and they could have grown deep enough for long enough so that 8 m of later coral deposition could have occurred, which would be eroded away between the MIS 5e peak and now, as indicated in the Ritidian research area. For example, if we take 116 ka as the date at which the sea level would drop from its maximum to the same level as the modern sea level (Muhs, 2002), the dated corals could be still ~10 m under water even if we account for ~2 m of uplift in 15 ka; at the MIS 5e peak ~125 ka ago they could be 20 m below the water surface, but by 116 ka the water would drop for ~6 m and the island would rise for ~2 m the corals would still be ~12 m or roughly ~10 m under water level at that time. Several thousand years would also be enough for a several meter thick sequence do be deposited on top of the dated corals.

Cave formation and constraints

Ritidian west

The Ritidian-west caves are all in Mariana Limestone so it is difficult to find temporal constraints. Because they are much bigger than the caves found in the Tarague Limestone at Ritidian-east and Tarague embayment, they are not likely to be directly related. However, they must have been flooded during the MIS 5e, at which time they could have even held a fresh water lens. This lens might or might have not caused the observed dissolution of secondary calcite deposits. The freshwater lens must have been at some level within the cliff of the first terrace above the backbeach deposits, where the caves would have formed. But because of the preexisting karst plumbing system, the

freshwater discharge might have simply followed the preexisting flowpaths and overprinted them.

The only sea-level indicator in Ritidian-west that probably belongs to the last interglacial cycle is the notch just above the backbeach deposits at the extreme east end of the Ritidian-west area (Figure 92). The notch should belong to either 5a or 5c, analogous to the sea-level indicators at Ritidian-east. The elevation of the notch is, however, ~10 above the modern sea-level, which is ~2-3 m higher than the caves at Ritidian-east area. The difference in elevation could be due to the differential uplift along the Ritidian Fault previously reported by Tracey et al. (1964) and Randall and Baker (1989). This fault could also explain the difference in elevation between the supposed MIS 5e notches at Ritidian-east and Ritidian-west area.

Interpretation of the tectonic history of northern Guam

General

Modern Pacific coral reefs usually grow to within a few meters of the sea level extant at the time of their growth. Reef margins can support algal ridges that grow in the surf zone to even slightly above the mean sea level. Given the elevation of an uplifted reef, if the time of deposition can be determined from a datable fossil, and the depth of the fossil with respect to the sea level at the time of deposition can be inferred (as from the known ranges of depths for the dated fossil species or surrounding organisms), one can further infer the relative uplift since the time of the reef formation. Reef limestones, however, are subject to surface erosion as soon as they are subaerially exposed. Erosional lowering (denudation) of the surface can be significant, especially in areas with high rainfall, which supports colonization by vegetation. Where such erosion occurs, it

must be accounted for in order to accurately estimate uplift and paleo sea-level. In tectonically active areas, such as the Mariana Islands, the tectonic uplift and subsidence must be accounted for as well.

If one can find a sea-level indicator other than a reef surface, however, such as a sea-level notch or flank margin cave, then denudation is not of concern. However other parameters, such as the time of the notch formation, still need to be resolved in order to calculate the uplift since the notch formation.

Uplift of the Mariana Limestone

The highest elevation at Ritidian Point is Mount Machanao, made of Mariana Limestone reef facies (Appendix A) which stands 183 m above sea level. To determine the long-term average uplift rate the time at end of Mariana Limestone deposition must be estimated, and the sea level at that time should also be considered. The end of the Mariana Limestone deposition has been estimated to be between 2 and 1.8 Ma (Randall and Siegrist, 1996). Though during the late Pleistocene the sea level has been generally lower than the present, evidence from the Western Pacific suggest that sea level around 2 Ma ago was similar to the present one (Wardlaw and Quinn, 1991). The denudation rates for bare limestone rock, which is at least nowadays the case of the top of the Ritidian cliff, are between ~30 and 50 mm/ky considering modern rainfall and evapotranspiration on Guam and 30 % average porosity of the rock. Based on these parameters, the estimated thickness of the section removed by dissolution in 1.8 M years would be ~54 to 100 m. Given the modern elevation, the calculated total uplift in this period would therefore be ~240 to 280 m, giving an average uplift rate of ~ 0.13 to 0.16 mm/yr.

Uplift of the Tarague Limestone

Though the exact sea level around Guam during MIS 5e is unknown, evidence from various sites across the Pacific (Chappell, 1974, Muhs, 2002) as well as the sea-level curve derived from oxygen isotope record (Waelbroeck et al., 2002) suggests that the sea level was ~6 m higher than the modern, and that the maximum sea level was reached ~125 ka BP (Waelbroeck, 2002). If we assume that the notch above the MIS 5e terrace that lies ~28-33 m above the modern sea level represents the MIS 5e sea level, then there was ~22-27 m of uplift in 125 ka, giving an average uplift rate of ~0.18 to 0.22 mm/yr.

Uplift of Merizo Limestone

The highest elevations of the coral-algal ridge facies of the mid-Holocene Merizo Limestone and associated sea-level notch were measured to be ~4.2 m while the modern notch is at ~ 0.6 m above mean sea level, implying a ~3.6 m of sea level change since mid-Holocene. The mid-Holocene sea-level highstand was estimated to have been only ~1.8 above the modern sea level (Dickinson, 2000), which if correct, implies 1.8 m of uplift since the mid-Holocene sea-level highstand. The estimations for the end of the sea-level highstand range between 3.1 and 2.75 ka, however. The average uplift rate since mid-Holocene time, depending on the date selected, thus ranges between 0.58 and 0.65 mm/yr.

Recent tectonic movements

Based on the average displacement from three benchmarks in northern Guam between 1963 and 2004 (Carlson, 2009), there has been 0.030 m of subsidence in 41 years, giving an uplift rate of -0.73 mm/yr. Recent GPS measurements from a station also

located in northern Guam, not far from the site of the above benchmarks, give an average uplift value of 1.18 ± 0.73 mm/yr in a nearly 10-year period between January 1997 and November 2006 (Bouin and Wöppelmann, 2010). GPS measurements in 1992 and 1994 in a time span of 18 months (1.5 year) showed an average subsidence of ~10 cm of the island, which suggest a coseismic subsidence during the 1993 earthquake (Beavan et al.). The average uplift in the period between the two measurements in the span of 18 months (1.5 yr) would therefore be -66.67 mm/yr, though most of the subsidence probably occurred in less than a minute during the earthquake in 1993 (Bureau and Hengesh, 1994).

Summary of the tectonic activity of the island

A quick look at the evidence for tectonic movement gives an impression that the tectonic behavior of the island is quite complex. It can be noticed, however, that the shorter the period of observation, the larger the magnitude of the uplift or subsidence rate.The long-term average, which incorporates both uplift and subsidence, however, gives a small positive uplift rate. The tectonic activity of Guam could thus be interpreted to be similar to the typical behavior of the shares on the stock market; on short time scale the value can change dramatically up or down but the longer the time period taken into account, the steadier the rise of the value (Figure 99).

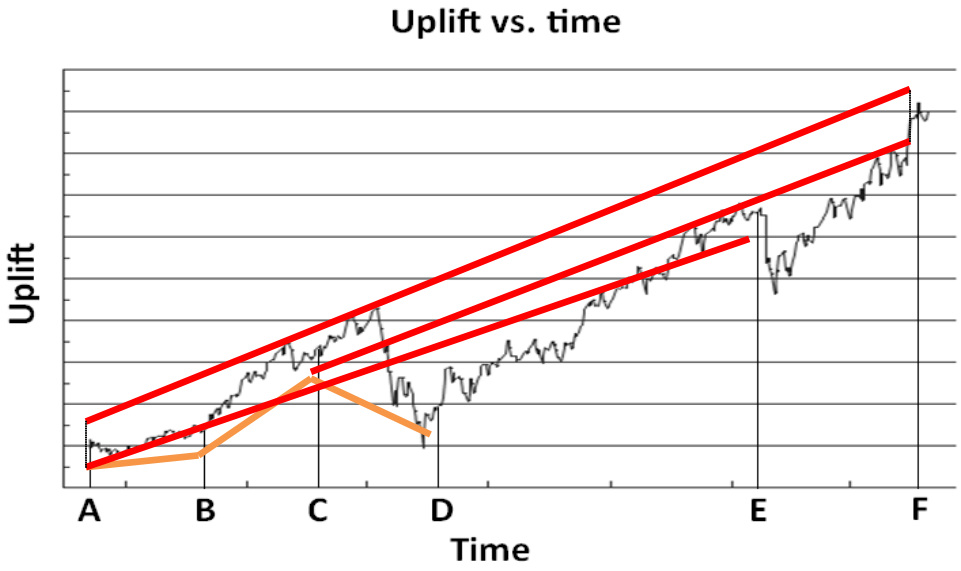

Figure 99 A schematic uplift curve for Guam. If we average short periods of time we get various average uplift values. For example, almost steady state results from averaging the time period between A and B, but a relatively rapid average uplift if the time period between B and C is taken, or a rapid average subsidence if the period between C and D is taken, even if we had uplift during this period. Instantaneous uplift or subsidence can also occur as a syntectonic event sometimes after e.g. time D or E, etc. But if we take long enough periods, e.g. between A and E, C and F, or A and F, we get similar average uplift values (red lines).

Concluding remarks about the denudation rates

From the observation of the *Karrentische* a minimum denudation of ~5 m can be deduced, which is also supported by less reliable indicators such as the observed karst pinnacles. Considering that the elevation of the inferred MIS 5e notch at Ritidian-east is ~8 m above the MIS 5e terrace, the actual denudation must have been ~8 m since the MIS 5e maximum, ~125 ka ago. This yields a denudation rate of ~64 mm/ka, which is in good agreement with the theoretically derived values for the given geologic and climatic conditions in northern Guam, and estimated values from other tropical regions with similar geology.

CHAPTER VI

SUMMARY AND CONCLUSION

Synthetic story

After the penultimate glacial maximum (MIS 6), sea level started to rise rapidly. As it was rising, it was flooding some preexisting karstified topography at Ritidian-east, as well as at Ritidian-west. At Ritidian-east, a less pronounced terrace must have existed, while at Ritidian-west well-developed terraces must have been in place before the MIS 5e transgression. The Tarague coral reef (Tarague Limestone) started to grow on both sides. While in the Ritidian-east area the reef had a continuous growth, at Ritidian-west it grew on two levels; on the terrace where Holocene backbeach deposits now occur, and at MIS 5e maximum veneering the first terrace *above* modern backbeach deposits. The remnants of the former are visible in patches near the cliff of this terrace, the best one being the ~3 m pinnacle (Figure 35), while the latter grew especially at the edge of the first terrace above the modern backbeach deposits where a well-preserved fossil coral reef with aragonitic corals can be observed. Boulders kept falling on the terrace where the reef was forming and they were overgrown as the reef growth was catching up with the sea-level rise.

When the sea level reached its MIS 5e maximum, i.e. ~6 m above the present sea level, ~125 ka ago, a bioerosional notch started to form in the Ritidian cliff, which is presently found at the elevation of ~28 m above the modern sea level. Simultaneously, flank margin caves were forming somewhere behind the notch. It seems likely that a

relative sea-level change occurred during the MIS 5e, either due to a tectonic movement or glacio-isostatic readjustments. Another possible explanation for sea-level change during this time is an oscillation in temperature that would have caused a eustatic, as well as a regional, sea-level change. In any case, it appears that one of the two MIS 5e sea-level substands was longer, causing a retreat of the bioerosional notch and cliff so that the flank margin caves in the back of the cliff were breached and filled with coral cobbles. Assuming a glacioisostatic adjustment analogous to the mid-Holocene one, the upper notch would have formed before the present one during a "mid-MIS 5e" highstand. Boulders would have kept falling on the reef that kept growing and prograding seawards, creating a relatively massive new terrace in the Ritidian-east area, and adding a new veneer on the two preexisting terraces in the Ritidian-west area. A buttress and channel reef morphology developed, especially in the Ritidian-central area. Meanwhile, the island had been rising tectonically.

The sea-level drawdown that followed the end of the MIS 5e, exposed the recently formed reef (Tarague Limestone). Dissolutional denudation and karstification of the Tarague reef began. The boulders that fell on the reef protected the reef surface beneath them from denudation while themselves dissolving, initiating the tropical *Karrentisch* development. On the top of the terrace, a layer of paleosol started to form. The inherited buttress and channel morphology became enhanced because of the differential dissolutional denudation, even as it was also destroyed by the colonizing vegetation at the same time. Some karst pinnacles started to form out of the preexisting reef morphology.

During MIS 5c, approximately 100 ka BP, Pepe, Tokcha, Old Cove, Sesgao, and Batingting caves and voids could have formed in the Tarague Limestone at the level ~19

m lower than the MIS 5e notches. Assuming an average of ~0.2 mm/yr uplift, there would be ~4 m of uplift in the ~20 ka span between MIS 5e and MIS 5c, so that the actual sea-level would be only ~15 m below the MIS 5e sea level, i.e., 9 m below the modern sea level.

Following MIS 5c, sea level dropped again to well below the present one, so that the record of that sea-level low stand (MIS 5b) must still be beneath the modern sea level, in spite of the subsequent uplift.

Assuming the subsequent MIS 5a sea-level highstand at ~80 ka BP reached about the same level as MIS 5c, and assuming 4 m of tectonic uplift in the 20 ka between MIS 5c and MIS 5a, the relative sea level would have been 4 m below the MIS 5c caves. Mayulang Cave, being 4 m lower than the rest of the caves at Ritidian-east, therefore probably formed during MIS 5a. Such deductions are highly speculative, of course, because the local sea-level curve is unknown, and eustatic sea-level curves and local sea-level curves like the one obtained from the terraces study at Huon Peninsula can be used only as rough references for the general trend of the sea-level change and its timing. For instance, if the MIS 5a was *higher* than MIS 5c, as suggested by some sea-level curves, then MIS 5c caves could have been uplifted to the later MIS 5a level and the cave record of the two sea-level stands would overlap. In such a case, the MIS 5c level would be ~15 m below the MIS 5e level (~9 m below the modern sea level) and the MIS 5a level would be ~11 m below the MIS 5e level (~5 m below the modern sea level). Given the local sea-level curve uncertainties, other scenarios area also possible.

The more recent sea-level stands after MIS 5a or MIS 5c were too low for their indicators to be uplifted high enough to be exposed above modern sea level. So, for the next 80 ka the Tarague Limestone surface kept denuding and karstifying. If we assume a

denudation rate ~64 mm/ka, the boulder of Mapi Fina' Mames must have fallen on the terrace surface about 90 ka BP. Some of the boulders that fell during the deposition of the reef and were swallowed by the reef growth have since been exhumed.

Sea-level began to rise again after the Last Glacial Maximum, ~20 ka BP. During the mid-Holocene, ~5 to ~3 ka BP, it was probably 1.8 m higher than the modern sea level (Dickinson, 2000). During the mid-Holocene highstand the Merizo reef had formed as well as a sea-level notch. After the sea-level drop to the modern sea level, the reef was exposed and eroded. The reef flat of the Merizo Limestone fossil reef was subsequently covered with backbeach (storm) deposits.

Since the deposition of the Merizo Limestone there has been a tectonic uplift of ~1.8 m, which has placed the Merizo Limestone as well as the mid-Holocene sea-level notches at ~4 m above the modern sea level. At this elevation, we also have Mayulang Cave, which could have thus also formed during the mid-Holocene. Whether it formed then or not is not certain, but it has breached since then, because it is filled with Holocene deposits. No U/Th stalagmite data are available for Mayulang Cave, however, to eliminate the mod-Holocene speleogenesis option. By the mid-Holocene, the original surface of the Tarague Limestone terrace had retreated about ~8 m from dissolutional denudation.

Conclusions

- During the MIS 5e sea-level highstand, the Tarague reef limestone was deposited, which is nowadays present up to 20 m above sea level.
- MIS 5e stage left two notch-records in the Ritidian cliff: a cave notch and a bioerosional notch. These are 28 m above the modern sea-level

- The original Tarague surface has retreated ~8 m since the MIS 5e maximum. The average denudation rate is therefore 0.064 mm/yr or 64 mm/ka, which is in a very good agreement with theoretically calculated values.
- Tropical *Karrentische* can be successfully used as denudation indicators, but requires a high number of observations. Karst pinnacles should be used with discretion as sea-level indicators in a reef environment because their shape can be constructional.
- Flank margin caves proved to be good sea-level indicators on gentle slopes where sea-level notches are difficult to form and are poorly preserved.
- There has been approximately 22 m of cumulative tectonic uplift since MIS 5e, which gives an average value of 0.18 or rounded 0.2 mm/yr uplift rate, which matches well with uplift rates estimated from other indicators.
- The tectonic movements on Guam include a complex sequence of rapid uplift and subsidence but a general long term trend of uplift at ~0.2 mm/yr.
- The caves found at the elevation of ~8 m above the modern sea level at Ritidian point formed during MIS 5c or 5a sea-level stand.
    - If they formed during MIS 5c sea-level stand, they formed 6 m below the modern sea level.
    - If they formed during MIS 5a sea-level stand, they formed 10 m below the modern sea level.

REFERENCES

Allaby, A., Allaby, M., 1999, Dictionary of Earth Sciences, Second Edition. Oxford. University Press, Oxford, 640 pp.

Ayan, T., 1965, Chemical staining methods used in the identification of carbonate minerals: Bulletin of Mineral Resources Exploration, v. 65, p. 133-147.

Ayers, J.F., Clayshulte, R.N., 1984, A preliminary study of the hydrogeology of Northern Guam. Universitiy of Guam, Water and Energy Research Institute, Technical report No. 56, Guam, pp. 77.

Beavan, J., Murata, I., Nakao, S., Kato, T., Hirahara, K., Tanaka, T., Abad, R., Scholz, C., Roecker, S., Davis, D., 1994, Determination of the Philippine Sea plate velocity from Global Positioning System observations, and effects of the 1993 Guam earthquake (abstract), Eos Transactions, AGU, 75, West Pacific Geophysical Meeting Supplement, v. 59.

Bouin, M. N., Wöppelmann, G., (2010), Land motion estimates from GPS at tide gauges: a geophysical evaluation, Geophysical Journal International, v. 180, p. 193-209.

Bottrell, S.H., Carew, J.L., Mylroie, J.E., 1993, Bacterial sulphate reduction in flank margin environments: Evidence from sulphur isotopes. *In* White, B., (ed.), Proceedings of the 6th Symposium on the Geology of the Bahamas, Port Charlotte, Florida, Bahamian Field Station, p. 17-21.

Bureau, G., Hengesh, R.G., 1994, Earthquake hazard vulnerability study, Guam, Mariana Islands. Prepared for Government of Guam, Civil Defense/Emergency Services Office, Agana, Guam. Dames and Moore, 41 pp. and appendices and plates.

Cabioch, L.F., Montaggioni, G., Faure, G., Ribaud-Laurenti, A., 1999, Reef coralgal assemblages as recorders of paleobathymetry and sea level changes in the Indo-Pacific province. Quaternary Science Reviews, v.18, p. 1681–1695.

Carlson, E., Doyle, D., Smith, D., 2009, Development of Comprehensive Geodetic Vertical Datums for the United States Pacific Territories of America Samoa, Guam, and the Northern Marianas. Surveying and Land Information Science, v. 69, n. 1, p. 5-17.

Carson, M.T., PhD Anthropology, Richard F. Taitano Micronesian Area Research Center (MARC), University of Guam.

Carson, M.T., 2010, Radiocarbon chronology with marine reservoir correction for the Ritidian archaeological site, Northern Guam. Radiocarbon, v. 52, n. 4, p. 1627-1638.

Campos, J., Madariaga, R., Scholz, C., 1996, Faulting of the August 8, 1993, Guam earthquake: A thrust event in an otherwise weakly coupled subduction zone. Journal of Geophysical Research, v. 102, n. 17,581-17,596.

Chappell, J., 1974, Geology of coral terraces at Huon Peninsula, Papua New Guinea; a study of Quaternary tectonic movements and sea level changes. Geological Society of America Bulletin, v. 85, p. 553–70.

Cheng, H., Edwards, R. L., Hoff, J., Gallup, C. D., Richards, D. A. and Asmerom, Y., 2000, The half-lives of uranium-234 and thorium-230. Chemical Geology, v. 169, p. 17–33.

Coe, A., Bosence, D.W. J., Church, K.D., Flint, S.S., Howell, J.A., Wilson, R.C.L, 2005, The Sedimentary Record of Sea-Level Change. Cambridge University Press, New York, 287 pp.

Dansgaard, W. , Johnsen, S. J. , Clausen, H. B., Dahl-Jensen, D. , Gundestrup, N. S. , Hammer, C. U. , Hvidberg, C. S. , Steffensen, J. P., Sveinbjrnsdottir, A. E. , Jouzel, J. and Bond, G., 1993, Evidence for general instability of past climate from a 250-kyr ice-core record. Nature, v. 364, p. 218-220.

Dasher, G.R., 1994, On station: A complete handbook for surveying and mapping caves. National Speleological Society, Huntsville, AL, 242 p.

Dickinson, W.R., 2000, Hydro-Isostatic and tectonic influences on emergent Holocene paleoshorelines in the Mariana Islands, Western Pacific Ocean. Journal of Coastal Research, v. 16, n. 3, 735-746.

Dickinson, W.R., 2001, Paleoshoreline record of relative Holocene sea levels on Pacific islands. Earth-Science Reviews, v. 55, 191-234.

Dickinson, W.R., 2004, Impacts of eustasy and hydro-isostasy on the evolution and landforms of Pacific atolls. Palaeogeography, Palaeoclimatology, Palaeoecology, v. 213, p. 251-296.

Dreybrodt, 2000, Equilibrium chemistry of karst waters in limestone terrains. *In* Klimchouk, A.B., Ford, D.C., Palmer, A.N., Dreybrodt, W. (eds), Speleogenesis – evolution of karst aquifers. National Speleological Society, p. 126-135.

Edwards, R.L., Chen, J.H., and Wasserburg, G.J., 1986, 238U-234U-230Th-232Th systematics and the precise measurement of time over the past 500 000 years. Earth and Planetary Science Letters, v. 81, p. 175-192.

Emery, K.O., 1962, Marine Geology of Guam. Geological Survey Professional Paper 403 (B), 76 pp.

Fleming, K., Johnston, P., Zwartz, D., Yokoyama, Y., Lambeck, K., Chappell, J., 1998, Refining the eustatic sea-level curve since the Last Glacial Maximum using far- and intermediate-field sites. Earth and Planetary Science Letters, v. 163, p. 327-342.

Ford, D., Williams, P., 2007, Karst Hydrogeology and Geomorphology, John Willey and Sons Ltd. Chicester, U.K., 562 pp.

GRIP members, 1993, Climate instability during the last interglacial period recorded in the GRIP ice core. Nature, v. 364, p. 203–207.

Grossman, E.E., C.H. Fletcher III, Richmond, B.M., 1998, The Holocene sea-level highstand in the equatorial Pacific: analysis of the insular paleosea-level database. Coral Reefs, v. 17, p. 309-327.

Higgins, C.G., 1980, Nips, Notches, and the solution of coastal limestone: an overview of the problem with examples from Greece. Estuarine and Coastal Marine Science, v. 10, p. 15-30.

Hopley, D., 1986, Beachrock as a sea-level indicator. *In* van de Plassche (ed.), Sea-Level Research: A manual for the Collection and Evaluation of Data. Geo Books, Norwich, UK, pp. 361-400.

Jenson, J.W., Keel, T.M., Mylroie, J.R., Mylroie, J.E., Stafford, K.W., Taboroši, D., Wexel, C., 2006, Karst of the Mariana Islands: The interaction of tectonics, glacio-eustasy, and freshwater/seawater mixing in island carbonates. Geological Society of America, Special paper v. 404, p. 129-138.

Jocson, J.M.U., Jenson, J.W., Contractor, D.N., 2002, Recharge and Aquifer Response: Northern Guam Lens Aquifer, Guam, Mariana Islands. Journal of Hydrology, v. 260, p. 231-254.

Jozuel, J., Lorius, C., Petit, J., Genthon, C., Barkov, N., Kotlyakov, V., Petrov, V., 1987, Vostok ice core: a continuous isotope temperature record over the last climatic cycle (160,000 years). Nature 329, p. 403–408.

Karig, D.E., 1971, Structural history of Mariana Island Arc System, Geological Society of America Bulletin, v. 82, p. 323-344.

Kato, T., Beavan, J., Matsushima, T., Kotake, Y., Camacho, J.T., Nakao, S., 2003, Geodetic evidence of back-arc spreading in the Mariana Trough. Geophysical Research Letters, v. 30, n. 12, doi: 10.1029/2002GL016757.

Kayanne, H., Ishi, T., Matsumoto, E., Yonekura, N., 1993, Late Holocene sea-level change on Rota and Guam, Mariana Islands, and its constraint on Geophysical Predictions. Quaternary Research, v. 40, p. 189-200.

Kayanne, H., Hiroya, Y., Randall, R.H., 2002, Holocene sea-level changes and barrier reef formation on an oceanic island, Palau Islands, western Pacific. Sedimentary Geology, v. 150, p. 47-60.

Kindler, P., Mylroie, J.E., Curran, H.A., Carew, J.L., Gamble, D.W., Rothfus, T.A., Savarese, M., and Sealey, N.E. 2010. Geology of central Eleuthera, Bahamas: a field trip guide. 15th Symposium on the Geology of the Bahamas and Other Carbonate Regions.Gerace Research Centre, San Salvador, Bahamas, 75 p.

Kobayashi, K., 1995, Role of subducted lithospheric slab in uplift and subsidence of the northwestern Pacific margins. Marine Geology, v. 127, n. 1-4, p. 119-144.

Lambeck, K., 2004, Sea-level change through the last glacial cycle: geophysical, glaciological and paleogeogrphic consequences. Compte Rendus Geoscience, v. 336, p. 677-689.

Lambeck, K., Chappell, J., 2001, Sea level change through the last glacial cycle. Science, v. 292.

Lambeck, K, Nakada, M., 1992, Constraints on the age and duration of the last interglacial period and on sea-level variations. Nature, v. 357.

Lambeck K., Esat, T.M., Potter, E-K., 2002, Links between climate and sea levels for the past three million years. Nature, v. 419.

Lander, M., Ph.D. Meteorology, Water and Environmental Research Institute of the Western Pacific, University of Guam.

Lander M.A., Guard, C.P., 2003, Creation of a 50-Year Rainfall Database, Annual Rainfall Climatology, and Annual Rainfall Distribution Map for Guam. WERI Technical Report No. 102, 31 pp.

Lascu, I., 2005, Speleogenesis of large flank margin caves of the Bahamas. Master's thesis, Mississippi State University, 214 pp.

Lincoln, J. M., and Schlanger, S. O., 1987, Miocene sea-level falls related to the geologic history of Midway Atoll. Geology, v. 15, p. 454–457.

Martinson, D.G., Pisias, N.G., Hays, J.D., Imbrie, J., Moore, T.C., Shackelton, N.J., 1987, Age dating and orbital theory of the ice ages: Development of a high-resolution 0 to 300,000-year chronostratigraphy. Quaternary Research, v. 27, p. 1-29.

Martinez, F., Fryer, P.F., 2000, Geophysical characteristics of the southern Mariana Trough, 11º50'N-13º40'N. Journal of Geophysical Research, v. 105 n. B7, p. 16,591-16,607.

McGregor, H. V., Abram N. J., 2008, Images of diagenetic textures in *Porites* corals from Papua New Guinea and Indonesia, Geochemistry Geophyics Geosystems., 9, 17 pp., Q10013

Milne, G., Shennan, I., 2007, Isostasy, *In* Scott A. Elias, (ed.), Encyclopedia of Quaternary Science, Elsevier, p. 3043-3051.

Mink, J.F., Vacher, H.L., 1997: Hydrogeology of northern Guam. *In* Vacher, H.L., Quin, T. (Eds): Geology and Hydrogeology of Carbonate Islands. Developments in Sedimentololgy, 54. Elsevier Science B.V., p. 743-761.

Mitrovica, J.X., Milne, G.A., 2002, On the origin of late Holocene sea-level highstands within equatorial ocean basins. Quaternary Science Reviews, v. 21, p. 2179-2190.

Mitrovica, J.X., Peltier, W.R., 1991, On postglacial geoid subsidence over the equatorial oceans. Journal of Geophysical Research, v. 96, p. 20,053-20,071.

Muhs, D.R., 2002, Evidence for the Timing and Duration of the Last Interglacial Period from High-Precision Uranium-Series Ages of Corals on Tectonically Stable Coastlines. Quaternary Research. v. 58, p. 36–40.

Murray-Wallace, C.V., 2007, Eustatic sea-level changes, glacial interglacial cycles, *In* Scott A. Elias, (ed.), Encyclopedia of Quaternary Science, Elsevier, p. 3024-3034.

Mylroie, J. E., 1990, Sea Level. Magill's Survey of Science: Earth Science Series, Pasadena, p. 2267-2273.

Mylroie, J.E., and Carew, J.L., 1991, Erosional notches in Bahamian carbonates: Bioerosion or groundwater dissolution? *In* Bain, R.J., (ed.), Proceedings of the 5th Symposium on the Geology of the Bahamas, Port Charlotte, Fla, Bahamian Field Station, p. 185–191.

Mylroie, J.E., Jenson, J.W., Taboroši, D., Jocson, J.M.U., Vann, D.T., Wexel, C., 2001: Karst features of Guam in terms of a general model of carbonate island karst. Journal of Cave and Karst Studies, v. 63, n.1, p. 9-22.

Mylroie, J.R., Mylroie, J.E., 2007, Development of the carbonate island karst model. Journal Of Cave And Karst Studies, v. 69, n. 1, p. 59-75.

Mylroie, J.E., Mylroie, J.R., 2009, Flank margin caves as syndepositional caves: examples from the Bahamas. *In* White, W.B., (ed): Proceedings, 15th International Congress of Speleology, Kerville, Texas, 1(1), p. 533-539.

Mylroie, J.E., Mylroie, J.R., Nelson, C.S., 2008, Flank margin cave development in telogenetic limestones of NewZealand. Acta Carsologica, v. 37, n. 1, p. 15-40.

Mylroie, J. E. and Mylroie, J. R., 2009, Flank margin cave development as syndepositional caves: Examples from The Bahamas. *In* White, W. B., ed., Proceedings of the 15th International Congress of Speleology, National Speleological Society, Huntsville, Alabama, v. 2, p. 533-539.

NOAA, 2011, http://tidesandcurrents.noaa.gov/data_menu.shtml?stn=1630000%20Apra%20Harbor,%20Guam,%20%20andtype=Bench%20Mark%20Data%20Sheets.

Nunn, P.D., 1998, Pacific Island Landscapes, Institute of Pacific Studies, The University of the South Pacific. 302 pp.

Nunn, P.D., 1999, Envrionmental Change in the Pacific Basin, John Wiley and Sons, 357 pp.

Otoničar, B., Buzjak, N., Mylroie, J.E., Mylroie, J.R., 2010, Flank margin cave development in carbonate breccia facies: an example from Cres island, Coratia. Acta Carsologica, v. 39, p. 79-91.

Peltier, W.R., 2001, On eustatic sea-level history: Last Glacial Maximum to Holocene: Quaternary Science Reviews, v. 21, p. 377-396.

Pirazzoli, P.A., Montaggioni, L.F., 1986, Late Holocene sea-level changes in the Northwest Tuamotu Islands, French Polynesia: Quaternary Research, v. 25, p. 350-368.

Pirazzoli, P.A., 1986, Marine notches. *In* van de Plassche (ed.), Sea-Level Research: A manual for the Collection and Evaluation of Data. Geo Books, Norwich, UK, 361-400 pp..

Pirazzoli, P.A., 2007, Sea level studies, Geomorphological indicators, *In* Scott A. Elias, (ed.), Encyclopaedia of Quaternary Science, Elsevier, p. 2974-2983.

Purdy, E.G., Winterer, E.L., 2001, Origin of atoll lagoons. Geologic Society of America Bulletin, v. 7, p. 837-854.

Radke, G., Le Campion-Alsumard, Golubi, S., 1996, Microbial assemblages of the bioerosional "notch" along tropical limestone coasts. Algological Studies, v. 83, p. 469-482.

Randall, R.H., D.E. Baker, Jr., 1989, Appendix A: A geological and biological survey of the Ritidian Point coastal region of Guam. pp. 1-136. *In* H. Kurashina, J.A. Simons, J.A. Toenjes, J. Allen, S.S. Amesbury, G.M. Heathcote, R.H. Randall, D.E. Baker, Jr., Smith, B.D., Stephenson, R.A., Wells., E.F., Archaeological investigations at the Naval Facility (NAVFAC) Ritidian Point, Guam, Mariana Islands. Micronesian Area Research Center, University of Guam.

Randall, R.H., Siegrist, H.G., 1996, The Legacy of Tarague Embayment and Its Inhabitants, Anderson AFB, Guam, Volume III: Geology, Beaches, and Coral Reefs. Prepared for Andersen Air Force Base. International Archaeology, Inc., Honolulu, 462 pp.

Reagan, M., Meier, A., 1983, Geology and geochemistry of early arc-volcanic rocks from Guam. Geological Society of America Bulletin, 95, 701-713.

Reale, T., Carew, J. L., Thomas, C., Dumars, A., and Siegrist, G., 2004, Petrology of limestones from Guam, U.S.A.: A predictable pattern of diagenesis? *In* Lewis, R., and Panuska, B. (eds.), Proceedings of the 11th Symposium on the Geology of the Bahamas and Other Carbonate Regions (2002): San Salvador, Bahamas, Gerace Research Center, p. 157-164.

Reece, M. A., Mylroie, J. E., and Jenson, J. W., 2006, Notches in Carbonate Cliffs and Hillslopes: Origin and Implications. *In* Davis, R. L., and Gamble, D. W., (eds.), Proceedings of the 12th Symposium on the Geology of the Bahamas and Other Carbonate Regions, Gerace Research Center, San Salvador, Bahamas, p. 143-152.

Ruddiman, W.F., Raymo, M. McIntyre A., 1986, Matuyama 41,000-year cycles: North Atlantic Ocean and northern hemisphere ice sheets: Earth and Planetary Science Letters, v. 80, n. 1-2, p. 117-129.

Sandberg, P.A., 1985, Aragonite cements and their occurrence in ancient limestones, *In* Schneidermann, N. and Harris, P.M. (eds.), Carbonate Cements: SEPM Special Publication, 36, p.33-57.

Scoffin, T.P., Stoddard, D.R., 1978, Beachrock and intratidal cements. *In* Goudie, A.S. and Pye, K. (eds.), Chemical Sediments and Geomorphology, p. 401-425

Shepard F.P., Curray J.R., Newman W.A., Bloom A.L., Newell N.D., Tracey J.I. Jr, Veeh H.H.,1967, Holocene changes in sea level: evidence in Micronesia. Science, v. 157 n. 3788, p. 542-544.

Siegrist, H.G., and Reagan, M.K., 2008, Geologic Map and Sections of Guam, Mariana Islands (1:50,000), Revision of original map from USGS Professional Report 403A, by Tracey et al. (1964).

Schlanger, S.O., 1964, Petrology of the limestones of Guam. United States Geological Survey Professional Paper 403 – D, 52 pp.

Smith, D., Atkinson, T.C. 1976, Process, landforms and climate in limestone regions. *In* Derbyshire, E., editor, Climate and geomorphology, p. 367-409.

Spencer, T., 1988, Coastal biogeomorphology. *In* Viles, H.A. (ed.): Biogeomorphology, p. 255-318.

Stern, R.J., Bloomer, S.H., 1992, Subduction zone infancy: Examples from the Eocene Izu-Bonin-Mariana and Jurassic California arcs. Geological Society of America Bulletin, v. 104, p. 1621-1636.

Stern, R.J., Fouch, M.J., Klemperer, S., 2003, An overview of the Izu-Bonin-Mariana subduction factory, *In* J. Eiler and M. Hirschmann (ed.), Inside the Subduction Factory. Geophysical Monograph, 138, American Geophysical Union, p. 175–222.

Strecker, M. R., A. L. Bloom, L. M. Gilpin, and F. W. Taylor, 1986, Karst morphology of uplifted Quaternary coral limestone terraces: Santo Island, Vanuatu. Zeitschrift zur Geomorphologie, v. 30, p. 387-405.

Taboroši, D., 2002, Biokarst on a tropical carbonate island, Guam, Mariana Islands, Theoretical and Applied Karstology, v. 15, p. 73-91.

Taboroši, D., 2004, Field guide to cave and karst of Guam. Bess Press, Honolulu, HI, 109 pp.

Taboroši, D., 2006, Karst Inventory of Guam, Mariana Islands. WERI Technical Report No. 112: 214 pp.

Taboroši, D., Jenson, J.W., Mylroie, J.E., 2004, Karren features in island karst: Guam, Mariana Islands. Zeitschrift für Geomorphologie, v. 48, n. 3, p. 369-389.

Taboroši, D., Mylroie, J. E., and Kirakawa, K. 2006, Stalactites on tropical cliffs: Remnants of breached caves or subaerial tufa deposits? Zeitschrift fur Geomorphologie, v. 50, p. 117-139.

Tracey, J.I., Schlanger, S.O., Stark, J.T., Doan, D.B., May, H.G., 1964: General geology of Guam: United States Geological Survey Professional Paper 403 – A, 104 pp.

Waelbroeck, C., Labeyrie, L., Michel, E., Duplessy, J.C., McManus, J.F., Lambeck, K., Balbon, E., and Labracherie, M., 2002, Sea-level and deep water temperature changes derived from benthic foraminifera isotopic records: Quaternary Science Reviews, v. 21, p. 295-305.

Wang, J. G. Z. Q. and Law, K. T., 1994, Sitting in Earthquake Zones, A. A. Balkema, Rotterdam, 115 p.

Waterstrat, W. J., Mylroie, J. E., Owen, A. M., and Mylroie, J. R., 2010, Coastal caves in Bahamian eolian calcarenites: Differentiating between sea caves and flank margin caves using quantitative morphology: Journal of Cave and Karst Studies, v. 72, p. 61-74.

Whitaker, F.F., Smart, P.L., 1997, Hydrogeology of the Bahamian Archipelago. *In* Vacher, H.L., Quin, T. (eds), Geology and Hydrogeology of Carbonate Islands. Developments in Sedimentololgy, 54.

White, W.B., 1984, Rate processes: chemical kinetics and karst landform development. *In* La Fleur RG (ed.), Groundwater as a geomorphic agent. Allen and Unwin, London Boston Sydney, p. 227-248.

Wigley, T.M.L., Plummer, L.N., 1976: Mixing of carbonate waters. Geochimica et Cosmochimica Acta, 40, p. 989-999.

Young, F.L., 1988, Soil Survey of Territory of Guam. United States Department of Agriculture Soil Conservation Service, 166 pp.

Zong, Y., 2007, Sea levels, Late Quaternary, tropics. *In* Scott A. Elias, (ed.), Encyclopaedia of Quaternary Science, Elsevier, p. 3087-3094.

APPENDIX A

GEOLOGIC MAP AND SECTIONS OF GUAM

.pdf of geologic map and sections of guam

APPENDIX B

RESULTS OF XRD QUANTITATIVE ANALYSIS OF THE SAMPLES OF THE BEDROCK OF THE SURFACE OF TOKCHA CAVE

Sample*	Aragonite (%)	Calcite (%)	Mg-calcite (%)	Halite (%)
8ca	77 ± 2	13 ± 2	10 ± 2	
7c:	74 ± 2	17 ± 2	9 ± 2	
5c	87 ± 2	8 ± 2	4.8 ± 2	0.2 ± 0.1 **
3c	66 ± 2	24 ± 2	8.7 ± 2	1.3 ± 0.5
1c2	97 ± 2	1.3 ± 0.5	1.7 ± 0.5	
1c	23 ± 2	77 ± 2		
6a	35 ± 2	32 ± 2	33 ± 2	
5ah	35 ± 2	28 ± 2	27 ± 2	
4a	40 ± 2	29 ± 2	40 ± 2	
2h	44 ± 2	32 ± 2	24 ± 2	
1h	42 ± 2	31 ± 2	27 ± 2	

*The letters of the sample names are abbreviations of the visible fossils present in the sample:

- c – coral
- a – algae
- h – *Halimeda*

** Halite is present only in trace amounts.

APPENDIX C

RESULTS OF U-Th DATING OF THE SPELEOTHEMS FROM TOKCHA CAVE AND OLD COVE CAVE

																		Model Ages (Years)			
	Sample	Spike *1	238 U		delta 234U		230 Th		232 Th		230/232		230/234		230/238		230/238				
	weight	weight	(ppb)	uncert.	today	uncert.	(pg/g)	uncert.	(pg/g)	uncert.	(ppm)	uncert.	activity	uncert.	activity	uncert.	atomic	if (230/232)i		if (230/232)i	
Sample ID	(g)	(g)																= 4.4 ppm	uncert.	= 15 ppm	uncert.
Tokcha, Tai 1s (bottom)	0.238	0.3503	212.8	0.2	102.1	1.6	1.097	0.005	28.5	7.8	38800	10600	0.268	0.001	0.315	0.002	0.0000053	36560	220	36550	220
Tokcha, Dong 1s (bottom)	0.237	0.3571	302.3	0.4	103.4	1.4	1.550	0.010	59.1	7.9	26450	3500	0.284	0.002	0.313	0.002	0.0000053	36240	290	36220	290
Tokcha, Tai 6s (tip)	0.141	0.2624	318.5	0.5	101.3	1.8	1.051	0.010	39.5	13.2	26900	9000	0.183	0.002	0.202	0.002	0.0000034	22010	230	22010	230
Tokcha, Dong 1s (bottom)	0.400	0.3528	221.4	0.3	104.5	1.5	1.145	0.005	51.5	4.7	22400	2000	0.286	0.001	0.316	0.002	0.0000054	36590	220	36570	220
Old Cove C. 1 (bottom)	0.623	1.0303	578.8	0.6	106.8	1.0	1.674	0.006	5064	12	334	1	0.160	0.001	0.177	0.001	0.0000030	18710	240	18160	790
Old Cove C. 2	0.240	0.5154	238.2	0.3	110.4	2.1	5.82	0.03	19020	66	309	2	1.345	0.007	1.493	0.007	0.000025	not calculated			